

**STRUCTURAL CONTROLS ON GROUNDWATER
FLOW IN THE YUCCA MOUNTAIN REGION**

Prepared for

**Nuclear Regulatory Commission
Contract NRC-02-97-009**

Prepared by

**David A. Farrell
Amit Armstrong
James R. Winterle
David R. Turner
David A. Ferrill
John A. Stamatakos
Neil M. Coleman
Mary Beth Gray
Stewart K. Sandberg**

**Center for Nuclear Waste Regulatory Analyses
San Antonio, Texas**

July 1999

ABSTRACT

Accurate prediction of radionuclide fluxes along transport pathways, and arrival times at receptor locations, are important considerations in the siting of a high-level nuclear waste repository at Yucca Mountain (YM), Nevada. The accuracy of these predictions is dependent on the identification and characterization of potential transport pathways and accurate estimation of groundwater flow rates along these pathways. Due to the limited geologic and hydrologic data available for the YM region potential transport pathways and associated groundwater flow rates have been the subject of much debate and speculation. One proposed conceptual model suggests that geologic structures, such as faults and fractures form the dominant flow and transport pathways at the site and that transport times to receptor locations that result from such pathways may be significantly less than those currently proposed in the Department of Energy Total System Performance Assessment-Viability Assessment. In an attempt to address conjectures related to the importance of structural controls on groundwater flow at YM, staff from the Center for Nuclear Waste Regulatory Analyses (CNWRA) and the U.S. Nuclear Regulatory Commission (NRC) formed a multidisciplinary working group tasked with reviewing the following site information: (i) geophysical data pertinent to identifying potential structural controls on groundwater flow, (ii) hydrologic data relevant to the characterization of transmissivity anisotropy in the tuffaceous aquifer units, (iii) stratigraphic controls on groundwater flow, (iv) deformation mechanisms in faults and their potential impacts on groundwater flow, (v) fracture block characterization and its implications with respect to groundwater flow, and (vi) hydrochemistry and its implications with respect to groundwater flow. In addition, the working group was encouraged, where possible, to illustrate the impacts of some of its findings on groundwater flow at the site using simple models. The findings of this multidisciplinary review identified regions where structural controls on groundwater flow at both the local and site scale appear plausible. In particular, fracture and stress field analyses conducted in the tuffaceous units indicated possible anisotropy in the hydraulic transmissivity field which were consistent with findings of hydrologic studies. Using existing geophysical studies, plausible structural explanations for observed hydrologic and hydrochemical data were presented. In addition, other structural features, such as fault zones, which could potentially impact groundwater flow, were identified and discussed. Hydrochemical data were also found to be useful for constraining potential flow paths and for identifying regions where structure likely resulted in the observed anomalous chemical signatures. Although the multidisciplinary approach provided insights into structurally controlled groundwater flow at YM sparse data limited a comprehensive understanding of the relative importance of this phenomenon.

CONTENTS

Section	Page
FIGURES	vii
TABLES	ix
ACKNOWLEDGMENTS	xi
1 INTRODUCTION	1-1
2 SITE DESCRIPTION	2-1
2.1 REGIONAL GEOLOGIC FRAMEWORK	2-1
2.2 STRATIGRAPHIC AND HYDROSTRATIGRAPHIC SETTING	2-1
2.2.1 Carbonate Aquifer	2-4
2.2.2 Tuff Aquifers	2-5
2.2.3 Alluvial Aquifer	2-6
2.3 STRUCTURAL SETTING	2-7
2.4 REGIONAL POTENTIOMETRIC SURFACE	2-8
3 REVIEW OF EXISTING FLOW MODELS OF THE SOUTHERN NEVADA REGION	3-1
3.1 D'AGNESE et al. (1997)	3-1
3.2 U.S. DEPARTMENT OF ENERGY (1997)	3-3
3.3 CZARNECKI et al. (1997)	3-5
3.4 COHEN et al. (1997)	3-7
3.5 LEHMAN AND BROWN (1995, 1996)	3-7
3.6 SUMMARY OF GROUNDWATER MODELS APPLIED IN THE SOUTHERN NEVADA REGION	3-9
4 REVIEW OF INFORMATION PERTINENT TO THE ASSESSMENT OF STRUCTURAL CONTROLS ON GROUNDWATER FLOW IN THE VICINITY OF YUCCA MOUNTAIN	4-1
4.1 INFLUENCE OF STRESS ON GROUNDWATER FLOW IN THE YUCCA MOUNTAIN REGION	4-1
4.1.1 Slip Tendency and Dilation Tendency	4-2
4.1.1.1 Slip Tendency	4-2
4.1.1.2 Dilation Tendency	4-3
4.1.2 Bulk Transmissivity Anisotropy	4-3
4.1.2.1 Prediction of Anisotropic Transmissivity at Yucca Mountain	4-5
4.1.3 Analyses of Slip And Dilation Tendencies of Yucca Mountain Faults	4-5
4.1.3.1 Slip-Tendency Analysis of Yucca Mountain Faults	4-5
4.1.3.2 Dilation-tendency Analysis of Yucca Mountain Faults	4-8
4.1.3.3 Summary of Implications of Stress in Evaluating Structural Controls on Groundwater Flow in the Yucca Mountain Region	4-8
4.2 TRANSMISSIVITY ANISOTROPY IN THE YUCCA MOUNTAIN REGION	4-8
4.2.1 Estimating Anisotropic Transmissivity at Yucca Mountain	4-8
4.2.1.1 Summary of Implications of Transmissivity Anisotropy in Evaluating Structural Controls on Groundwater Flow in the Yucca Mountain Region	4-11

CONTENTS (cont'd)

Section	Page
4.3 INFLUENCE OF FAULT ZONES GROUNDWATER FLOW IN THE YUCCA MOUNTAIN REGION	4-12
4.3.1 Deformation Mechanism and Fault Zone Widths	4-12
4.3.2 Crossing Faults	4-16
4.3.3 Summary of Implications of Fault Zone Deformation in Evaluating Structural Controls on Groundwater Flow in the Yucca Mountain Region	4-16
4.4 HYDROCHEMISTRY OF GROUNDWATER IN THE YUCCA MOUNTAIN REGION ..	4-23
4.4.1 Major Element Chemistry	4-23
4.4.1.1 Regional System	4-23
4.4.1.2 Yucca Mountain and Immediate Vicinity	4-24
4.4.2 Stable Isotope Chemistry (δD , $\delta^{18}O$, and $\delta^{13}C$)	4-27
4.4.2.1 Regional System	4-27
4.4.2.2 Yucca Mountain and Immediate Vicinity	4-27
4.4.3 Radiogenic Isotopes	4-30
4.4.3.1 Regional System	4-30
4.4.3.2 Yucca Mountain and Immediate Vicinity	4-31
4.4.4 Summary of Implications of Hydrochemistry in Evaluating Structural Controls on Groundwater Flow in the Yucca Mountain Region	4-31
4.5 GEOPHYSICAL STUDIES IN THE YUCCA MOUNTAIN REGION	4-34
4.5.1 The Heat Flow and Thermal Regime in the Yucca Mountain Region	4-34
4.5.1.1 Discussions of Heat Flow Data	4-34
4.5.1.2 Nonisothermal Modeling of Yucca Mountain Region	4-36
4.5.2 Gravity Studies	4-37
4.5.2.1 Discussions of Gravity Data	4-39
4.5.3 Magnetic Studies	4-45
4.5.3.1 Discussions of Magnetic Data	4-45
4.5.4 Electrical Resistivity Studies	4-46
4.5.4.1 Magnetotelluric Surveys	4-46
4.5.4.2 Telluric Studies	4-47
4.5.4.3 Electromagnetic and Standard Resistivity Surveys	4-48
4.5.5 Summary of Implications of Geophysics Studies in Evaluating Structural Controls on Groundwater Flow in the Yucca Mountain Region	4-52
4.6 NUMERICAL STUDIES OF THE POTENTIAL IMPACTS OF AQUIFER ANISOTROPY AND HETEROGENEITY ON GROUNDWATER FLOW IN THE YUCCA MOUNTAIN REGION	4-53
4.6.1 Summary of Implications of Numerical Studies in Evaluating Structural Controls on Groundwater Flow in the Yucca Mountain Region	4-55
5 SUMMARY AND CONCLUSIONS	5-1
6 REFERENCES	6-1

FIGURES

Figure	Page
2-1	Regional map of southwestern Nevada (taken from D'Agnese et al., 1997) 2-2
2-2	Generalized stratigraphic section for the rocks in the Yucca Mountain region 2-3
2-3	Regional potentiometric map of the Death Valley groundwater system (taken from D'Agnese et al., 1997) 2-10
2-4	Site-scale potentiometric map of the Yucca Mountain region 2-11
4-1	Conceptual illustration of effects of faults with high slip tendency or high dilation tendency on development of anisotropic permeability in areas like the Yucca Mountain region [the minimum principal compressive stress (σ_3) is horizontal] 4-4
4-2	Thematic mapper scene with potential repository location, wells (red dots), faults (irregular black lines), and water table contours (blue lines). 4-6
4-3	(a) Slip tendency map of Yucca Mountain faults mapped by Simonds et al. (1995); (b) Dilation-tendency map of Yucca Mountain faults. 4-7
4-4	Locations of wells and faults in the vicinity of Yucca Mountain fault locations are from Frizzel and Shulters (1990) 4-10
4-5	Directional hydraulic diffusivities estimated from observation wells based on the long-term pumping test conducted at the C-Holes beginning May 8, 1996. 4-12
4-6	(a) Conceptual model of fault zone showing the fault core and surrounding damage zone; (b) Diagram showing the fault zone of the Stillwater fault in Dixie Valley, Nevada (Seront et al., 1998). 4-14
4-7	Types of fault zones observed from the Exploratory Shaft Facilities at Yucca Mountain (the four fault zones were identified from detailed field and laboratory studies of fault zone deformation). 4-15
4-8a	X-ray results showing the clay mineralogy of the Solitario Canyon fault gouge (Randon mount of < 400 mesh fraction). 4-17
4-8b	X-ray results showing the clay mineralogy of the Solitario Canyon fault gouge (oriented sample: air-dried). 4-18
4-8c	X-ray results showing the clay mineralogy of the Solitario Canyon fault gouge (oriented sample: glycolated). 4-19
4-8d	X-ray results showing the clay mineralogy of the Solitario Canyon fault gouge (comparison: air-dried and glycolated samples). 4-20
4-9	Schematic diagram illustrating effects of crossing conjugate normal faults on developing permeability anisotropy in rock where (a) fault zone deformation results in permeability decrease and (b) where fault zone deformation produces permeability increase 4-21
4-10a	Contour map of dissolved calcium in groundwater in the Yucca Mountain region. (taken from Claassen, 1985). 4-25
4-10b	Contour map of dissolved sodium in groundwater in the Yucca Mountain region (taken from Claassen, 1985). 4-26
4-11a	Regional map for hydrochemical studies used by Davisson et al. (1999). 4-28
4-11b	Contour map of $\delta^{18}\text{O}$ in groundwater for the southern Nevada region [taken from Davisson et al. (1999)]. 4-29
4-12a	Contour map of ^{14}C in groundwater for the southern Nevada region [taken from Davisson et al. (1999)]. 4-32

FIGURES (cont'd)

Figure	Page
4-12b	Contour map of ^{14}C in groundwater for the Yucca Mountain region [taken from Claassen (1985)]. 4-33
4-13	Map showing isotherms at the water table under Yucca Mountain, contoured with an interval of 2°C [taken from Fridrich et al. (1994) and based on data from Sass et al.(1988)] 4-35
4-14	(a) Model grid for nonisothermal model domain showing the model grid on top of Paleozoic Carbonate; (b) Simulated temperatures at the water surface. 4-38
4-15	Map of the residual gravity field in the vicinity of Yucca Mountain; units in mGal 4-40
4-16	North-to-southeast geologic section across Yucca Mountain showing interpreted buried graben [taken from Fridrich et al. (1994)]. 4-41
4-17	Subsurface model developed from gravity and seismic data collected along geophysical line AV-1 located south of the town of Amargosa Valley 4-44
4-18a	Telluric lines 1 and 2 extending from Yucca Mountain across the northern portion of Fortymile Wash and into Jackass Flats [taken from Flanigan (1982)] 4-49
4-18b	Telluric lines 3 and 4 extending across the lower reaches of Fortymile Wash and the northern Amargosa Desert [taken from Flanigan (1982)]. 4-50
4-19	(a) Electromagnetic sounding locations in Fortymile Wash and Amargosa Desert used by the Center for Nuclear Waste Regulatory Analyses (Bouguer gravity map superimposed; (b) Model based on the electromagnetic data (triangles represent resistivity layer boundaries and numbers represent layer resistivities) 4-51

TABLES

Table		Page
4-1	Aquifer properties estimated from the 1996 long-term pumping test	4-11

ACKNOWLEDGMENTS

This report was prepared to document work performed by the Center for Nuclear Waste Regulatory Analyses (CNWRA) for the Nuclear Regulatory Commission (NRC) under Contract No. NRC-02-97-009. The activities reported here were performed on behalf of the NRC Office of Nuclear Material Safety and Safeguards, Division of Waste Management. The report is an independent product of the CNWRA and does not necessarily reflect the views or regulatory position of the NRC.

The authors thank Gordon Wittmeyer, Lawrence McKague, and Scott Painter for their thorough technical reviews, Barbara Long for her editorial expertise, Budhi Sagar for programmatic review, and Lee Selvey for format review. Also appreciated is Paulette Houston and Arturo Ramos for staff support and preparation of this document.

QUALITY OF DATA, ANALYSES, AND CODE DEVELOPMENT

DATA: CNWRA-generated original data contained in this report meet quality assurance requirements described in the CNWRA Quality Assurance Manual. Sources for other data should be consulted for determining the level of quality for those data. The estimation of anisotropic transmissivity was based on analysis of data collected near Yucca Mountain (YM) from May–December, 1996. These data include water table altitude data from wells ONC1, USW H-4, UE-25 wt#3, UE-25 wt#14, and atmospheric pressure data collected at the C-Holes. Data from well ONC1 were obtained from the Nye County Internet site www.nyecounty.com; these data were collected under the Nye County Nuclear Waste Repository Project Office (NWRPO) Quality Assurance Program (QAP). Nye County policy requires that NWRPO establish and maintain a documented QAP that meets the requirements of ANSI/ASME NQA-1 and the criteria of 10 CFR Part 50, Appendix B. Water elevation data for wells USW H-4, UE-25 wt#3, UE-25 wt#14 obtained from the Yucca Mountain Project (YMP) Technical Database (TDB), available from Internet site www.ymp.gov, data tracking number (DTN) GS970308312314.002. These data are listed in the data file as “Non Q,” which presumably indicates they were not collected under an approved QAP. Atmospheric pressure data collected at the C-Holes were obtained from YMP with the understanding that the data were preliminary and have not undergone a complete technical review. However, the C-Holes atmospheric pressure data reveals pressure fluctuations that are nearly identical to those measured by Nye County at well ONC-1, located 840 m away, under a QAP. The C-Holes atmospheric pressure data were chosen over the Nye County data because they provide a continuous record, whereas the Nye County data set has brief periods where no atmospheric pressure was collected.

ANALYSES AND CODES: The groundwater flow simulations performed in section 4.6 of this report were documented under scientific notebook no. 311E (electronic), a copy of which is maintained at the CNWRA. An “off-the-shelf” code, Micro-FEM, was used to perform the work. Information about Micro-FEM can be obtained on the internet at “<http://www.xs4all.nl/~microfem>.” The Micro-FEM code was validated using a problem for which an analytical solution, in this case the Thiem equation (Kruseman and de Ridder, 1994), is available.

The simulations reported in section 4.5.1.2 of this report were performed using the computer code METRA, which is part of the MULTIFLO system of coupled flow and reactive transport models (Lichtner and Seth, 1998).

The simulations reported in section 4.5.4.3 of this report were performed using Version 6 of the suite of electromagnetic codes dated August 7, 1998, that includes ZONGE, READZONG, T47INPUT, READ, SLUMBER, RAMPRES3 and EINVRT6. These codes are discussed in the software users manual "Inverse Modeling Software for Resistivity, Induced Polarization (IP), and Transient Electromagnetic (TEM, TDEM) Soundings" written by Stewart Sandberg and dated August 7, 1998.

1 INTRODUCTION

Yucca Mountain (YM), Nye County, Nevada, is currently being characterized by the U.S. Department of Energy (DOE) as a potential location for an underground high-level waste (HLW) disposal site. The proposed site is located near the Nevada Test Site (NTS) in southern Nye County, Nevada, approximately 105 km north of Las Vegas, Nevada. The current design requires that the waste be placed in engineered canisters prior to emplacement in drifts located within the unsaturated portion of Miocene Topopah Spring Tuff units.

The Nuclear Regulatory Commission (NRC) is required to review and decide on the DOE license application to construct and operate the proposed HLW repository. A key concern in making the licensing decision is whether the repository will provide effective long-term waste isolation from the accessible environment based on a dose- or risk-based compliance standard. A likely scenario for the release of radionuclides to the biosphere should the storage canisters fail, is that radionuclides will be transported by percolating groundwater through the unsaturated zone (UZ) to the saturated zone (SZ), where they will be transported by the regional groundwater flow system beyond the repository footprint to potential receptors.

For purposes of repository performance assessment (PA) analyses, SZ postulated flow paths from the repository footprint to potential receptor locations are typically considered to pass through two distinct flow systems. The first is a fracture-dominated flow system through the volcanic tuff aquifer that underlies YM. It is generally assumed that, owing to low effective porosities and specific surface area, groundwater velocities are relatively high and radionuclide sorption is relatively low in this fracture-flow system. At some distance downstream from YM, groundwater flow exits the volcanic tuff aquifer and enters an alluvial (valley fill) aquifer where effective porosities and the mineral surface area available for radionuclide sorption are generally thought to be orders of magnitude greater.

PA sensitivity analyses (Nuclear Regulatory Commission, 1999) also demonstrate that radionuclides may be attenuated so effectively by flow through saturated alluvium that the attenuation during flow in the fractured tuffs is negligible by comparison. It should be noted, however, that PA calculations to date have assumed that saturated alluvium in the Yucca Mountain region (YMR) is a homogenous porous medium in which flow is evenly distributed. The presence of heterogeneities, such as buried stream channels, in the saturated alluvium could result in shorter travel times and less attenuation of radionuclides than are currently predicted in PA. Thus, the relative importance of the fracture flow segments of transport flow paths away from YM should not be marginalized until ongoing characterization of the alluvial flow system and delineation of the SZ tuff-alluvium interface has been completed.

Although the fractured-tuff flow system may not be a major contributor to natural attenuation of radionuclides, its importance lies in the fact that the network of fractures and faults controls where SZ flow will cross the fracture-alluvium interface and, hence, the relative transport distance in tuff versus alluvium. For example, if flow in the fractured tuffs is in the direction of the hydraulic gradient, as would occur in an isotropic flow system, then groundwater would flow in an easterly direction before turning gradually to the south—the result being greater transport distance through the alluvial flow system. Conversely, if the tuff aquifer exhibits either anisotropic permeability, owing to preferential fault and fracture orientations, or preferential flow along fault zones, then flow away from the repository footprint could conceivably occur in a more southerly direction than the hydraulic gradient, resulting in much shorter transport distance through saturated alluvium.

Determination of groundwater flow paths in the YMR is complicated by myriad uncertainties related to the geology and hydrogeology of the site. Geologically, the YMR is complex due to the many tectonic, volcanic, and erosional processes that have occurred through geologic time. These events have resulted in complex stratigraphic unit geometries and the development of numerous subsurface faults and fractures which, in turn, has resulted in a complex hydrogeologic environment. An understanding of the hydrogeologic environment is further complicated by uncertainties in the spatial distribution of formation properties pertinent to groundwater flow, uncertainties related to boundary conditions, and uncertainties related to possible structural features that may impact groundwater flow.

Due to the complex geology and associated uncertainties, differing conceptual models for subsurface flow in the vicinity of YM have been postulated in the form of groundwater flow models for the region [e.g., Winograd and Thordarson (1975), Rice (1984), Czarnecki et al. (1997), D'Agnesse et al. (1997), Cohen et al. (1997), and Lehman and Brown (1995, 1996), among others]. Among the differences in the proposed groundwater flow models, the incorporation, or lack thereof, of possible structural controls on groundwater flow, such as faults and fractures, is one of the more significant. For example, the potential impacts of fast flow along faults in the tuff aquifer were explored by Lehman and Brown (1995, 1996). Their analyses showed that models which explicitly accounted for structural controls yielded groundwater travel times to receptor locations that were orders of magnitude less than those estimated by models that did not explicitly account for such structural features. Similar results may be envisioned for the alluvial flow system, which is also known to be structurally heterogeneous. From a regulatory perspective, such contrasting model results require careful consideration.

In an effort to evaluate possible structural controls on groundwater flow at YM, the Center for Nuclear Waste Regulatory Analyses (CNWRA) and NRC staffs assembled a multidisciplinary working group (Structural Controls on Groundwater Flow Working Group). The primary goal of this working group was to review available hydrogeological, geophysical, hydrochemical, and structural geology data that may lead to conceptual models of groundwater flow, in particular, structurally controlled groundwater flow. Where possible, the working group has attempted to express their findings in terms of potential effects on groundwater flow in the YMR.

Chapter 2 of this report provides a review of the geology and hydrogeology of the YMR and the geologic and hydrogeologic framework for subsequent chapters. Chapter 3 contains a broad review of existing groundwater flow models for the YMR, and includes models that have largely ignored structural controls on groundwater flow, and those that have explicitly accounted for structural controls on flow. Chapter 4 provides a more detailed discussion of geologic, hydrologic, hydrochemical and geophysical constraints on groundwater flow and the geologic and hydrostratigraphic architecture of the region. Specifically, section 4.1 summarizes recent CNWRA analyses of the in situ stress field at YM, and presents a conceptual model for the influence of existing faults and fractures, and resolved stresses, on the development of anisotropic hydraulic conductivity. Section 4.2 presents an analysis of pump test data from the C-Holes complex located east of YM that indicates the direction of the principal axis of anisotropy of the transmissivity for the tuff aquifer to be consistent with that predicted in section 4.1. Section 4.3 describes recent CNWRA investigations of fault zone deformation in YM tuffs, and its potential impact on groundwater flow. Section 4.5 reviews geophysical studies that help constrain the geometry of the hydrostratigraphic units and that indicate possible deformation adjacent to faults which may be of hydrogeologic significance. Finally, section 4.6 summarizes recent modeling conducted jointly by NRC and CNWRA staff to address the possible impact of aquifer anisotropy on groundwater flow in the YM area.

Finally, the intent of this report is to provide a qualitative assessment of possible structural controls on groundwater flow in the YMR based on existing data. In its current form, the report provides little discussion of the structural aspects of the alluvial deposits in Fortymile Wash and the Amargosa Desert and their potential impact on groundwater flow in the YMR even though the DOE (1998) and the NRC (1999) sensitivity analyses have tentatively identified the alluvial deposits as one of the most important natural barriers to radionuclide migration at the site. This lack of discussion is not intended to marginalize the importance of the alluvial deposits but reflects the limited characterization performed in these deposits. This data limitation is currently being rectified through well bore and hydrologic analyses being conducted by Nye County, and geophysical and field mapping studies being conducted by the CNWRA. The results of these studies will be incorporated in followup reports. Finally, the qualitative discussions provided in this report indicate that structure plays a role in groundwater flow at the site; however, a comprehensive quantitative understanding of the role of structure is still lacking and requires further study.

2 SITE DESCRIPTION

Because the site description presented in this section considers only those factors viewed as pertinent to evaluating structural controls on groundwater flow in the region, it is limited to providing information on the geology and hydrogeology of the site.

Figure 2-1 identifies the area of interest for this study, including the southwestern part of the NTS, the region immediately west of the NTS extending to Crater Flat, and the region south of the NTS extending into the Amargosa Desert.

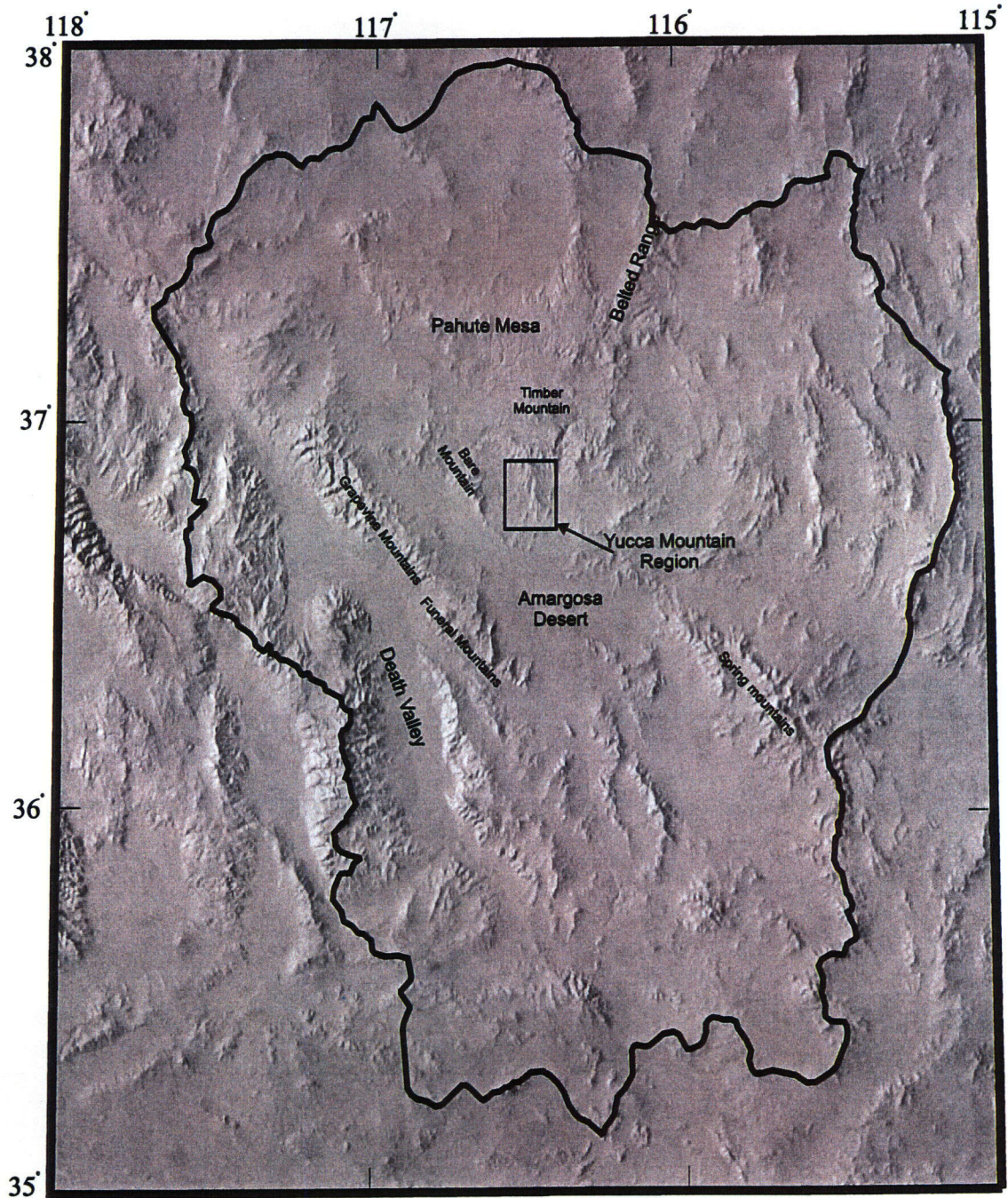
2.1 REGIONAL GEOLOGIC FRAMEWORK

The YM region is located in the Death Valley hydrologic system of the larger Western Great Basin system (figure 2-1). The Great Basin is part of the Central Basin and Range physiographic province of the western Cordillera. The Basin and Range is a wide zone of active extension and distributed normal faulting that spans east to west from the Wasatch Front and Colorado Plateau in Central Utah and Western Colorado to the Sierra Nevada Mountains in western Nevada and eastern California. Topography within the Basin and Range province reflects Miocene-to-Recent faulting in response to east-west extension, in which tilted and exhumed footwall blocks form subparallel north-south striking ranges separating elongated and internally drained basins. Ranges are up to several hundred km long with elevations up to 2 km above the basin floors. Much of the surface faulting is at the base of the ranges along normal faults that dip moderately ($\sim 60^\circ$) beneath the adjacent basins (herein defined as range-front faults), although complex faulting within the basins and ranges is also common.

YM proper lies within the Crater Flat basin, an extensional or transtensional half graben bounded on the west by master Bare Mountain fault and on the east by a series of antithetic west dipping faults, including the Paintbrush and gravity faults (Ferrill et al., 1996a). In this setting, YM forms a central graben high, separating two drainage basins, Crater Flat to its west and Fortymile Wash and Jackass Flat to its east. The basins and YM also contain northwest striking dextral strike-slip faults that are either remnants of discrete phases of regional dextral shear (Minor et al., 1997; Schweickert and Lahren, 1998) or transfer structures that accommodate differential extension within the basins (e.g., Fridrich 1998). Such faults at YM include the Drill Hole Wash, Sever Wash, Pagany Wash, and inferred Yucca Wash faults. These faults are poorly oriented for slip in the present day stress field (Ferrill et al. 1999b) and lack evidence of Quaternary displacement (Simonds et al., 1995). The orientation of these faults is, however, consistent with regional stress conditions prior to 10 Ma (Morris et al., 1996; McKague et al. 1996). Although they are inactive, these faults may nevertheless represent important pathways for groundwater flow.

2.2 STRATIGRAPHIC AND HYDROSTRATIGRAPHIC SETTING

Rocks of the YMR consist of thick accumulations (15 km in places) of Neoproterozoic and Phanerozoic sedimentary and igneous rocks resting on structurally complex crystalline basement, mainly 2.5 to 1.4 Ga gneiss, schist, quartzite, marble, and granite (figure 2-2). For the hydrologic framework, this stratigraphy can be subdivided into eight generic units. These are (i) Proterozoic clastics related to Neoproterozoic rifting; (ii) terrigenous detrital rocks (mainly quartzites) of the Early Paleozoic miogeocline; (iii) Cambrian shallow-marine and carbonate platform strata; (iv) continental shelf-slope-rise sequences of the mature Paleozoic Cordilleran passive margin; (v) Antler foredeep sediments; (vi) Early Tertiary basin



Universal Transverse Mercator projection, Zone 11.
 Shaded-relief base from 1:250,000-scale Digital Elevation Model;
 sun illumination from northeast at 30 degrees above horizon

25 0 25 50 KILOMETERS

Death Valley Regional
 Flow System Boundary

25 0 25 50 MILES

Figure 2-1. Regional map of southwestern Nevada (taken from D'Agnese et al., 1997)

Hydrostratigraphic Units

Precambrian and Paleozoic Section

Death Valley Bare Mountain

Upper Clastic Confining Unit	Pennsylvanian	Tihvipah Limestone		Foredeep Sequence		
	Mississippian	Rest Spring Shale				
		Perdido Fm.				
		Tin Mountain Limestone				
	Devonian	Lost Burro Fm.				
		Fluorspar Canyon Fm.	Rocks of Tarantula Canyon			
	Silurian	Hidden Valley Fm.				
		Lone Mountain Dolomite				
	Lower Carbonate Aquifer	Ordovician	Ely Springs Dolomite		Continental Shelf-Slope- Rise Sequence	
			Eureka Quartzite			
Pogonip Group		Antelope Valley Fm.	Antelope Valley Fm.			
		Ninemile Fm.	Ninemile Fm.			
		Goodwin Limestone	Goodwin Limestone			
Cambrian		Nopah Fm.		Platform Sequence		
		Bonanza King Fm.				
	Carrara Formation		Terrigenous Detrital Sequence			
	Zabriskie Quartzite					
	Wood Canyon Fm.					
	Stirling Quartzite					
Proterozoic Confining Unit	Johnnie Fm.		Rift Sequence			
	Noonday Dolomite					
	Pahrump Group	Kingston Peak Fm. and Beck Springs Dolomite				
		Crystal Springs Fm.				
		Basement Gneiss				

Hydrostratigraphic Units

Miocene Volcanic Section

Upper Volcanic Aquifer	Thirsty Canyon Group	Gold Flat Tuff	9.4 Ma	
		Trail Ridge Tuff		
		Pahute Mesa Tuff		
		Rocket Wash Tuff		
Upper Volcanic Confining Unit	Fortymile Canyon assemblage	Beatty Wash Fm.		
		Timber Mountain Group	Ammonia Tanks Tuff	11.5 Ma
			Rainier Mesa Tuff	11.6 Ma
Rhyolite of the Loop	12.5 Ma			
Lower Volcanic Aquifer	Paintbrush Group	Tiva Canyon Tuff	12.7 Ma	
		Yucca Mountain Tuff	12.8 Ma	
		Pah Canyon Tuff		
		Topopah Springs Tuff		
Lower Volcanic Confining Unit	Calico Hills Fm.		12.9 Ma	
	Wahmonie Fm.		13.0 Ma	
Lower Volcanic Confining Unit	Crater Flat Group	Prow Pass Tuff	13.25 Ma	
		Bullfrog Tuff		
		Tram Tuff		
Lower Volcanic Confining Unit	Belted Range Group	Dead Horse Flat Tuff	13.5 Ma	
		Grouse Canyon Tuff	13.7 Ma	
		Comendite of Split Ridge	14.0 Ma	
		Lithic Ridge Tuff		
Lower Volcanic Confining Unit	Older Tuffs	Lava of Tram Ridge	15.25 Ma	
		Tunnel Fm.		
		Tub Spring Tuff		
		Tuff of Yucca Flat		
		Redrock Valley Tuff		

2-3

Figure 2-2. Generalized stratigraphic section for the rocks in the Yucca Mountain region

deposits, mainly alluvial fan, fluvial, and lacustrine deposits; (vii) Miocene pyroclastic rocks of the Southwestern Nevada Volcanic Field; and (viii) Late Tertiary and Quaternary alluvial basin sediments with minor occurrences of basaltic volcanic rocks.

The groundwater flow system in the YMR is part of the larger Death Valley flow system which, in turn, forms a subregion within the Great Basin regional aquifer system (Plume, 1996). Within the Death Valley regional system, the YM flow system is centrally located within the Alkali Flats (Franklin Lake Playa)-Furnace Creek subbasin (Waddell, 1982). Alkali Flats, located in the southern Amargosa Desert, forms the discharge point for this subbasin. At this location, groundwater leaves the system in the form of evapotranspiration. It is believed that recharge for the Death Valley groundwater system occurs in the higher elevations of Timber Mountain, Pahute Mesa, Shoshone Mountain, the Sheep Range, and the Spring Mountains where precipitation exceeds evapotranspiration. Additional water may enter the system by subsurface flow from adjacent basins (Winograd and Thordarson, 1975). Within the immediate vicinity of YM, localized regions of recharge may exist in Fortymile Wash and Fortymile Canyon (Claassen, 1985; Savard, 1994).

Essentially the groundwater flow system of the YM region can be considered in terms of four aquifers, one within the lower Paleozoic carbonate rocks, two within the Miocene tuffs, and one within the alluvial and fluvial valley fill sediments. The alluvial aquifer is only important south of YM and in the Amargosa Desert where the groundwater table crosses from the tuffs into these younger sediments. The following sections provide very brief descriptions of these rocks, with emphasis on their role in the YMR hydrogeologic framework.

2.2.1 Carbonate Aquifer

The regional carbonate aquifer in the Death Valley hydrologic system consists of fractured and faulted Cambrian to Devonian carbonate rocks, overlying a lower confining unit that consists of Proterozoic to Cambrian clastics rocks and underlies an upper confining unit that consists of Late Devonian to upper Mississippian clastic rocks. These units are described separately in the following paragraphs.

The base of this stratigraphic section consists of 700- to 600-Ma supercrustal sedimentary and volcanic rocks deposited in deep, fault-bounded troughs (up to 3-km thick). These troughs and associated deposits are related to development of the Neoproterozoic rifted margin of North America (Laurentia) as fragments of East Gondwana separated from the rest of the supercontinent Rodinia (Dalziel, 1996; Prave, 1999). This sequence includes the Crystal Springs and Kingston Peak formations, which are some of the oldest sedimentary rocks exposed in the desert southwest.

Overlying the rift sequence rocks is a sequence of late Proterozoic to Cambrian terrigenous detrital rocks, which formed a westward-thickening miogeoclinal wedge. Unlike the localized deposition of supercrustal rocks, stratigraphic units within the terrigenous detrital sequence maintain remarkable lithological similarities along nearly the entire Cordilleran margin. These rocks represent the initial accumulation of sediments on the newly formed passive margin. Thickness of the miogeoclinal wedge is approximately 6,000 m. These rocks comprise the lower confining unit of the regional carbonate aquifer.

By Early Cambrian time, the Cordillera evolved into a sprawling carbonate platform, accumulating over 2,000 m of shallow or subtidal Early Cambrian carbonates. The Bonanza King formation is the dominant unit of the Carbonate platform sequence. By the Late Cambrian time, the Cordillera passive margin

matured, and a cratonic platform-shelf-slope-rise environment developed. With well-recognized cycles of transgression and regression of the proto-Pacific Ocean, the margin remained stable until the Late Devonian. The resulting sequence contains nearly 6,000 m of Middle Cambrian to Upper Devonian slope deposits, mainly thickly bedded limestones and dolomites with occasional siltstones and sandstones. These rocks comprise the bulk of the regional carbonate aquifer.

In the Late Devonian to Early Mississippian, the margin again became tectonically active with the approach and eventual collision of the Roberts Mountain allochthon, a series of telescoped lower Paleozoic rocks from the outer continental slope rift basins. A foreland trough (foredeep) developed in front of the allochthon, collecting a thick sequence of west-derived clastic flysch and east-derived debris flows and turbidities. Coeval muddy marginal shelf deposits inboard of the foredeep are considered potential source rocks for hydrocarbons generation in this part of Nevada (Trexler et al., 1996). These rocks comprise the upper confining unit of the carbonate aquifer.

Locally in the YMR, little information is available with regard to the hydrogeologic properties of the carbonate aquifer (Winograd and Thordarson, 1975). To date, aquifers within the Paleozoic carbonate unit have been only intersected by one borehole (UE-25 p#1) drilled in the vicinity of YM.

In other parts of the Great Basin, including Death Valley and the Spring Mountains near Las Vegas, Nevada thinly bedded carbonate rocks of Pennsylvanian and Permian age crop out. In these regions local aquifers exist within the younger carbonate rocks. Near YM, however, these rocks are not present in the stratigraphic record, either because they were never deposited or they were eroded during Mesozoic or early Cenozoic uplift.

2.2.2 Tuff Aquifers

Miocene volcanic rocks, mainly silicic tuffs, are up to 5-km thick and obscure much of the Precambrian and Proterozoic rocks, especially at YM. YM itself consists of a thick accumulation of volcanic tuff deposited on an irregular surface of the eroded and deformed Paleozoic and Precambrian basement. These tuffs were erupted from a series of Middle to Late Miocene (15 to 9 Ma) calderas that collectively form what has been defined as the Southwestern Nevada Volcanic Field (Sawyer et al., 1994). Each caldera eruptive sequence produced a sequence of tuffs that are stratigraphically organized into groups. Rocks of the Paintbrush Group, principally ash flows of the Topopah Spring Tuff (12.8 Ma) and Tiva Canyon Tuff (12.7 Ma), make up the main surface exposures of YM. The Paintbrush Group tuffs rest on a sequence of older tuffs, including the Calico Hills Formation and the Prow Pass and Bullfrog Members of the Crater Flat Group. The tuffs are generally flat-lying or moderately tilted in fault blocks bound by normal faults except along the northern margin of Bare Mountain. There, detachment faulting on the Fluorspar Canyon fault, as part of the Bullfrog Hills detachment system, appreciably attenuated the Miocene section. Younger tuffs related to the Timber Mountain Group are locally exposed at YM in topographic lows between large block-bounding faults. This observation, along with evidence for growth faults in the Paintbrush Group rocks in Solitario Canyon (Carr, 1990; Day et al., 1998a,b), suggests that faulting and tuff deposition were synchronous at YM.

The Tertiary volcanic sequences at YM may be divided into two aquifer systems and two confining units, based on permeability considerations: the upper and lower volcanic aquifer units and the upper and lower volcanic confining units (figure 2-2; also see figure 7 of Luckey et al., 1996). The lower volcanic aquifer includes most of the Prow Pass Tuff and the underlying Bullfrog and Tram units of the Crater Flat

Group (Luckey et al., 1996). Where the upper part of the Prow Pass Tuff is not fractured, it is considered part of the upper confining unit (Luckey et al., 1996). The lower volcanic aquifer underlies almost all of YM, and its units are often within the SZ. In general, the lower volcanic aquifer tends to be less densely fractured (Spengler et al., 1984) and more altered than the upper volcanic aquifer. The combination of the lower fracturing and the greater degree of alteration may account for this unit having a lower permeability than the upper volcanic aquifer (Luckey et al., 1996).

The lower volcanic confining unit consists of bedded tuffs, lava flows, and flow breccia beneath the Tram Tuff and includes the Lithic Ridge Tuff and the older flows and tuffs beneath the Lithic Ridge Tuff (Luckey et al., 1996). In the vicinity of YM, this unit has been encountered in Boreholes USW G-1, USW G-2, USW G-3, USW H-1, J-13, and UE-25 p#1. Luckey et al. (1996) pointed out that, although some zones in the lower volcanic confining unit may be fractured, the unit may be buried so deeply that the fractures are closed and do not transmit substantial quantities of water.

The upper volcanic aquifer consists of the variably welded ash-flow tuffs and rhyolite lavas of the Topopah Spring Tuff unit of the Paintbrush Group (Luckey et al., 1996). Luckey et al. (1996) described this aquifer as being saturated to the east and south of YM and in Crater Flat. This aquifer is the source of water for wells J-12 and J-13. At UE-25 wt#13, UE-25 wt#14, and UE-25 wt#15, only the lower part of the Topopah Spring Tuff is saturated. South of YM, only the lower part of the Topopah Spring Tuff is saturated in boreholes USW WT-11 and UE-25 wt#12. In Crater Flat, only the lower part of the Topopah Spring Tuff is saturated in boreholes USW WT-10; however, at borehole USW VH-1, the entire unit is saturated. Beneath the center of YM, the Topopah Spring Tuff unit is above the SZ due to the eastward dip of the unit and vertical displacements of this unit along the Bow Ridge, Midway Valley, Fran Ridge, and Paintbrush Canyon faults.

The upper volcanic confining unit consists of the unfractured part (or the area where the fractures are plugged) of the basal vitrophyre of the Topopah Spring Tuff, the bedded tuff beneath the Topopah Spring Tuff, the Calico Hills Formation, and the uppermost, nonwelded part of the Prow Pass Tuff of the Crater Flat Group (Luckey et al., 1996). Although the unit is not considered to be an aquifer, it nevertheless is capable of producing water (see figure 33 of Geldon, 1993). Beneath much of the southern part of YM, the upper confining unit is above the SZ (Fridrich et al., 1994; Luckey et al., 1996); in the remainder of the southern area, only the lower part of this unit is saturated. At USW WT-1, only 8 percent of this unit is saturated.

2.2.3 Alluvial Aquifer

Pliocene and Quaternary deposits in Crater Flat consist mainly of unconsolidated lacustrine sediments, alluvium, colluvium, and aeolian deposits. The stratigraphy of these units in Crater Flat and adjacent to Bare Mountain have been developed by Swadely and Parrish (1988) and Faulds et al. (1994). Corresponding maps of the surface distribution of these units generally show younging of the deposits toward the southern end of Crater Flat and Fortymile Wash, consistent with interpretation that the southern part of the basins have undergone greater subsidence, at least since about 1.0 Ma (Ferrill et al., 1996b; Stamatakis et al., 1997). Quaternary deposits are studded by a series of Pliocene and late Quaternary basaltic dikes and volcanoes. Pliocene volcanism, dated at 3.8 Ma (Fleck et al., 1996), is primarily confined to the eastern portion of the Crater Flat basin. Quaternary volcanism includes an alignment of at least four coeval volcanic cones, dated at about 1.0 Ma, in western Crater Flat and a basaltic cone at Lathrop Wells, thought to be between 70 and 140 ka (Heizler et al., 1997; Turrin et al., 1991). These rocks constitute the alluvial aquifer south of YM in the vicinity of the critical group.

Little is known about the details of the alluvial aquifer. In most flow models, described below, the hydrologic properties are considered isotropic and uniform, despite the presence of well-developed paleosols and a complex network of paleodrainages within the basins (Lundstrom et al., 1998). The details of the hydrogeologic properties of the alluvial aquifer are the subject of ongoing technical investigations by the CNWRA.

2.3 STRUCTURAL SETTING

Late Proterozoic and Paleozoic rocks in the Southern Great Basin have been deformed during several late Paleozoic and Mesozoic episodes of contractional deformation, including the emplacement of the late Permian Last Chance allochthon (Snow, 1992) and the Jurassic-Cretaceous Sevier orogeny (Cowen and Bruhn, 1992). These contraction events formed a roughly north-south fold-thrust belt contiguous with the Sevier fold-thrust belt across much of the western United States. That fold-thrust belt was later distended by Cenozoic extensional faulting (Wernicke, 1992) such that only parts of the remnant fold-thrust belts remain exposed in exhumed fault-bound ranges. These same structures also exist beneath Cenozoic basins and form an important framework for groundwater flow in the carbonate aquifer like the large hydraulic gradient just north of YM (Fridrich et al., 1994).

The majority of faults at YM are either north-trending normal faults or northwest-trending dextral strike-slip faults. The larger faults in these two orientations bound the fault blocks that underlie the study area. These two sets of faults are interpreted to be coeval, based on mutual terminations and secondary structures between them such as pull-apart basins (Day et al., 1998b) consistent with their origination during pre-10 Ma east-west extension in the region (Morris et al., 1996; Ferrill et al., 1996a; McKague et al., 1996). Some northwest-trending faults are dominantly normal faults, accommodating extension in relay ramps between overlapping normal faults (Ferrill et al., 1999a). Only four reverse faults with north-south or northeast-southwest strikes have been identified, but they are potentially key features for constraining the kinematic history of the region (Day et al., 1998a,b) and for identifying infiltration pathways (Levy et al., 1997). Much of the detailed fieldwork to study faults in the central block focused on the Ghost Dance and Sundance faults, which are close to the subsurface trace of the Experimental Studies Facilities (ESF) (Spengler et al., 1994; Potter et al., 1996).

YM itself consists of a sequence of north- to north-northeast-trending fault-bound ridges crossed by occasional northwest-trending dextral-strike-slip faults. Faults dip almost uniformly to the west and separate blocks of gentle to moderate east-dipping tuff strata. From north to south, both fault displacement and stratal tilt increase, indicating progressively greater extension of the Crater Flat basin southward. This pattern is most profound on the west flank of YM, which is defined by a series of left-stepping and north-trending *en echelon* faults. The southward increase in fault offset is coupled with greater block rotation, both horizontal and vertical (Scott, 1990). Work by the U.S. Geological Survey (USGS) (Hudson et al., 1994; Minor et al., 1997) suggests that this pattern of faulting, along with rotated paleomagnetic directions in the tuffs, resulted from a discrete period of extension followed by a discrete period of dextral shear, akin to an oroclinal bending model. More recent re-analyses of these data suggest an alternative explanation. The north-to-south displacement gradient and rotation of fault blocks is simply a result of increased rollover deformation in the hangingwall above a listric Bare Mountain fault (Stamatatos and Ferrill, 1998).

An *en echelon* pattern of faulting is best expressed along the western edge of Yucca Crest and the fault line escarpment that follows the west-dipping Solitario Canyon, Iron Ridge, and Stagecoach Road faults (Simonds et al., 1995). The geometry of faults and ridges defines a scallop trend, composed of linear north-

trending fault segments connected by discrete curvilinear northwest-trending fault segments. For example, the ends of the northwest-trending curvilinear Iron Ridge fault bend to the northwest near its overlap with both the Stagecoach Road and Solitario Canyon faults (SCF). YM also contains numerous swarms of small northwest-trending faults that connect the large north-trending faults. One example is at West Ridge, which is cut by numerous small faults that connect segments of the Windy Wash and Fatigue Wash faults. This geometry strongly suggests that the entire YM fault system is an *en echelon* branching fault system (Ferrill et al., 1999a), in which faulting on the large block-bounding fault triggers relatively widespread, but predictable, secondary faulting on connecting and linking faults. Linkage of the *en echelon* system is either by lateral propagation of curved fault tips or formation of connecting faults that breach the relay ramps (see figure 1 of Ferrill et al., 1999a; Peacock and Sanderson, 1994; Trudgill and Cartwright, 1994). More importantly, from this interpretation of *en echelon* faulting, it follows that locally developed faults and fractures were produced by local variations of the stress field (Crider and Pollard, 1998), rather than dramatic swings of the regional extension direction (Throckmorton and Verbeek, 1995). The amount, orientation, and degree of faulting directly depend on the relative position of the rock within the *en echelon* fault system either in relay ramps that connect overlapping *en echelon* fault segments or in the hangingwall or footwall blocks of the block bounding faults.

Of the three main northwest-striking, strike-slip faults exposed at YM (the Sever Wash, Pagany Wash, and Drill Hole Wash faults), only the Drill Hole Wash fault is intersected by the ESF. The structural blocks near YM, which are bounded by strike-slip faults, generally tilt approximately 5° east-southeast to southeast (Day et al., 1998a,b). Vertical displacements along these faults are generally small. Major washes and drainage features such as Pagany Wash appear to develop parallel to these strike-slip faults. Unexposed strike-slip faults in the region have been inferred from geophysical data. For example, Scott and Bonk (1984) inferred a northwest-striking fault beneath Yucca Wash based on their interpretation of aeromagnetic data. Fridrich (1998) presents structural evidence for the Yucca Wash fault.

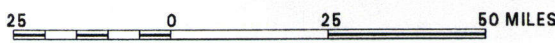
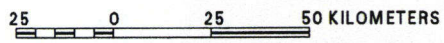
Minor faults that are fully contained within the rock mass between major block-bounding faults are termed intrablock faults. In some cases, intrablock faults are expressions of hanging-wall and footwall deformation and thus penetrate only to within a few hundred meters of the block-bounding faults (Day et al., 1998a,b). Examples of intrablock faults in the YMR include the Ghost Dance fault (GDF), Abandoned Wash fault, the Busted Butte fault, the Boomerang Point fault, as well as unnamed faults in the blocks west of Dune Wash on East Ridge. Vertical displacements along these faults can exceed 100 m (Day et al., 1998a). The GDF is the primary intrablock fault within the central part of the potential repository. It is a north-striking normal fault zone that dips steeply westward with down-to-the-west displacement. This fault connects to the Abandoned Wash fault at Ghost Dance Wash. The combined length of this fault is approximately 7 km. Dips on this intrablock fault were described by Day et al. (1998a) as being steeper than those of block-bounding faults and range from 75° to vertical.

2.4 REGIONAL POTENTIOMETRIC SURFACE

The first attempt at constructing a potentiometric map of the NTS and surrounding region was performed by Winograd and Thordarson (1975). The Winograd and Thordarson map illustrated possible southward flow from Pahute Mesa to the Amargosa desert. However, because of the lack of data for the Timber Mountain region, this southern flow path could not be confirmed. An updated potentiometric surface map for the region, extending from Timber Mountain to the Amargosa desert, based on additional data was produced by Czarnecki and Waddell (1984). The map also illustrated possible southern flow from north of YM into the Amargosa desert and beyond. As with the map of Winograd and Thordarson (1975), however,

the map of Czarnecki and Waddell (1984) was limited by little data north of YM and by no data for the Timber Mountain region. The most recent regional potentiometric surface map for the Death Valley system (figure 2-3) has been provided by D' Agnese (1997). The D' Agnese map, based on data collected since the Czarnecki and Waddell (1984) map, indicates flow from Pahute Mesa southward beneath YM and then to the Amargosa desert and beyond. As with its predecessors, a potential shortcoming of the model is lack of data for the Timber Mountain area.

Site-scale potentiometric surface maps have been developed for YM and adjacent regions. Robison (1984) developed a site-scale potentiometric surface map based on 1983 water level data. On the basis of the Robison map, the hydraulic gradient in the region was divided into three categories: (i) a large southward hydraulic gradient (0.12–0.13) north of the proposed repository location, (ii) a moderate eastward hydraulic gradient (0.05) in the vicinity of Solitario Canyon and just west of the crest of YM, and (iii) a region of low hydraulic gradient east of the area described in (ii). Ervin (1993, 1994) revised the potentiometric surface in the region of the low hydraulic gradient. The revised map (figure 2-4) illustrates that, in this region, the predominant direction of the groundwater gradient is east-southeast. The low hydraulic gradient region is believed to extend south into the Amargosa Desert.



- Death Valley Regional Flow System Boundary
- 1,000— Potentiometric contour- Shows altitude of potentiometric surface. Contour interval 100 meters. Datum is sea level.

Figure 2-3. Regional potentiometric map of the Death Valley groundwater system (taken from D'Agnese et al., 1997)

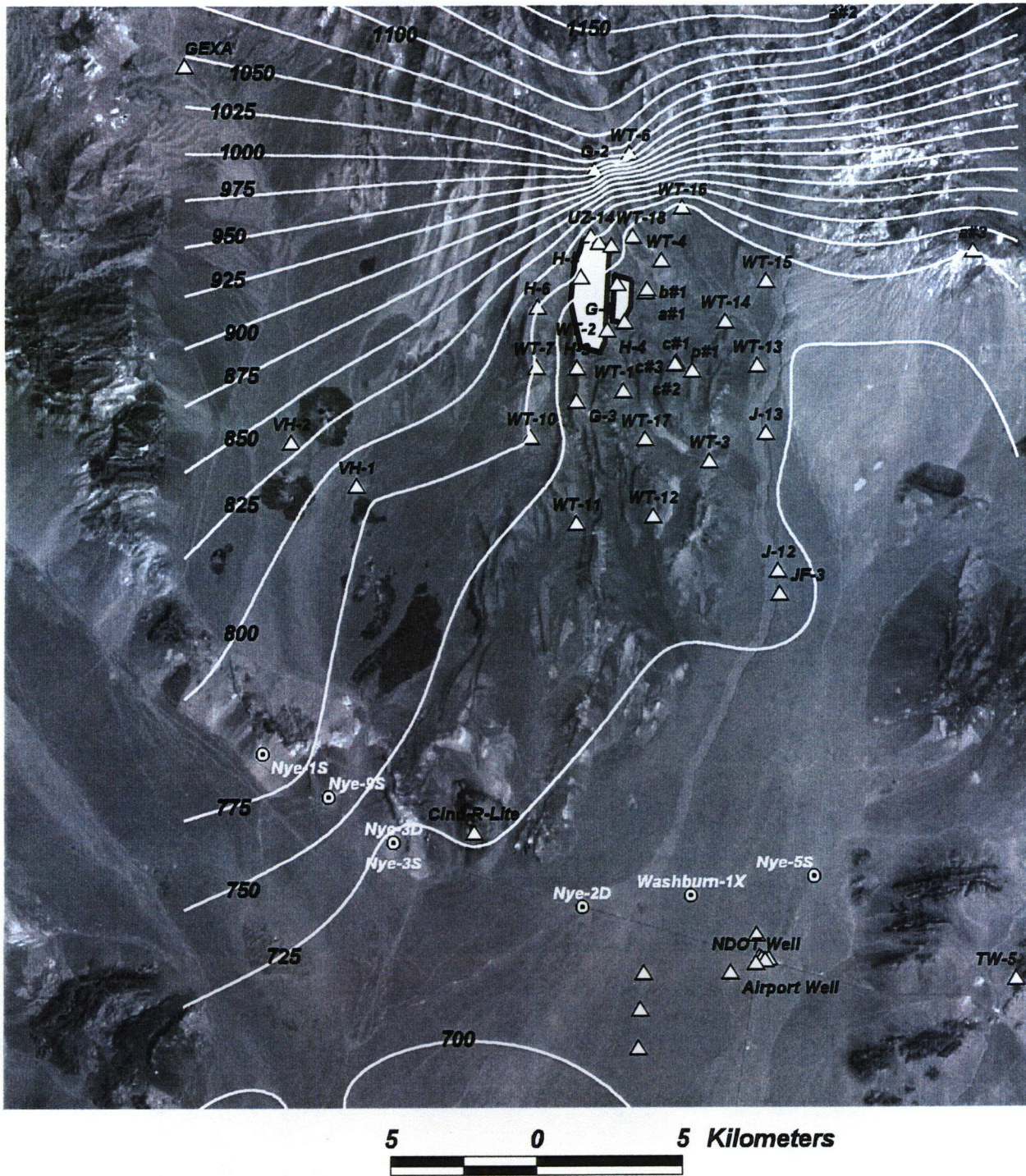


Figure 2-4. Site-scale potentiometric map of the Yucca Mountain region

3 REVIEW OF EXISTING FLOW MODELS OF THE SOUTHERN NEVADA REGION

Hydrological studies in the Death Valley region in the early 1960's assessed the potential for radionuclides released from underground nuclear tests to contaminate groundwater at the NTS and estimated the amount of water available for use at the NTS (Wittmeyer and Turner, 1995). Since that time, several hydrological studies have been conducted in southwestern Nevada and, more specifically, in the Death Valley groundwater flow system. This chapter provides a review of concepts behind the models proposed to describe saturated groundwater within this region.

Among the studies discussed by Wittmeyer and Turner (1995) are Schoff and Moore (1964), Rush (1970), and Winograd and Thordarson (1975), all examined the groundwater system across the NTS using hydrochemical facies data, hydrostratigraphic data, and hydraulic data; Waddell (1982) and Rice (1984), both involved the development of numerical models of the NTS and the Greater Death Valley regional groundwater flow systems; Czarnecki and Waddell (1984) and Czarnecki (1985, 1989), both developed conceptual modeling studies at YM designed to assess the effects of neotectonism and climate change on the proposed repository; Feeney et al. (1987) described numerical models of the western NTS groundwater system and Sadler et al. (1992) described the Greater Death Valley groundwater system both using deuterium calibrated mixing models; and Ahola and Sagar (1992) developed regional and subregional models to assess the effects of increased recharge, neotectonism, and dike or sill emplacement on YM. Because Wittmeyer and Turner (1995) presented comprehensive reviews of pre-1995 regional-scale models for the Death Valley flow system and the site-scale models for the YM flow system, no further discussion of these models is provided here. Instead, this chapter will focus on post-1995 regional- and site-scale modeling efforts.

Several post-1995 hydrogeological studies of the YM and Death Valley systems have been reported: D'Agnese et al. (1997), who presented a hydrogeologic evaluation and numerical simulation of the Death Valley regional groundwater flow system based on geographic information systems and geoscientific information systems; DOE (1997), which presented a regional groundwater flow model designed to predict the large-scale movement of tritium from underground tests areas on the NTS; Cohen et al. (1997), who developed a sub-site-scale model for YM that examined the impact of fault properties on flow geometry; and Czarnecki et al. (1997), who developed a subscale numerical groundwater model based in part on the regional model of D'Agnese (1997).

All models appear to indicate a general south to southeastern flow from the YMR to the Amargosa Desert. This general flow direction has been supported by the DOE expert elicitation panel, who concluded, based on available data, that the dominant flow direction is from YM southeast to Fortymile Wash and then south to the Amargosa Valley (Geomatrix Consultant, Inc., and TRW Environmental Safety System, Inc. 1998). The expert elicitation panel also concluded that the primary flow paths more than likely would remain within the lower volcanic aquifer near YM and enter the alluvium farther south. Due to the higher heads in the carbonate aquifer relative to those of the volcanic units, the expert elicitation panel suggested it is unlikely that radionuclides will migrate into this unit.

3.1 D'AGNESE et al. (1997)

A regional groundwater flow model for Death Valley was developed by the USGS. The objective of this study was to estimate aquifer parameters, provide boundary conditions for a site-scale model, and estimate the water budget. D'Agnese et al. (1997) modeled an area of 100,000 km² using MODFLOWP, a

three-dimensional (3D) finite difference mathematical model with nonlinear least squares regression for parameter estimation. This regional model is based on a 3D hydrologic framework model developed by using a digital elevation model, geologic maps and cross sections, and lithologic well logs. This framework model provides a description of the geometry, composition, and hydraulic properties of the materials that control the regional groundwater flow system. Most surface recharge to the regional flow system is provided by high-altitude areas. Discharge from the groundwater system occurs through evapotranspiration, spring discharge, and well pumping. The water budget for the regional system suggests that the outflow exceeds inflow. This can be attributed to the poor definition of both the pumping and evapotranspiration discharge volumes. It was also surmised that the Death Valley system is not a closed system, and an interbasinal transfer of water in the deeper Paleozoic system was necessary to achieve a water balance during the modeling.

The regional system was simulated using a finite difference grid consisting of 163 rows, 153 columns, and 3 layers. The grid cells were oriented north-south and of uniform size $1,500 \times 1,500$ m. The three layers occur at the following intervals below the water table: 0–500 m, 500–1,250 m, and 1,250–2,750 m. This simulation exercise supported the analyses of interactions between the relatively shallow local and subregional flow paths and the deeper regional flow paths controlled by the carbonate aquifer. A series of conceptual models was evaluated to test the validity of various interpretations about the flow system. The conceptual model providing the best fit during the calibration exercise was retained as the final optimized model. This final model, although a reasonable representation of the hydrological system, showed evidence of model errors in the form of water balance errors ($117,100 \text{ m}^3/\text{d}$) and high head residuals (up to 300 m).

The boundaries selected for the flow system were modified from Waddell et al. (1984), Harrill et al. (1988), and Bedinger et al. (1989). Most system boundaries were no-flow boundaries. Inflows to the model, however, may occur from Pahranaagat Valley, Sand Springs Valley, Railroad Valley, Stone Cabin Valley, Ralston Valley, Fish Lake and Eureka Valley, Saline Valley, Panamint Valley, Pilot Knob Valley, and Soda Lake Valley. The flux estimate for Pahranaagat Valley is $20,000 \text{ m}^3/\text{d}$ (Winograd and Friedman, 1972). No estimate is available for other inflows. The Death Valley regional system was modified and divided into three major subregional flow systems: Northern Death Valley, Central Death Valley, and Southern Death Valley. There is evidence of groundwater flow across the subregional boundaries. In each subregion, the flow paths are grouped in groundwater basins containing various groundwater sections. The Northern Death Valley subregion was divided in four dominant groundwater sections: Lida-Stonewall, Sarcobatus Flats, Grapevine Canyon, and Oriental Wash. The Central Death Valley subregion was divided in three groundwater basins: Pahute Mesa-Oasis Valley, Ash Meadows, and Alkali Flat-Furnace Creek. The Southern Death Valley subregion was divided into four groundwater sections: Pahrump Valley, Shoshone-Tecopa, California Valley, and Ibex Hills.

Numerous conceptual models were evaluated to test the validity of various flow system interpretations. These conceptual models were tested for (i) location and type of flow system boundaries, (ii) extent and location of recharge areas, and (iii) configuration of the hydrogeologic framework model. Changes to the conceptual model that produced significant improvements in the flow model results were incorporated in the final model. Model calibration was performed by estimating a total of 18 parameters. During calibration, however, some of these parameters were lumped together. After calibration, the model was evaluated by comparing the measured and estimated values with simulated values. The comparison included (i) hydraulic heads and spring flows; (ii) hydraulic conductivities, vertical anisotropy, and infiltration; and (iii) water budgets. The residuals for hydraulic heads showed a good match with the observed heads in small hydraulic gradient areas and a relatively good match in large hydraulic gradient areas. The simulated spring flows were generally lower than the observed flows. Evaluation of estimated

parameters indicated that the values of hydraulic conductivity, vertical anisotropy, and recharge rates are all within the expected ranges. The model simulation also indicated a reasonable water budget for the system. The model errors, which were attributed to the coarse vertical discretization of the system, are displayed in the nonnormal distribution of weighted residuals of hydraulic head and spring flow. It was surmised that a further calibration of the system will provide improved accuracy in model prediction. This model is currently being refined to incorporate a higher vertical resolution with 16 hydrostratigraphic layers and a better representation of structural features.

3.2 U.S. DEPARTMENT OF ENERGY (1997)

The NTS regional groundwater flow system covers approximately 26,200 km² of the Death Valley groundwater flow system. The area is bounded by Death Valley, the Funeral Mountains, Bullfrog Hills, and the Cactus Range on the west; by the Kawich, Reveille, and Quinn Canyon ranges on the north; by the Timpahute, Pahrnatagat, and Sheep ranges on the east; and by parts of the Spring Mountains, the Resting Spring Range, and the Greenwater Range on the south. The digital geologic model includes the distribution and thicknesses of the aquifers and confining units and their depths relative to the hydrologic basement. The geologic model also incorporates major structural features that control groundwater flow and migration of contaminants within the regional flow system.

Hydraulic parameters included hydraulic conductivity and effective porosity. Data on hydraulic parameters were gathered and evaluated to help describe the hydrogeologic framework of the groundwater flow system. Within the NTS region, groundwater occurs within alluvial, volcanic, and carbonate geologic units.

The direction of groundwater flow is influenced locally in areas where structural and geologic conditions have controlled the distribution and thickness of the Lower Carbonate Aquifer. In some areas of the regional flow system, groundwater encounters geologic features, such as structural highs of the Lower Clastic Confining Unit, that promote an upward flow component. Upward flow components may cause discharge at the ground surface in the forms of wet playas or springs where groundwater may be lost by evapotranspiration. Such discharge characteristics are observed at Oasis Valley, Penoyer Valley, and Amargosa Flat. There is groundwater flow between basins in the form of subsurface inflow and outflow. Ultimately, however, the groundwater is lost from the flow system at other surface discharge areas located downgradient.

Recharge and discharge occur either through the surface or through the external boundary of the groundwater flow system, although a little groundwater crosses the boundary by underflow along much of its length. Areas where underflow occurs include the boundaries with Pahrnatagat Valley, Sarcobatus Flat, Pahrump Valley, and the Amargosa Valley near Eagle Mountain. An inflow in the range of 5,400–60,800 m³/d occurs from the Pahrnatagat Valley to the Desert Valley. The inflow from Pahrump Valley is in the range of 5–7,600 m³/d. The outflow in the range of 850–3,400 m³/d occurs at Eagle Mountain. Areas of recharge were assumed mostly to correspond to precipitation areas. The greatest recharge occurs along the Spring Mountains in the south, followed by the Sheep Range to the east. Other mountain ranges in the NTS groundwater flow system are areas of moderate recharge. Lower-elevation areas, such as Death Valley, are not recharge areas. In some areas such as Fortymile Canyon, however, recharge is known to occur. Thus, some of the recharge assumed to occur at higher elevations was redistributed to lower elevations in the vicinity of the NTS. Eight surface-discharge areas were identified. The estimated total amount of

groundwater recharge to the NTS regional groundwater flow system ranges 1.83×10^5 to 3.60×10^5 m³/yr. The estimated total amount of groundwater discharge ranges 1.36×10^5 to 3.06×10^5 m³/yr.

The groundwater flow model was designed to provide a basis for predicting the movement of contaminants from the underground test areas on a regional scale. It was also intended to provide a means for evaluating the range of uncertainty in these predictions due to uncertainties associated with the geologic and hydrologic data. In the future, the model will be used also to provide boundary conditions for more detailed models of the underground testing areas consistent with the regional groundwater budget. The geologic model domain was subdivided into a grid consisting of 68 columns by 76 rows and 20 layers. The large number of layers was used to simulate accurately the geologic complexity of the thinner, yet hydrologically significant, hydrostratigraphic units, primarily located in Pahute Mesa and Yucca Flat and to increase numerical accuracy. The grid was constructed to simulate more accurately the hydrology of the areas of concern, which include the underground testing areas and downgradient regions. It was also aligned with the direction of the mean fracture orientation in the primary testing areas of concern, Pahute Mesa and Yucca Flat. Boundary conditions were specified to match communication of the NTS groundwater flow system with neighboring flow systems.

The calibrated model, based on the MODFLOW simulator, provided a good match overall and accurately reproduced several prominent features of the hydrology of the NTS and surrounding areas. The high gradient between Emigrant Valley and Yucca Flat (along the northern border of Yucca Flat) was present, as was the high gradient north of the YM area. The higher water levels in the western part of Yucca Flat above the Upper Clastic Confining Unit were present also. A moderately low gradient across Timber Mountain, increasing to the north beneath Pahute Mesa, was well simulated. The low gradient throughout most of the area underlain by the Lower Carbonate Aquifer was present, as was the moderate gradient between the Penoyer and Desert Valleys. The high gradient between the Amargosa Desert and Death Valley was reproduced, along with recharge mounds in the Spring Mountains, the Sheep Range, the Kawich Range, and the Grant Range. The eastward gradient present in the western part of the Pahute Mesa testing area was not well-represented in the model, and there was a slight gradient reversal in this area.

Flowpaths from selected nuclear test locations were identified with the particle-tracking code. Particle-starting locations were chosen (415 of them) so that each test area (Pahute Mesa, Rainier Mesa, Yucca Flat, Climax Stock, Shoshone Mountain, and Frenchman Flat) was represented. Results indicated that particles originating in the Pahute Mesa testing area discharge in Oasis Valley. Particles originating in the eastern testing areas (Yucca Flat and Frenchman Flat) discharge in Death Valley or the Amargosa Desert, but not at Ash Meadows. Particles originating in other testing areas did not leave the NTS during the simulated time period of 200 yr.

Extensive sensitivity analyses were performed to evaluate the impact of parameter uncertainty on water level and boundary flux responses and on particle-tracking results. Two types of sensitivity analyses were performed. The first type involved changing basic assumptions of the model such as using different versions of the regional geologic model and different recharge distributions. The second type was a systematic variation of the hydraulic-conductivity parameters. The sensitivity analysis of the different geologic models confirmed that a barrier to flow in the area of Calico Hills westward to Bare Mountain was needed to match estimated discharge rates at Oasis Valley together with observed gradients in that area. This barrier was based on structural relationships associated with the Belted Range Thrust together with alteration of volcanic rocks in the Claim Canyon caldera segment and northern YM. This interpretation was consistent with geologic and hydrologic information in the area. Changes in the geologic model near Penoyer Valley resulted in an improvement in the hydrologic model; however, a lower hydraulic conductivity for the Lower

Carbonate Aquifer in the northeastern part of the model was needed to match water levels and estimated fluxes. The sensitivity analysis performed on 116 hydraulic conductivity values showed that the effect on water levels and boundary fluxes was small. The response in specific areas was dependent on local conditions such as the geometric relationships between hydrogeologic units and the 3D extent of the hydrogeologic unit.

The groundwater pathlines from underground test locations at or below the water table were calculated from the flow model. Three of the fastest pathlines, closest to the southern edge of a test area, were selected for transport simulations to represent each of the main underground test areas. This transport model was used to calculate the tritium concentration in groundwater downgradient from the underground test locations and to assess the impacts of flow and transport parameter uncertainties on the predicted downgradient tritium concentrations. The transport model required the following parameters to be defined at each node: initial tritium concentrations, radioactive decay coefficient, specific discharge, dispersivity, effective and matrix porosities, and effective diffusion coefficient. The maximum flow path length was 99 km, based on preliminary scoping simulations.

The transport modeling results suggested that (i) the regional geology is the dominant factor controlling the horizontal and vertical position of flow paths, (ii) matrix diffusion is an important mechanism governing the migration of tritium in fractured carbonate and volcanic rocks, (iii) source-term concentration uncertainty is most important near the nuclear test locations and decreases in importance as the travel distance increases, and (iv) the recharge coefficient which accounts for the total groundwater flux uncertainty, is as important as matrix diffusion at downgradient locations.

3.3 CZARNECKI et al. (1997)

The site-scale flow model developed by the USGS (Czarnecki et al., 1997) covers an area of approximately 1,350 km² (30 × 45 km) over a saturated thickness of about 1,500 m. The specific objectives of this models were to (i) estimate groundwater flow velocity from the repository to the accessible environment, (ii) characterize the complex 3D behavior of flow through heterogeneous media, and (iii) identify the potential role of faults in groundwater flow. The results from this modeling exercise were not directly used in the Total System Performance Assessment-Viability Assessment for various reasons listed in Civilian Radioactive Waste Management System, Management & Operating Contractor report (1998).

The model grid was based on a digital hydrogeologic framework model. The framework model was sampled at a spatial resolution of 1,500 × 1,500 m with variable thicknesses to maintain hydrostratigraphic continuity. The fully 3D model domain was discretized in a tetrahedral finite element mesh consisting of 9,279 nodes and 51,461 elements with 16 layers representing different hydrogeologic units. The faults were not incorporated as distinct hydrologic features. Only the top two layers were selected from the regional model. Flow simulations were performed using the Finite Element Heat Mass Nuclear groundwater flow and transport code. Calibration of the flow model was performed with the Parameter ESTimation (PEST) code. The constant head boundary condition was derived from the regional model of D'Agnesse et al. (1997). The results from the flow simulations were presented by Czarnecki et al. (1997). Results from the transport simulations were presented by Zvoloski et al. (1997).

The site-scale model assumed constant head boundaries along all lateral boundaries. The constant head values for the boundaries were obtained from the regional flow model. No flow was assumed from the

lower boundary of the model; the upper boundary of the model, (i.e., water table) received recharge along the upper reaches of Fortymile Wash. The large hydraulic gradient was assumed part of the SZ and represented by a low-permeability fault. The moderate hydraulic gradient was also represented by a low-permeability fault. Recharge due to infiltration was not applied in this model and no pumpage was assumed in the model domain.

Model calibration was performed by an automated parameter estimation method to match the observed hydraulic heads at 94 locations by varying selected permeability values. During the calibration, it was indicated that the available data are not sufficient to estimate all parameters individually. The hydrogeologic units with similar permeability values were lumped to minimize the number of estimated parameters. For various combinations of fixed and estimated parameters, 40 PEST parameter estimation runs were completed.

The simulation results suggest that the model predictions were most accurate when the low-permeability barriers were added corresponding to the SCF and the downgradient side of the large hydraulic gradient and also when the permeability of the upper volcanic confining unit was isolated and optimized. The hydraulic head residuals in the optimized model occurred between -5 and +5 m. A greater disparity was noticed in flux across the model boundaries when compared with the regional-scale model. Comparison between the site-scale and the regional-scale models showed almost twice the amount discharging from the southern end of the site model and substantially different amounts for the north and east sides. It was suggested that at the northeast corner of the site model the major flux difference between the two models was due to recharge from the north. The groundwater is diverted eastward and discharges from the model domain, in part, because of the interaction of constant head boundaries and the low-permeability east-west barrier representing the large hydraulic gradient.

Although the preliminary results provide a good fit with the measured values, the permeability values used to attain this good fit show a large range for each aquifer; especially for the middle volcanic aquifer, where the value used to fit the model is three orders of magnitude smaller than the values reported for the C-Hole complex. The authors attributed this either to model error or to a local, large-permeability zone (near the C-Hole complex) not represented in the model.

The major assumptions of the site-scale flow model include (i) bulk permeability is uniform within each hydrogeologic unit, (ii) the flow system is at steady state, (iii) the SZ can be represented as a single continuum, and (iv) the groundwater flow system is isothermal at 44 °C. The model may be used to provide a large-scale description of the hydrogeologic framework of the SZ flow system and to provide groundwater velocity estimates for preliminary transport simulations. In addition, the calibrated model may be used to provide initial permeability estimates for the 16 hydrogeologic units and recharge from the Fortymile Wash. The authors listed the following limitations due to inadequate calibration for the model: (i) simulations are restricted to fully saturated conditions from the water table and below; (ii) the model does not account for the variations in temperature observed within the flow system; (iii) it is likely the flow model is nonunique; (iv) the large hydraulic gradient is poorly understood and greatly affects model calibration, simulated permeability values, and flux; (v) flux into the site model domain is poorly defined; (vi) limited hydraulic test data exist for constraining permeability values used in the model; and (vii) definition of the hydrogeologic units within the model is limited by the sampling interval. The authors also suggested numerous ways to improve the model: (i) conducting sensitivity studies to identify the parameter that has the greatest effect on the sum of the squared residuals for head; (ii) refining the hydrogeological framework model; (iii) using higher resolution sampling; (iv) using faults explicitly as surfaces; (v) using additional

hydrochemical, flux, and isotopic data for model calibration; and (vi) including vertical flux through the bottom of the model.

3.4 COHEN et al. (1997)

Cohen et al. (1997) developed a sub-site-scale SZ model that covers an area of approximately 150 km² (10 × 15 km). The 3D integrated finite difference numerical model is based on the TOUGH2 numerical simulator. The model consists of 23 layers and is discretized into approximately 50,000 gridblocks. The model represents the SZ from the water table down to the confining unit separating the volcanic and carbonate aquifers. The geologic units were divided to account for vertical variation of rock properties as evidenced by welding characteristics and vertical flow surveys in the borehole. The model preserved the thickness, orientation, dip, and lateral continuity of the strata as defined in the 3D geologic model of YM, ISM 2.0 (Clayton et al., 1997). Displacement by faults was also explicitly considered, however, the faults were assumed vertical. The faults are discretized such that the fault zone properties can either be explicitly assigned or faults can be displacement-only features.

The steady-state model has been calibrated to measured hydraulic heads and to long-term pumping tests at the C-Hole pumping complex. The calibrated heads were within approximately 1 m of measured heads. The initial C-Hole pumping test results match steady-state results, however, the grid size was not large enough to study transient effects. The model results suggested that the flow geometry is greatly influenced by fault properties, whether faults are high-permeability fault zones, low-permeability fault zones, or fault with displacement only. The majority of flow is contained within the Bullfrog Tuff and follows the down dip direction. When the Bullfrog unit is offset by faults, vertical flow is induced and flow can return to the water table from below. On the basis of the model results, it was recommended that an additional multihole complex be designed to characterize groundwater flow parameters in the southern portion of the model area.

3.5 LEHMAN AND BROWN (1995, 1996)

The State of Nevada has funded a number of studies to independently assess the hydrogeology of the YMR. Although the effort is active on several fronts, state consultants have proposed conceptual models of the hydrogeology of the region that differ from those currently proposed by the DOE and the NRC. One such model, which has received considerable attention, is the model of Lehman and Brown (1995, 1996).

In this report, the authors proposed two conceptual models of nonisothermal groundwater flow in the YMR. One model focused on the possible structural dependence of flow, while the second model is similar in approach to the model currently under consideration by the DOE (1997). The aim of the modeling exercise was to explain the observed distributions of hydraulic head and temperature seen in the tuff aquifers.

Conceptual Model 1: (structurally controlled groundwater flow model)

This model, reported in Lehman and Brown (1995, 1996), assumes that groundwater flow in the tuff aquifers in the YMR is structurally controlled, with faults and fractures exerting strong influences on recharge, velocity fields, and flow geometry. The basis for this model lies in independent determination of the water table topography and temperature distributions within the SZ.

Lehman and Brown (1995) asserted that observed differences in response to recharge events between wells located east and west of YM indicate that groundwater flow on both sides of the mountain is not

coupled. This indicates that faults in the YMR may be either impermeable or at least semipermeable to flow. Water table responses following the Landers, California, the Big Bear, California, and the Little Skull Mountain, Nevada, earthquakes (June 28–29, 1992) were also used by Lehman and Brown (1995) to support fault-controlled flow. Plots of DOE waterlevel data following these earthquakes showed four distinct responses: (i) an upward temporary spike, (ii) a rapid upward change with an apparent long-term stabilization at a higher level, (iii) a downward temporary spike, and (iv) a rapid downward change with an apparent long-term stabilization at a lower level. Plots of the observation well locations relative to the positions of mapped faults in the region led Lehman and Brown (1995) to conclude that wells (in the YMR) that experienced increases in water table elevation were associated with shear zones and compressive stress environments that led to reductions in pore volumes, whereas downward trending waterlevels were associated with normal faults and tensile stress environments that led to increases in pore volumes. No discussions were presented by Lehman and Brown (1995, 1996) to explain the other observed hydraulic head patterns following the earthquakes.

Additional arguments in support of flow along and across faults in the YMR were presented by Lehman and Brown (1995) based on observed temperature differences at the site. The authors argued that the cold water plume, which coincides with the GDF, represents cold water moving from the high hydraulic gradient north of YM via the Drill Hole Wash or other nearby faults, across the SCF and into the GDF. The authors argued this scenario presents a plausible mechanism by which flow can cross the SCF. Lehman and Brown (1996) also proposed that flow across Solitario Canyon may occur south of the repository location along an unmapped fault, inferred from a revised contour map of the water table elevation in the region.

In the proposed conceptual model, the authors argued that, in addition to faults, fractures within the repository block form significant flow conduits, the hydraulic conductivities of which exceed the matrix hydraulic conductivity by five to six orders of magnitude. Based on the tectonic history of the region, the authors propose that fracture and other hydraulic properties should show spatial and temporal variations. They argued that, in compressive strain environments, reductions in pore volumes could lead to increases in water levels, whereas, in tensile strain environments, increases in effective pore volumes could lead to lowering water levels. Further, changes in the local stress field may result in changes in fracture aperture, which could introduce anisotropic behavior.

Lehman and Brown (1996) tested this conceptual model using a coupled groundwater flow and heat transport two-dimensional (2D) numerical model based on the VTOUGH simulator. The authors reported that, with regard to groundwater, the simulation results showed good agreement between the simulated and observed hydraulic heads, with high flux rates observed through fracture and fault zones. With regard to heat flow, the authors reported that the 2D concept could not achieve the temperatures indicated in the measured data along the SCF and along the Paintbrush fault. The authors argued that, although the anomalies do not appear in the model predictions, they can be explained or modeled by including upward vertical flow from the carbonates or by fixing temperature boundary conditions.

Estimated groundwater velocities were also examined in two areas of interest, the GDF and a fault free zone further east. For this conceptual model, the groundwater velocities are southward in the GDF and equate to 1,466 m/d while east of the fault zone lower velocities on the order of 181.7 m/yr are estimated.

Conceptual Model 2: (equivalent porous medium groundwater flow model)

The second conceptual model proposed by Lehman and Associates is an equivalent continuum model, which assumes that fault and fracture zones do not control groundwater flow pathways. Groundwater

in this model is assumed to flow across the steep hydraulic gradient area toward the hydraulic lows south and east of YM. Calibration was achieved by adjusting the hydraulic conductivities of the model until a match was achieved between the simulated and observed hydraulic gradients.

The authors concluded that, while the potentiometric surface can be matched, the temperature field of this model does not match the basic shape of the observed temperature distribution. In particular, the characteristic spike of cold water along the trace of the GDF is missing. Groundwater velocities in the vicinity of the GDF were estimated on the order of 278.5 m/yr, while those further east of the repository were estimated approximately 444 m/yr. The groundwater velocities in the region of the GDF calculated using this model are approximately 3 orders of magnitude less than those estimated using the previous model.

3.6 SUMMARY OF GROUNDWATER MODELS APPLIED IN THE SOUTHERN NEVADA REGION

The previous sections demonstrate that differences in conceptual approach and assumptions adopted in the various models designed to simulate groundwater flow in the YM region and beyond can significantly impact estimated groundwater velocities and fluxes. The structurally controlled model of Lehman and Brown differs conceptually from other models for the YM site. As demonstrated by Lehman and Brown (1995; 1996), groundwater velocities derived from conceptually different groundwater flow models designed for the YM site can range over several orders of magnitude. Such differences can significantly impact decision making processes related to siting a nuclear waste repository at YM. Among the factors contributing to the differing conceptual models are (i) poor understanding of the geology within the YM region and beyond, (ii) limited data for characterizing the hydraulic properties of hydrostratigraphic units, (iii) limited data characterizing the interactions between hydrostratigraphic units, and (iv) limited hydrogeologic data on geologic structures which have the potential to impact groundwater flow at the YM site- and regional-scales. Improvements in these areas are essential if decision makers are to have confidence in the data generated by numerical models.

4 REVIEW OF INFORMATION PERTINENT TO THE ASSESSMENT OF STRUCTURAL CONTROLS ON GROUNDWATER FLOW IN THE VICINITY OF YUCCA MOUNTAIN

The conceptual models presented in the previous chapter demonstrate the differing views regarding SZ flow within the YMR. These views range from classic continuum approaches to dual permeability models, in which fractures and faults dominate the groundwater flow system. The fundamental differences in these approaches are reflected by Lehman and Brown (1995) who stated, "...it is our opinion that the primary groundwater pathways are not adequately understood nor represented in the DOE Total System Performance Assessment analyses as shown to date. The groundwater velocities and volumetric flux rates as estimated by the DOE have been greatly underestimated for the YM." These differences are further illustrated by the fact that travel times to receptor locations differ by several orders of magnitude depending on the approach chosen. From a regulatory perspective, these conceptual differences need to be investigated with respect to their effect on dose estimates.

In an attempt to understand better the hydrogeology of the YMR, and in particular the impact of geologic structures on groundwater flow, the CNWRA and the NRC adopted a multidisciplinary approach that focuses on available hydrogeologic, geophysical, hydrochemical, and structural geology information. This chapter presents a summary of the review findings.

4.1 INFLUENCE OF STRESS ON GROUNDWATER FLOW IN THE YUCCA MOUNTAIN REGION

Interpretation of aquifer borehole tests (Geldon, 1997; Ferrill et al., 1999b) and groundwater temperature data (Bredehoeft, 1997) indicates that hydraulic conductivities at YM may be anisotropic and inhomogeneous. The apparent anisotropy and inhomogeneity are because of preferentially oriented fracture planes that develop and then respond to *in situ* stress. Analysis of faults at YM shows average strike is approximately north-south (azimuth $\sim 005^\circ$). Slip and dilation-tendency analyses indicate that faults and fractures ideally oriented for slip in the current stress field at YM strike $025\text{--}030^\circ$ and dip moderately to steeply, whereas faults and fractures ideally oriented for dilation strike $025\text{--}030^\circ$ and are vertical. Faults with favorable orientations for slip or dilation present potential flow pathways. These constraints support the interpretation of anisotropic transmissivity at YM, with the direction of maximum transmissivity in the azimuth range of approximately 005° (based on the dominant fault trend) to 030° (based on slip- and dilation-tendency constraints). Reinterpretation of pump-test data from the C-Holes at YM by CNWRA staff (see section 4.2) indicates a subregional anisotropic transmissivity with a maximum principal transmissivity direction of approximately 030° . This is consistent with the development of anisotropic transmissivity controlled by faults and fractures and the *in situ* stress field.

The permeability of the Miocene welded tuffs, the underlying Paleozoic and Precambrian carbonate, the clastic strata at YM, and the surrounding area is primarily controlled by faults and fractures (Waddell, 1982; Winograd and Thordarson, 1975; Fridrich et al., 1994). Based on alignment of springs (e.g., Ash Meadows fault: Winograd and Thordarson, 1975; Dudley and Larson, 1976) and elevated groundwater temperatures along faults (e.g., Midway Valley and SCF: Sass et al., 1995), studies have concluded that faults control groundwater flow locally and are paths for upward flow in the SZ at YM (Fridrich et al., 1994; Bredehoeft, 1997). The importance of faults and fractures on the hydrology of the YMR is further

emphasized by the anomalous concentrations of ^{36}Cl produced as a result of atmospheric nuclear testing in the Pacific Ocean in the 1950's, recently identified in samples from the ESF. This anomalous concentration has been interpreted as indicating rapid downward transport of meteoric water along faults and fractures in the UZ (Levy et al., 1997; Fabryka-Martin et al., 1998).

Anisotropic permeability in fractured rock aquifers results from the abundance and distribution of faults and fractures associated with damage zones (e.g., breccia). Although it is known that faulted and fractured aquifers commonly have anisotropic transmissivity (National Research Council, 1996), maps depicting regional-scale groundwater flow usually assume flow parallel to the gradient of the potentiometric surface. This is true only if the transmissive properties of the aquifer are isotropic or if the major or minor semiaxis of the transmissivity tensor is parallel everywhere to the potentiometric gradient.

Recent studies, including one example from YM, show that faults favorably oriented for slip in the current stress field tend to be the most active groundwater flow pathways (Barton et al., 1995; Finkbeiner et al., 1997). This observation has been explained by increased small-scale fracturing and faulting in the vicinity of faults on the verge of shear failure (Barton et al., 1995). The ability to recognize such faults allows the loci of increased fracturing to be identified.

A secondary but measurable influence on permeability is the effect of contemporary stress on reducing apertures of existing faults and fractures (Carlsson and Olsson, 1979; Barton et al., 1995; Finkbeiner et al., 1997). Faults and fractures perpendicular to the maximum principal stress are preferentially closed, thereby reducing permeability perpendicular to the maximum principal stress. Permeability perpendicular to the minimum principal compressive stress direction is relatively enhanced because lower resolved normal stress results in less fracture aperture reduction (e.g., Carlsson and Olsson, 1979).

In the following, a model is developed to assess the impact of the regional stress on existing faults and fracture systems at YM together with its subsequent influence on groundwater flow in the SZ beneath YM. The model is then tested using data from a long-term aquifer pumping test at YM. Finally, the possible implications of the model results on the proposed HLW repository at YM are discussed.

4.1.1 Slip Tendency and Dilation Tendency

The approach employed to analyze stress involves calculating resolved stresses on fault and fracture surfaces to analyze likelihood for slip or dilation in crustal stress fields. The resulting slip-tendency data and dilation-tendency data are displayed by color coding 3D models or trace maps of the fault and fracture array.

4.1.1.1 Slip Tendency

Slip-tendency analyses are applicable to planar discontinuities like faults, extension fractures, or layering (Morris et al., 1996; Ferrill et al., 1998). For faults and fractures, slip is likely to occur on a surface when the resolved shear stress, τ , on that surface equals or exceeds the frictional resistance to sliding. Frictional resistance is proportional to normal stress, σ_n , acting across that surface (Jaeger and Cook, 1979). The slip tendency, T_s , of a surface is the ratio of shear stress to normal stress acting on that surface (Morris et al., 1996).

$$T_s = \frac{\tau}{\sigma_n} \quad (4-1)$$

As such, T_s depends solely on the stress field (stress tensor) and surface orientation. Whether or not a surface slips depends on its cohesive strength, if any, and the coefficient of static friction, μ . The coefficient of static friction, μ , is the value of T_s that causes slip on a cohesionless surface and is often referred to as the fault strength in earthquake focal mechanism analysis (Harmsen, 1994). Under most crustal conditions, faults with $T_s = 0.6$ are ideally oriented for slip (Byerlee, 1978). Slip-tendency analysis provides a way to assess which faults are near the ideal orientation for slip and are the most likely to be associated with zones of increased fracture density and enhanced fracture permeability.

4.1.1.2 Dilation Tendency

Dilation of fractures is largely controlled by the resolved normal stress, which is a function of lithostatic and tectonic stresses and fluid pressure. The normal stress exerted on a fracture depends on the magnitude and direction of the principal stresses relative to the fracture plane. The ability of a fracture to dilate and transmit fluid is directly related to its aperture, which in turn is a function of the effective normal stress acting on it. The magnitude of the normal stress can be computed for surfaces of all orientations within a known or hypothesized stress field. This normal stress can be normalized by comparison with differential stress. The resulting dilation tendency (T_d) for a surface is then defined as

$$T_d = \left(\frac{\sigma_1 - \sigma_n}{\sigma_1 - \sigma_3} \right) \quad (4-2)$$

where σ_1 is the maximum principal compressive stress, and σ_3 is the minimum principal compressive stress.

4.1.2 Bulk Transmissivity Anisotropy

A population of steep, aligned, relatively permeable faults and fractures cutting a less permeable rock mass will tend to orient the maximum directional transmissivity parallel to the structural grain. In the case of unequal horizontal stresses acting on a population of steep faults and fractures, those with strikes *parallel* to the maximum horizontal compressive stress tend to open. Those with strikes *perpendicular* to the maximum horizontal stress tend to close. Similarly, some faults in an anisotropic stress field will be more ideally oriented for slip and others for locking. Thus, even if fault and fracture orientation distribution is isotropic, transmissivity in the maximum horizontal stress direction can be enhanced, producing transmissivity anisotropy.

Because fault and fracture populations commonly exhibit preferred orientations and *in situ* horizontal stresses are commonly unequal, both are likely to occur together in nature and lead to anisotropic transmissivity. For example, in cases where σ_3 is horizontal, vertical faults and fractures perpendicular to σ_3 have the highest dilation tendency and are likely to be more conductive than those in other orientations (figure 4-1a). Faults and shear fractures are sensitive to the σ_1 direction and commonly form two conjugate sets intersecting at an acute angle ($\sim 60^\circ$) centered on σ_1 (figures 4-1b and 4-1c). In normal fault regimes where σ_1 is vertical, two sets of opposite-dipping conjugate normal faults commonly develop (figure 4-1b). In strike-slip fault regimes where σ_1 is horizontal, two sets of vertical conjugate strike-slip faults commonly develop (figure 4-1c). In areas where σ_3 is horizontal, fault and fracture preferred orientations together with slip and dilation tendencies all promote development of a net bulk transmissivity anisotropy with a maximum horizontal transmissivity perpendicular to σ_3 (figure 4-1d). The interaction of aquifer transmissivity with fault and fractures can be field tested by aquifer pumping tests. As shown in the next sections, the results can be used to determine the full transmissivity tensor and compare the orientation of the principal components of

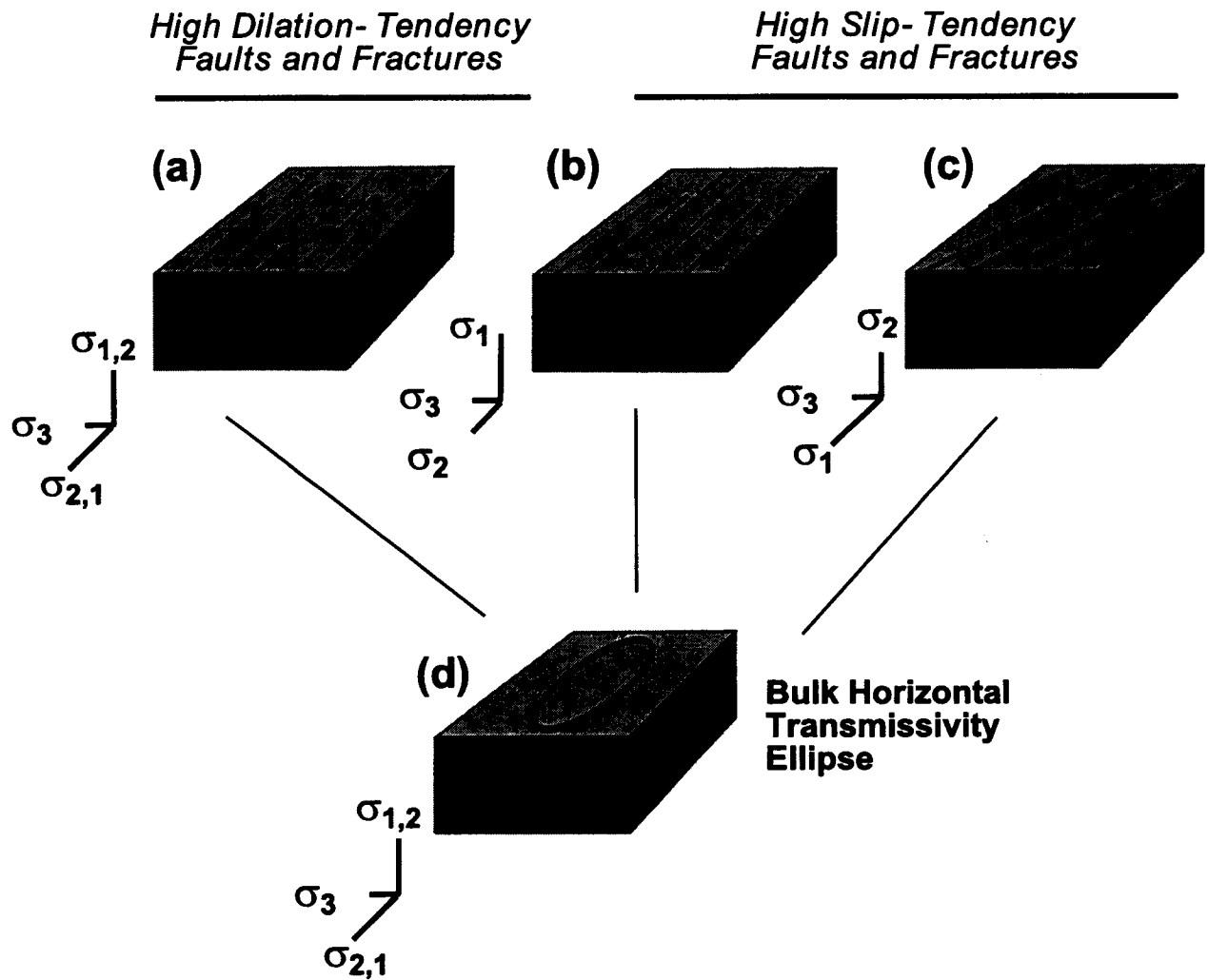


Figure 4-1. Conceptual illustration of effects of faults with high slip tendency or high dilation tendency on development of anisotropic permeability in areas like the Yucca Mountain region [the minimum principal compressive stress (σ_3) is horizontal]

this tensor with the maximum and minimum *in situ* horizontal stress orientations and the distribution of faults and fractures.

4.1.2.1 Prediction of Anisotropic Transmissivity at Yucca Mountain

The pattern of faults and fractures in the YMR (figure 4-2) resulted from deformation in a regional stress field that evolved from east-west extension before 10 Ma to west-northwest-east-southeast extension after 10 Ma (Zoback et al., 1981) and from thermoelastic contraction during cooling of the ash-flow tuffs (Sweetkind and Williams-Stroud, 1996). The result is a dominant population of north-south to northeast-southwest-trending normal faults, a subordinate population of northwest-southeast-trending strike-slip faults, and a group of minor connecting faults and curved fault tips (Day et al., 1998b; Ferrill et al., 1999a). Fault growth by connection of overlapping fault segments produced irregular fault traces with cusps at fault intersections. Although faults at YM are related to several deformational episodes, some faults are unlikely to slip because of unfavorable orientations relative to the contemporary stress state.

YM lies within the western Basin and Range in a region characterized by both normal and strike-slip earthquakes. The regional occurrence of both normal and strike-slip earthquakes indicates that the maximum (σ_1) and intermediate (σ_2) principal compressive stresses have similar magnitudes (Zoback, 1992; Zoback et al., 1992). The least principal compressive stress (σ_3) is approximately horizontal and trends west-northwest-east to southeast. Therefore, σ_3 is the odd axis of Krantz (1988) and has the most direct control on the pattern of fault-slip tendency. Stock et al. (1985) estimate the following effective principal stresses (corrected for fluid pressure) at a depth of 1 km: $\sigma_1 = \text{vertical} = 21 \text{ MPa}$, $\sigma_2 = \text{N}25^\circ\text{--}30^\circ\text{E} = 17 \text{ MPa}$, and $\sigma_3 = \text{N}60^\circ\text{--}65^\circ\text{W} = 11 \text{ MPa}$ for the region.

4.1.3 Analyses of Slip And Dilation Tendencies of Yucca Mountain Faults

4.1.3.1 Slip-Tendency Analysis of Yucca Mountain Faults

Slip-tendency analysis of YM faults used the relative stress values of Stock et al. (1985) given previously, a 3D fault model for western YM, and the faults mapped by Simonds et al. (1995, figure 4-3a). Maximum slip tendencies are experienced by faults that strike parallel to the north-northeast-trending maximum horizontal stress (025–030°; 028° in figure 4-3) and dip 55°. Slip tendencies are also near maximum (>0.3) for moderately to steeply dipping (40–65°), north-south to northeast-southwest (000–055°) striking faults. Faults at 1 km depth have moderate slip tendencies relative to typical failure conditions. In contrast, at depths of earthquake rupture initiation (e.g., 5–15 km), stresses resolved on similarly oriented faults produce near-failure slip tendencies (Morris et al., 1996). As described by Harmsen (1994), the pattern of slipped faults in the Little Skull Mountain (figure 1) earthquake sequence is dominated by dip-slip on southeast-dipping normal faults and right-lateral strike-slip on vertical north-south trending faults. This is the pattern is predicted by slip-tendency analysis of the YM stress field and supports simultaneous activity of strike-slip and normal faults in this area (Morris et al., 1996).

Examination of Simonds et al. (1995) reveals that nearly all faults with known or suspected late Quaternary displacement are in orientations of high slip tendency (figure 4-3a). Some noteworthy examples are the Northern and Southern Windy Wash, Fatigue Wash, Solitario Canyon, Iron Ridge, and Stagecoach Road faults (figure 8a). In contrast, the northwest-southeast trending Pagany Wash, Sever Wash, and Yucca Wash faults are in low slip-tendency orientations (figure 4-3a) and lack evidence of late Quaternary slip (Simonds et al., 1995).

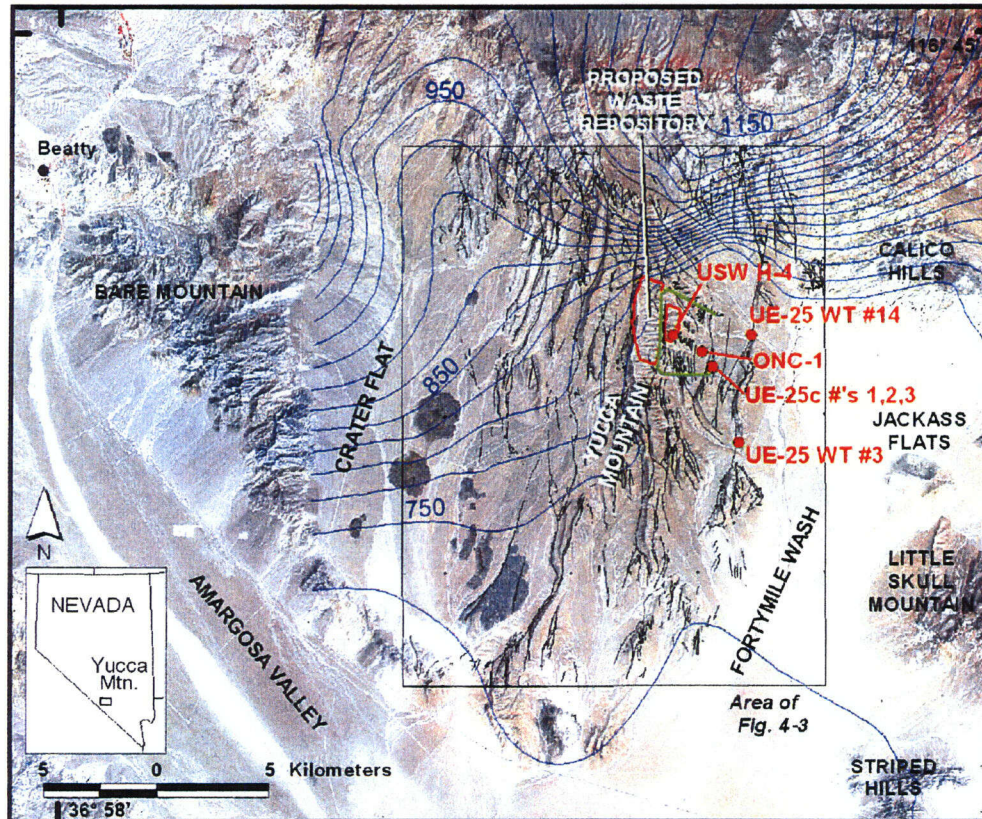


Figure 4-2. Thematic mapper scene with potential repository location, wells (red dots), faults (irregular black lines), and water table contours (blue lines). Water table contours are from Czarnecki et al. (1997). Green lines show the path of the exploratory studies facility.

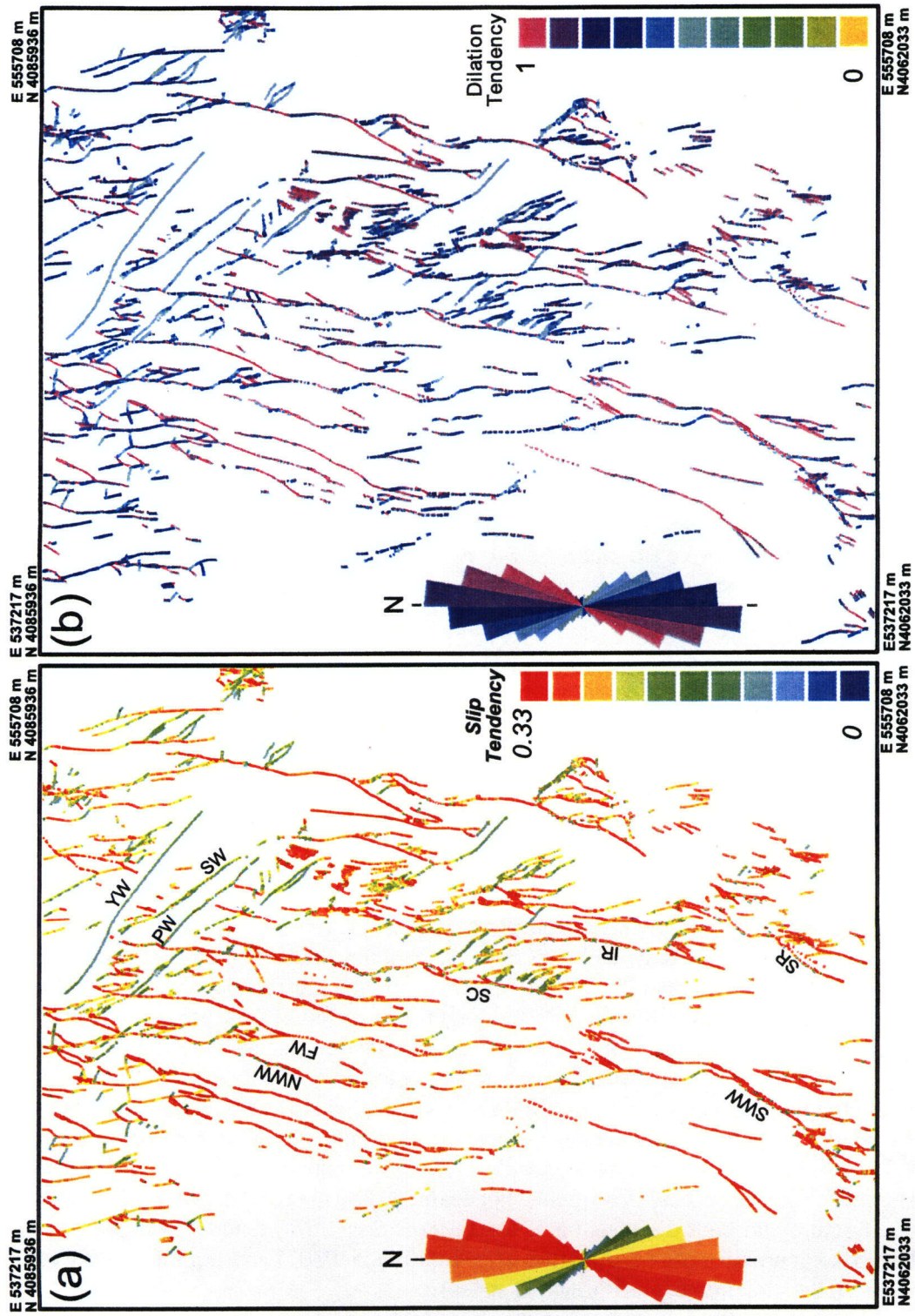


Figure 4-3. (a) Slip-tendency map of Yucca Mountain faults mapped by Simonds et al. (1995). Inset rose diagram shows cumulative fault length in 10° strike azimuth bins. Map and rose diagram are colored according to slip tendency as shown by slip-tendency plot and color bar in figure 3b. Named faults discussed in text are labeled on map according to these abbreviations: NWW = Northern Windy Wash, SWW = Southern Windy Wash, FW = Fatigue Wash, SC = Solitario Canyon, IR = Iron Ridge, SR = Stagecoach Road, PW = Pagany Wash, SW = Sever Wash, and YW = Yucca Wash. (b) Dilation-tendency map of Yucca Mountain faults.

4.1.3.2 Dilation-tendency Analysis of Yucca Mountain Faults

Dilation-tendency analysis of faults and associated fractures at YM (e.g., figure 4-3b) assumed the same relative stresses and mapped faults used for slip-tendency analysis. The results show that maximum dilation tendencies are experienced by vertical faults and fractures that strike parallel to the maximum horizontal stress (025–030°; 028° in figure 4-3). Faults trending $028 \pm 35^\circ$ and dipping 65–90° have dilation tendencies of 0.8 or greater in the present stress field. Dilation-tendency analysis of faults at YM illustrates an abundance of steeply dipping north-northeast trending faults that have high dilation tendency.

4.1.3.3 Summary of Implications of Stress in Evaluating Structural Controls on Groundwater Flow in the Yucca Mountain Region

Faults with favorable orientations for slip or dilation present potential flow pathways. Although only large map-scale faults were explicitly considered in the analysis described above, the processes that alter permeability of large faults and fracture systems also apply to abundant smaller scale fractures and faults like those seen in outcrops, boreholes, and the ESF (cf., Sweetkind and Williams-Stroud, 1996), resulting in an effective hydraulic continuum at the site scale. The dominant trend of faults at YM is approximately north-south (005°; see rose diagrams in figure 4-3). The dominant fault population strike, maximum slip tendencies, and maximum dilation tendencies indicate the possibility of anisotropic transmissivity, with the direction of maximum transmissivity in the azimuth range between 005° (based on dominant fault trend) and 030° (based on slip- and dilation-tendency constraints). As will be shown in the next section, the presence of anisotropic transmissivity is supported by long-term pumping test data from the C-Holes. The anisotropic transmissivity estimated at YM has a maximum principal direction of approximately 030°, consistent with the hypothesis that anisotropy is controlled by faults and fractures in the present-day *in situ* stress field. As will be discussed in section 4.6, such aquifer anisotropy has the potential to alter groundwater flow paths to more southward directions. Modeled flow directions are sensitive to the degree of anisotropy, and the direction of maximum principal transmissivity.

4.2 TRANSMISSIVITY ANISOTROPY IN THE YUCCA MOUNTAIN REGION

4.2.1 Estimating Anisotropic Transmissivity at Yucca Mountain

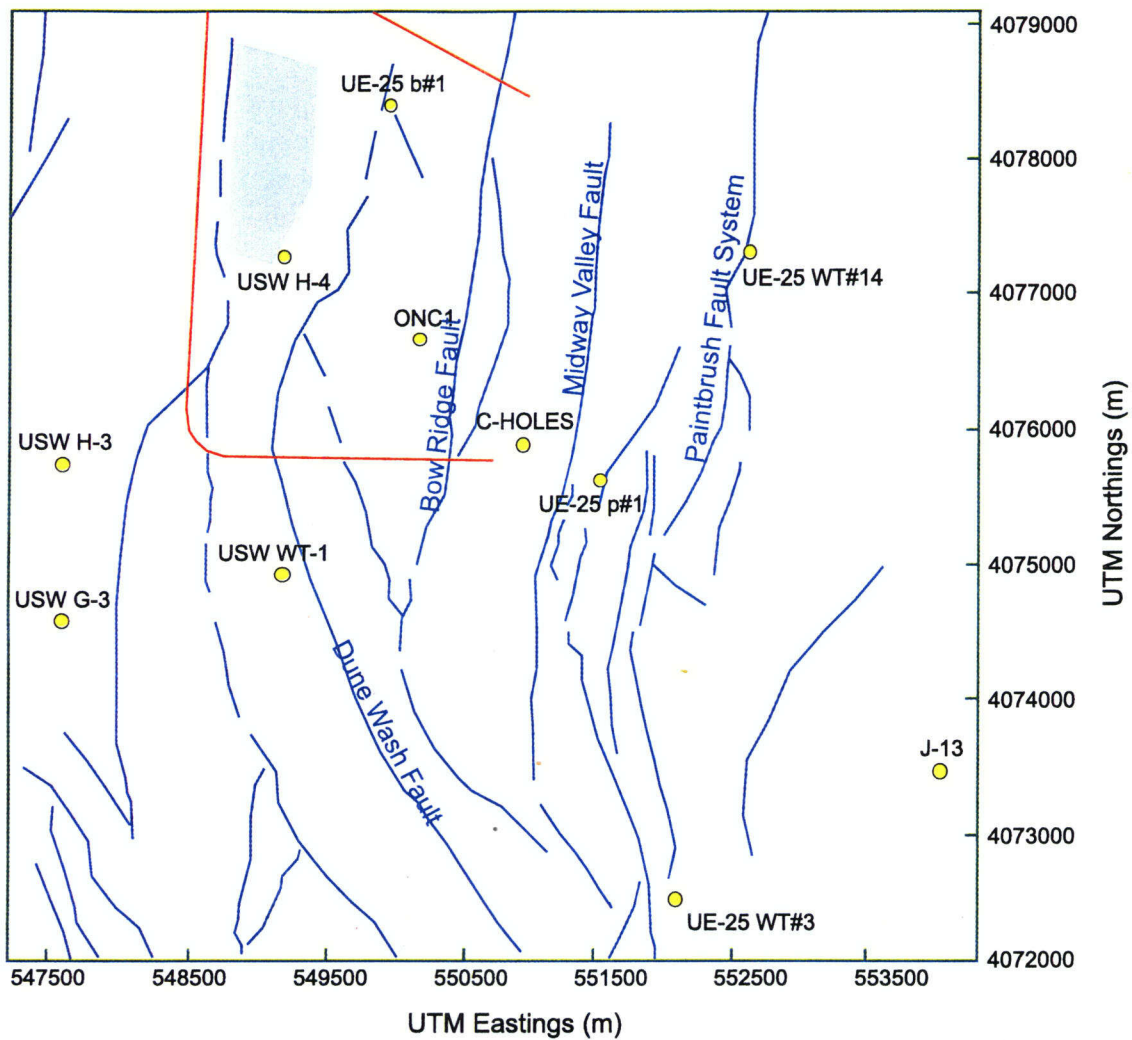
Anisotropy occurs in a porous medium when the permeability is different for flow in different directions. Horizontal anisotropy can occur for a number of reasons, the most likely of which, in a fractured rock aquifer, is the presence of vertical fractures. If vertical fractures exhibit a preferential orientation or if regional stresses result in the opening of fractures that strike along the direction of maximum stress, then movement of fluid may be enhanced in that direction. Although minimal fracture data exist for the saturated tuff aquifer beneath YM, large-scale 3D properties of fracture permeability fields in the UZ have been estimated based on fracture frequencies and orientations in the ESF (Sonnenthal et al., 1997). For most units, strong vertical and north-south permeabilities are predicted due to the predominance of north-south striking, near-vertical fractures. These anisotropy predictions exclude the effects of directional variability in fracture aperture that may be caused by regional or local stress fields. For example, Ferrill et al. (1999b) explain that, due to regional stresses, fracture and fault dilations (and, hence, transmissivities) tend to be highest for fractures and faults that strike approximately north-northeast (azimuth 025–030°) and dip moderately to steeply (i.e., perpendicular to the direction of least principal stress).

Data collected during a long-term aquifer pumping test, conducted at the C-Holes Complex on the eastern flank of YM from May 1996 to March 1997, provide a means for assessing horizontal anisotropy on the intrafault-block scale in the tuff aquifer. The C-Holes Complex consists of three wells (UE-25 c#1, UE-25 c#2, and UE-25 c#3) that approximately form a right angle with sides of 100 m and 30 m. During this aquifer test, well UE-25 c#3 was pumped at a rate of 9.5 L/s. Water levels in four distant observation wells (USW H-4, ONC-1, UE-25 wt#3, and UE-25 wt#14) were monitored at 15-min intervals. The locations of these observation wells, shown in figure 4-4, range in distance from 0.84 to 3.5 km from the pumped well. Locally, wells UE-25 c#1 and UE-25 c#2 were also monitored; however, data from these wells are not used in this analysis because (i) over the small scale of observation at the C-Hole Complex, pump test results are likely dominated by discrete features; (ii) the production interval in the pumped well included only a fraction of the aquifer thickness, resulting in 3D flow not accounted for in the analytical method used; and (iii) results may have been influenced by water recirculation from a simultaneously conducted tracer test.

Horizontal anisotropy was evaluated using the method of Papadopoulos (1965) for homogenous, anisotropic confined aquifers of infinite areal extent. To apply this method, at least three observation wells must be used to determine (i) the angle (θ) of the observation wells relative to the pumped well; (ii) the bulk aquifer transmissivity, which should be similar for all observation wells if the assumption of homogeneity is valid; and (iii) the directional hydraulic diffusivity for each well. It is important to distinguish between directional transmissivity [$T(\theta)$], a vector quantity, and the bulk aquifer transmissivity (T_e), which is a scalar quantity equal to the geometric mean of the minimum and maximum directional transmissivities. Directional hydraulic diffusivity [$D(\theta)$] is defined as the directional transmissivity [$T(\theta)$] divided by the dimensionless bulk aquifer storage coefficient (S). Although the primary interest is in $T(\theta)$, neither it nor S can be estimated separately from $D(\theta)$ until both the ratio of maximum to minimum $D(\theta)$ and the direction of maximum $D(\theta)$ are known. These important aquifer characteristics can be determined by fitting an ellipse to a polar plot of the square-root of $D(\theta)$ if estimates are available from at least three observation wells (Papadopoulos, 1965).

Pumping test data were first filtered using a two-step data correction that accounts for the influence on water levels exerted by both direct borehole coupling to atmosphere pressure changes and the delayed atmospheric pressure signal that arrives through the overlying geologic formation. Estimates of T_e and S were obtained for each observation well using the solution of Theis (1935). Note that, in this interpretation, it is assumed that S is constant throughout the aquifer (i.e., a homogenous aquifer), and thus differences in $D(\theta)$ between observation wells are attributed to $T(\theta)$. The value of $D(\theta)$ for each well was taken to be the quantity T_e/S . Table 4-1 lists the well azimuth (the direction from the pumped well with respect to north) and the estimated values of T_e and $D(\theta)$ for each observation well. Note that the T_e estimates obtained from this analysis are broadly consistent with, but less variable than, the aquifer transmissivities reported by Geldon et al. (1997).

Analysis of aquifer anisotropy begins with a test of the assumption of a homogenous aquifer system. In a purely homogenous aquifer, the T_e estimated from each observation well should be the same. At the site scale and regional scale, it is clear that the assumption of homogeneity is not valid, as transmissivity estimates range from less than 10 m²/d to the north and west of YM to as high as 14,000 m²/d in well JF3 to the southeast. Transmissivity estimates are somewhat less variable, however, within the area monitored during the long-term pumping test at the C-Holes. From table 4-1, it can be seen that the T_e values for each well are quite similar for all wells except H-4. The estimate for H-4 may be affected by a fault system that lies between it and the pumped well. Geldon et al. (1997) and Geldon et al. (1998) suggested that a preferential flow path between the C-Holes and H-4 may exist along the postulated Antler Wash fault. For this reason, well H-4 is excluded from the analysis of horizontal anisotropy. Because the estimated values





 Experimental Studies Facility
 Repository footprint

Figure 4-4. Locations of wells and faults in the vicinity of Yucca Mountain; fault locations are from Frizzel and Shulters (1990)

of T_e for wells ONC1, wt#3, and wt#14 are similar, the assumption of a homogenous continuum is deemed valid, at least for the aquifer area between those wells and the pumped well. The geometric mean value of T_e for these wells is $1,300 \text{ m}^2/\text{d}$. This value is the assumed bulk aquifer transmissivity tensor used to calculate minimum to maximum values of $T(\theta)$.

A polar plot of $D(\theta)$ for the three wells is shown in figure 4-5. The ellipse shown in figure 4-5 provides a close match to the observation well data with the major semiaxis oriented at an azimuth of approximately 033° (N 33° E). Because of the uncertainty associated with aquifer pumping tests and the limitation of only the minimum number data points necessary to define an ellipse, the ratio of minimum to maximum directional transmissivity is poorly constrained. A maximum $T(\theta)$ of $2,900 \text{ m}^2/\text{d}$, oriented at 033° , a minimum $T(\theta)$ of $580 \text{ m}^2/\text{d}$, oriented at 123° , and a bulk S value of 0.003 are estimated from figure 4-5.

Table 4-1. Aquifer properties estimated from the 1996 long-term pumping test

Well ID	Azimuth, θ	Distance from pumped well	Bulk Aquifer Transmissivity, T_e	Square-Root of Hydraulic Diffusivity, $\sqrt{D(\theta)}$
USW H-4	310°	2,245 m	670 m ² /d	560 m d ^{-0.5}
ONC1	327°	843 m	1,340 m ² /d	416 m d ^{-0.5}
UE-25 wt#3	161°	3,526 m	1,230 m ² /d	506 m d ^{-0.5}
UE-25 wt#14	050°	2,249 m	1,330 m ² /d	820 m d ^{-0.5}

These aquifer parameter estimates are obtained from the orientation angle and the minimum and maximum values of $D(\theta)$ obtained from the fitted ellipse, and knowledge that $\sqrt{T(\theta)_{max} T(\theta)_{min}} = T_e$. In this case, $\sqrt{T(033^\circ) T(123^\circ)} = 1,300$ m²/d. Because of the considerable degree of uncertainty in the anisotropy ratio and direction obtained from this analysis, the degree of confidence in this horizontal anisotropy analysis should be regarded as low. This analysis does, however, indicate that a north-northeast orientation of horizontal anisotropy in the tuff aquifer near YM is certainly a reasonable conceptual model. It is also encouraging that the predicted 033° direction of maximum horizontal transmissivity is consistent with the maximum fault and fracture dilation tendency azimuth range of 025–030° predicted by Ferrill et al. (1999b).

4.2.1.1 Summary of Implications of Transmissivity Anisotropy in Evaluating Structural Controls on Groundwater Flow in the Yucca Mountain Region

Admittedly, the preceding anisotropy analysis uses a number of simplifying assumptions. For example, the structural heterogeneity, held to be so important a consideration throughout this report, is ignored. Additionally, the analysis is based on data from the minimum number of wells necessary to evaluate anisotropic conditions. Thus, as already mentioned, the estimated anisotropy ratio of minimum to maximum transmissivity is poorly constrained. Despite the current low confidence in the results of this anisotropy evaluation, the authors conclude from the analysis that the existence of an intra-fault-block, NNE-oriented, horizontal anisotropy in the tuff aquifer is a viable alternative conceptual model that should be considered by DOE investigators in their characterization of flow and transport in the vicinity of YM. This conclusion is supported by the fact that the estimated orientation of the principal horizontal anisotropy axes is consistent with predictions based on regional stress analyses.

Additional data from a May–June 1995 aquifer pumping test at the C-Holes have recently become available. During this test, well UE-25 c#3 was pumped at nearly twice the rate as in the May 1996–March 1997 test, and hourly water-level data were collected at 12 wells in the tuff aquifer, although for a shorter duration. Future plans call for an additional anisotropy analysis using these recently acquired data. The increased number of observation wells are expected to provide a much improved basis for evaluating the potential for preferential flow directions.

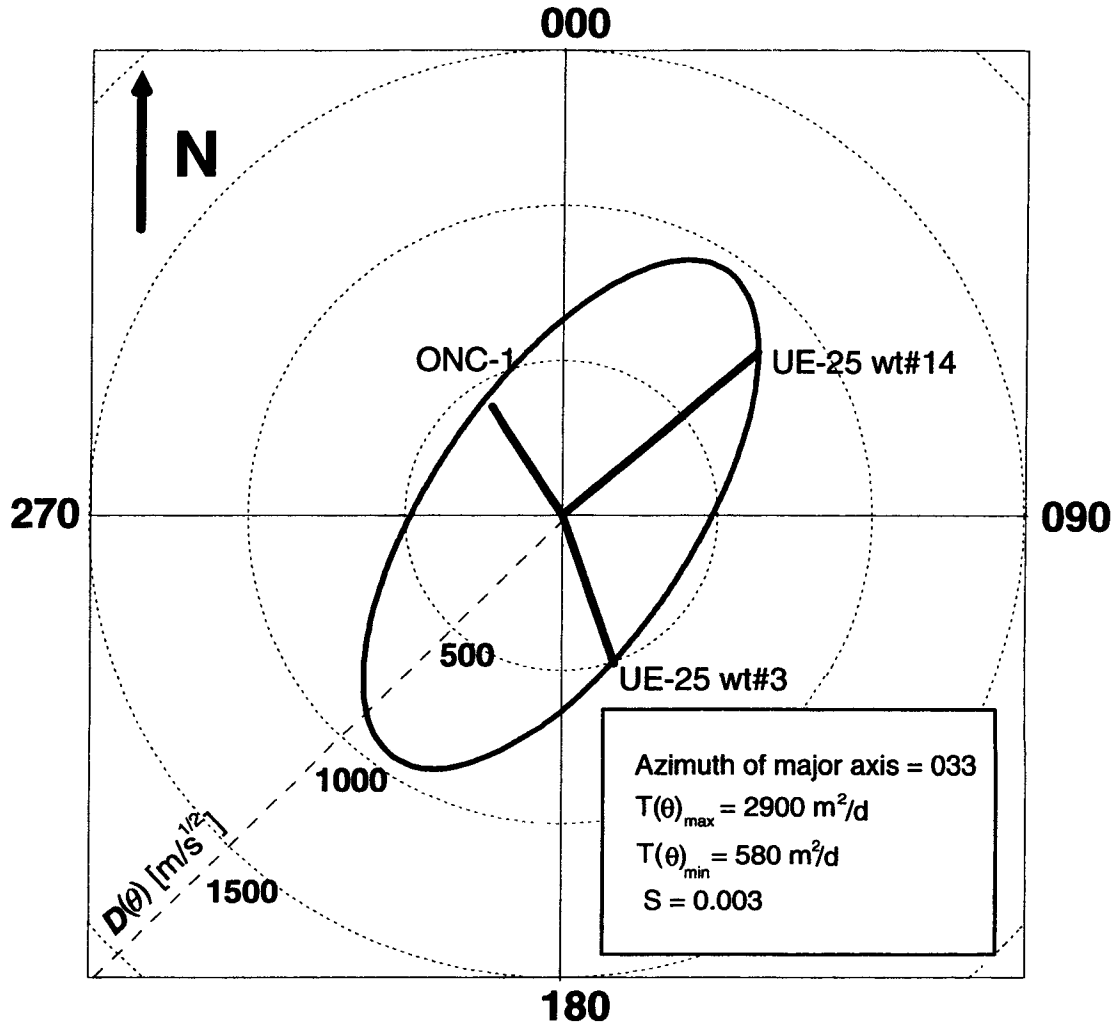


Figure 4-5. Directional hydraulic diffusivities estimated for observation wells based on the long-term pumping test conducted at the C-Holes beginning May 8, 1996. Raw pump test data were corrected for barometric effects prior to estimation of aquifer properties. The ellipse shown represents a maximum to minimum transmissivity ratio (T_x/T_y) of 5:1, with the maximum transmissivity axis (x') oriented at an azimuth of 033°.

4.3 INFLUENCE OF FAULT ZONES GROUNDWATER FLOW IN THE YUCCA MOUNTAIN REGION

4.3.1 Deformation Mechanism and Fault Zone Widths

Fault zone deformation in the upper crust produces a wide variety of textures that affect the overall permeability structure of the crust. Idealized faults consist of two textural zones (Sibson, 1977; Caine et al., 1996; Seront et al., 1998): a fault core and a damage zone. The fault core is a zone of high strain and accommodates most of the fault displacement by flow in gouge, cataclasite, breccia, or mylonite. The

surrounding damage zone is less deformed, accommodates less displacement, and may contain subsidiary structures such as veins, fractures, and minor faults (see figure 4-6a).

Deformation mechanisms govern the behavior of the fault zone with time and produce microstructures and microtextures that may inhibit or enhance permeability in the fault zones. At YM the protolith (volcanic tuff) has undergone brittle deformation by cataclasis at shallow levels in the upper crust. Changes in deformation mechanisms with time and deformation, the presence of fluids in the fault zone, mineral transformations, and syndeformational mineralization can affect the rheology of the fault zone and may cause it to widen or narrow with increasing displacement. If the products of the deformation produce fault rocks that inhibit continued cataclasis, then additional fault displacement will tend to fracture the protolith, and the fault zones will widen with time (i.e., strain harden). In contrast, if the fault rocks become progressively easier to deform, as faulting renews (strain localization and strain softening), then deformation will tend to localize within a narrow portion of the fault zone. The result will be an intensely deformed fault core with no increase in fault zone width.

Fault zone architecture and related structural permeability may strongly control fluid flow (e.g., Caine et al., 1996) into and out of the repository. Fault zones within which grain size has been reduced and secondary minerals have been precipitated generally contain core gouge zones with lower permeability and porosity than the adjacent protolith (e.g., Goddard and Evans, 1995; Caine et al., 1996). These faults would form barriers to flow. In contrast, faults with cores of coarse-grained breccias and wide damage zones containing numerous subsidiary structures may have greater permeability and porosity than the protolith, thereby enhancing fluid flow (e.g., Chester and Logan, 1986). These faults would potentially act as conduits to fluid flow depending on the degree of secondary mineralization. Faults commonly contain a less permeable core and a more permeable fault damage zone (Caine et al., 1996). Such fault zones have enhanced permeability parallel to the fault, but reduced permeability perpendicular to the fault.

Investigations of faulting at YM, especially studies of ESF faults, reveal that all these deformation processes and related features are present (Gray et al., 1998). Based on detailed field and microscope analyses of the ESF faults, four stylized fault types are recognized (figure 4-7). These four types essentially correspond to the four permeability fault zone structures defined in Caine et al. (1996). The discrete faults and shears (figure 4-7a) act like localized conduits. The minor faults with well-cemented fault zones (figure 4-7b) correspond to localized barriers. The GDF (figure 4-7c) corresponds to a distributed conduit. The SCF (figure 4-7d) corresponds to a combined conduit-barrier.

Of the faults exposed in the ESF, only the SCF has a well-developed fault foliated gouge. The orientation of the foliation is indicative of dip-slip displacement on the fault. To assess the mineralogy in the gouge, x-ray analyses were performed.¹ These included random powder-mount x-ray diffraction and oriented powder-mount x-ray diffraction runs. For the random powder mounts, the fraction of fault-rock material that passed through the 400 mesh sieve was placed inside a back-holding loader and inserted into the x-ray diffractometer. Some results peak at 14.42 angstroms, indicative of some clay minerals (figure 4-8a).

¹Gouge specimen SPC00543707 collected at Enhanced Characterization at the Repository Block Drift Station 25+85.1. Analyses were performed by Brad Jordan and Mary Beth Gray, Bucknell University, February 26, 1999.

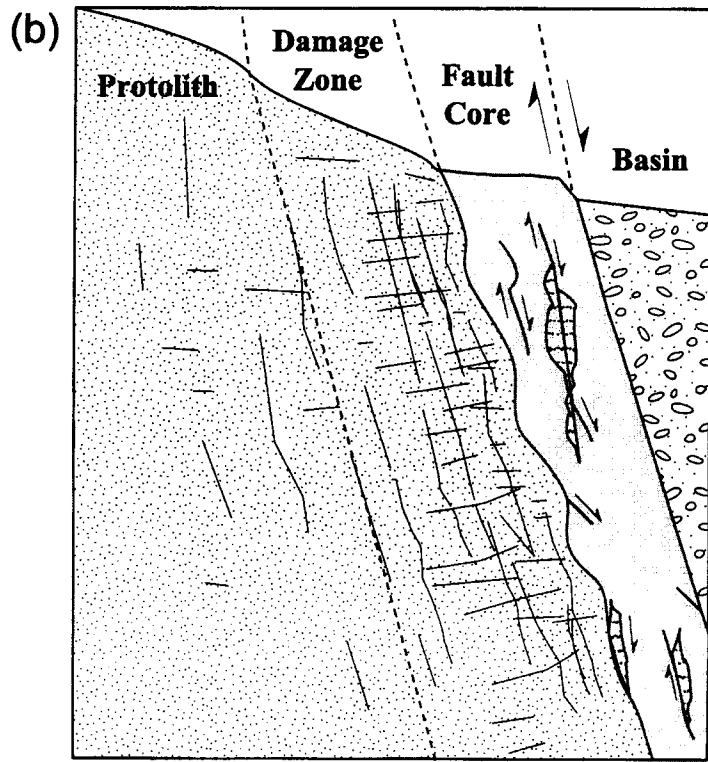
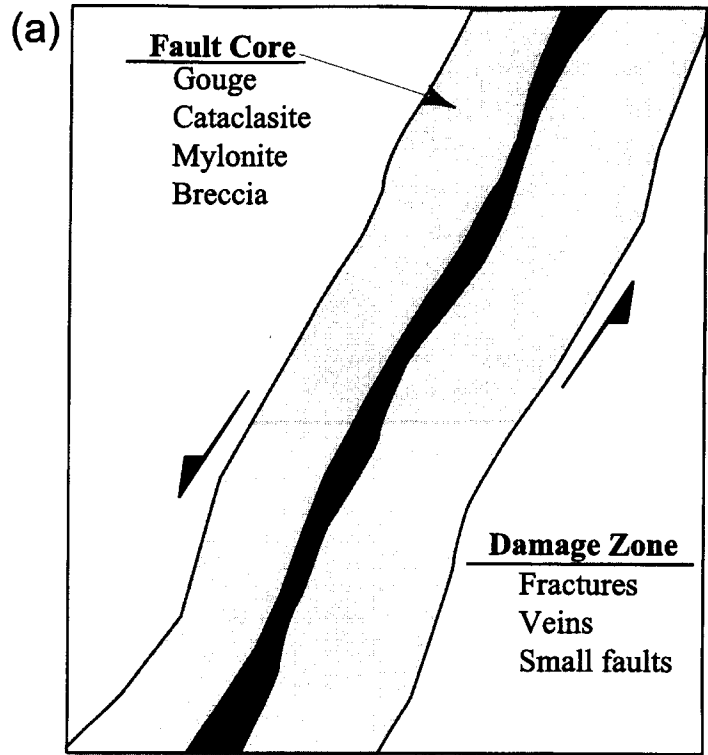


Figure 4-6. (a) Conceptual model of fault zone showing the fault core and surrounding damage zone; (b) diagram showing the fault zone of the Stillwater fault in Dixie Valley, Nevada (Seront et al., 1998)

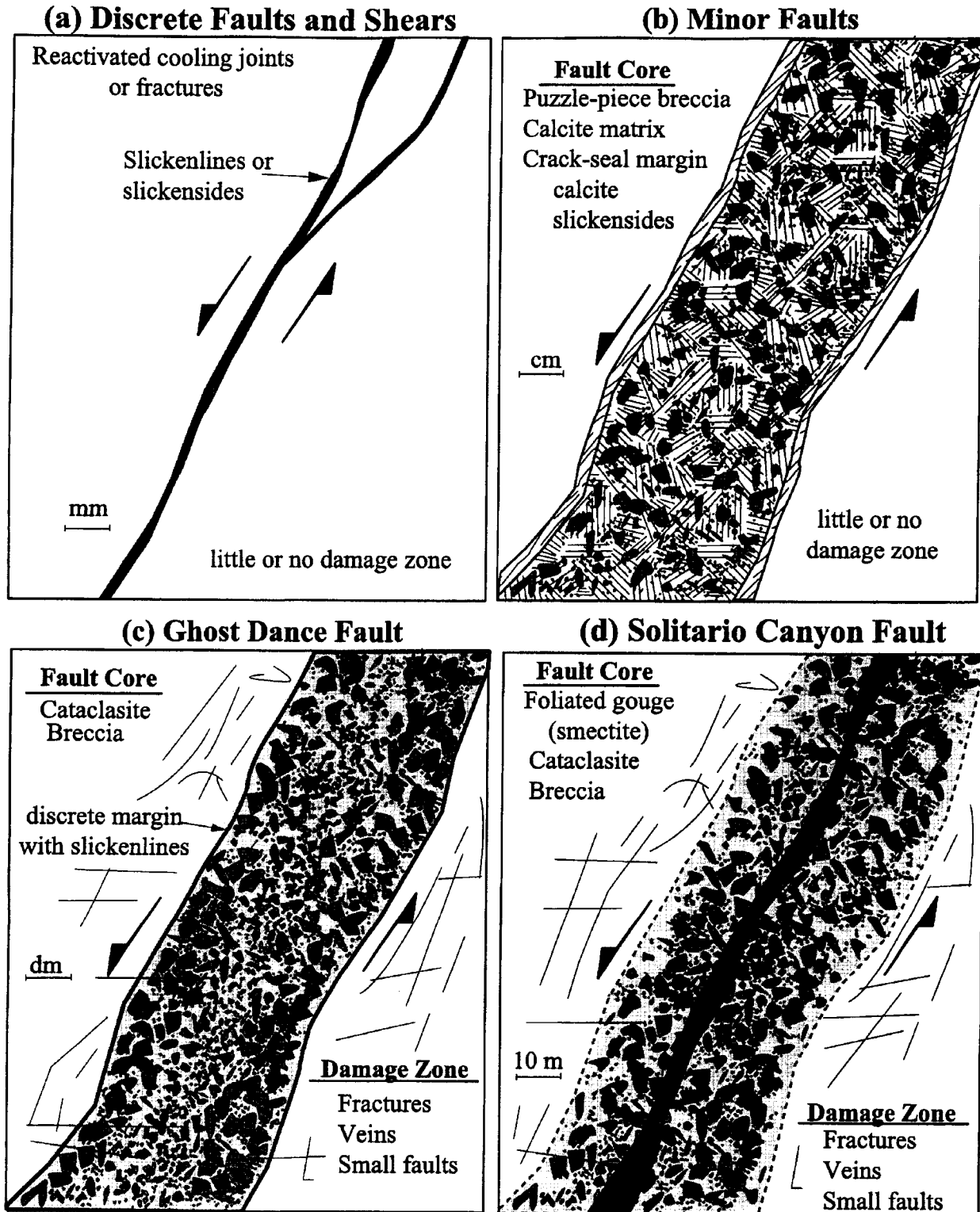


Figure 4-7. Types of fault zones observed from the Exploratory Studies Facility at Yucca Mountain (the four fault zones were identified from detailed field and laboratory studies of fault zone deformation)

Three oriented powder mounts were prepared from the fraction of fault-rock sample that did not pass through the 400 mesh sieve after further crushing. The mounts were prepared using the Millipore® Filter Transfer Method detailed in Moore and Reynolds (1989). The resulting x-ray diffraction pattern (figure 4-8b) shows a broad peak at 14.42 angstroms. One oriented powder was exposed to ethylene glycol vapors at 60 °C for 4 hr in a closed container and analyzed. The resulting x-ray diffraction pattern showed a peak at 16.6 angstroms (figure 4-8c). Comparison of the air dried and glycolated x-ray patterns (figure 4-8d) shows the shift in peaks characteristic of smectites (Starkey et al., 1984). This result is significant because smectites form effective barriers to flow. If much of the SCF zone contains a similar clay smear, then this fault would form a highly effective barrier to flow.

4.3.2 Crossing Faults

Extensional regions commonly develop two sets of steeply dipping normal faults with parallel strikes but opposite dips (Anderson, 1951), commonly referred to as conjugate normal faults. Intersecting and crossing conjugate normal faults are relatively common and range from micro- and meso-scale (e.g., Horsfield, 1980; Nicol et al., 1995; Watterson et al., 1998) to macro-scale features like those developed in many oil fields (Horsfield, 1980; Woods, 1988, 1992; Castagna, 1996). Crossing of conjugate normal faults produces a graben above a horst. Crossing faults play an important role in the development of permeability anisotropy in aquifers and reservoirs. At YM, faults and fractures represent the dominant permeability and potential fast pathways for groundwater infiltration, percolation, and flow in the fractured aquifers. Many of the surface traces collected in the vicinity of YM suggest crossing faults at depth. This is best exemplified by the intersection of the steeply-dipping to near-vertical GDF with the moderately west-dipping Bow Ridge Fault (BRF).

The effects of crossing conjugate normal fault networks on the bulk permeability of the host aquifer or reservoir rock is to essentially enhance permeability parallel to the line produced by their intersection. This occurs whether the crossing-fault networks consist of permeability-reducing or permeability-enhancing fault zones (figure 4-9). If the fault cores become barriers to flow, then flow will be restricted to within each of the resulting fault blocks (figure 4-9a). Those blocks are elongated parallel to the crossing fault intersection, and thus flow will parallel the crossing fault intersection. In contrast, if the fault zones develop enhanced permeability relative to the host rock, then flow will likely follow the fault zones or the crossing fault intersection (figure 4-9a).

4.3.3 Summary of Implications of Fault Zone Deformation in Evaluating Structural Controls on Groundwater Flow in the Yucca Mountain Region

Because brittle fault zones are lithologically heterogeneous and structurally anisotropic, they can act as either barriers and/or conduits that can impede or enhance groundwater flow in both the SZ or UZ. The manner in which fault zones affect groundwater flow depends in large part on how the rocks within the fault zone were deformed. In an idealized shallow fault, the fault zone is characterized by a fault core composed of gouge or cataclasite surrounded by a damage zone of highly fractured and brecciated wall rock. Permeability is reduced in the fault core and enhanced, at least initially, in the damage zone. In such faults, fluid flow would be heightened parallel to the fault zone, within the damage zone, and restricted along or across the core. The damage zone may have reduced secondary porosity and diminished permeability due to secondary mineralization.

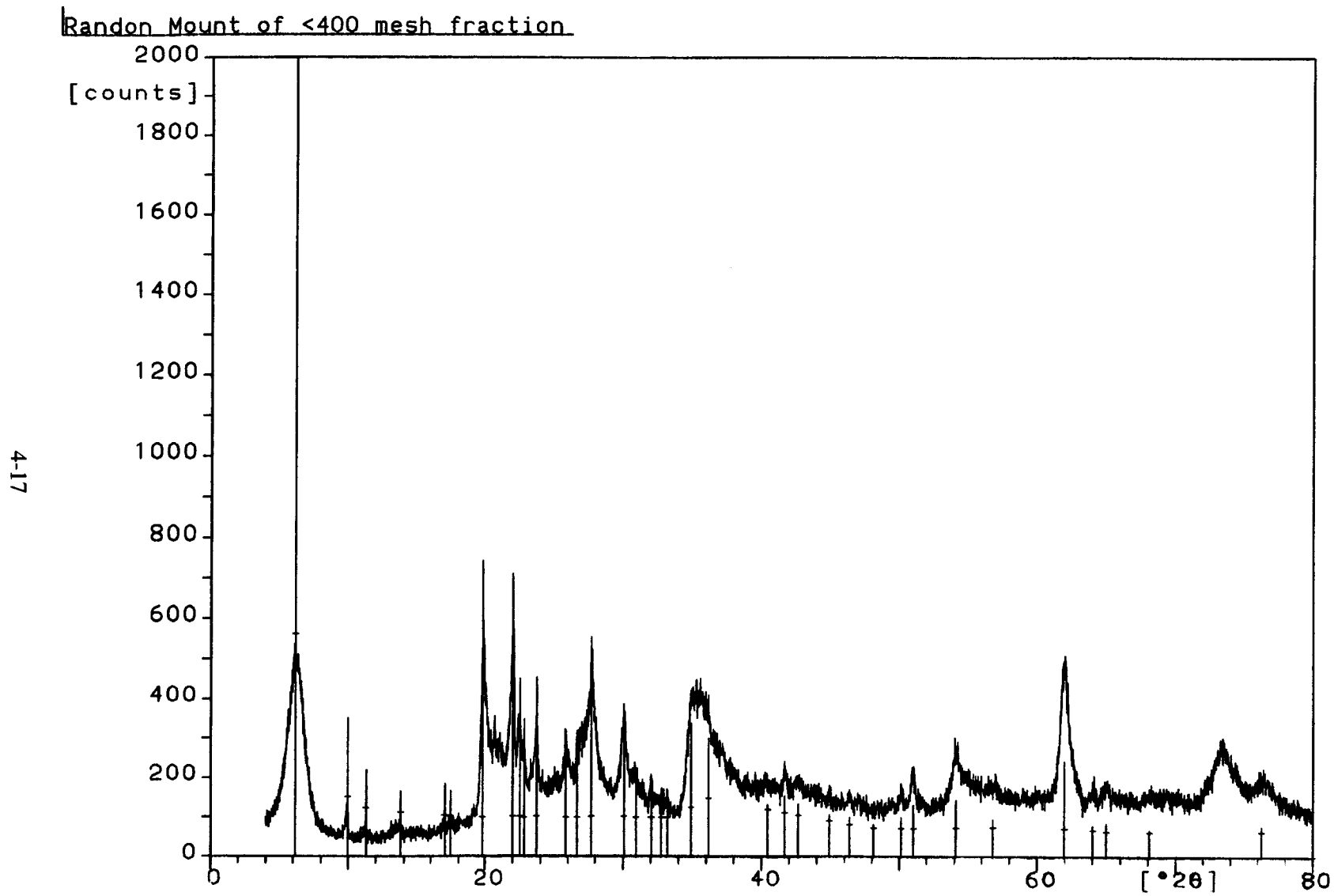


Figure 4-8a. X-ray results showing the clay mineralogy of the Solitario Canyon fault gouge (Randon mount of <400 mesh fraction)

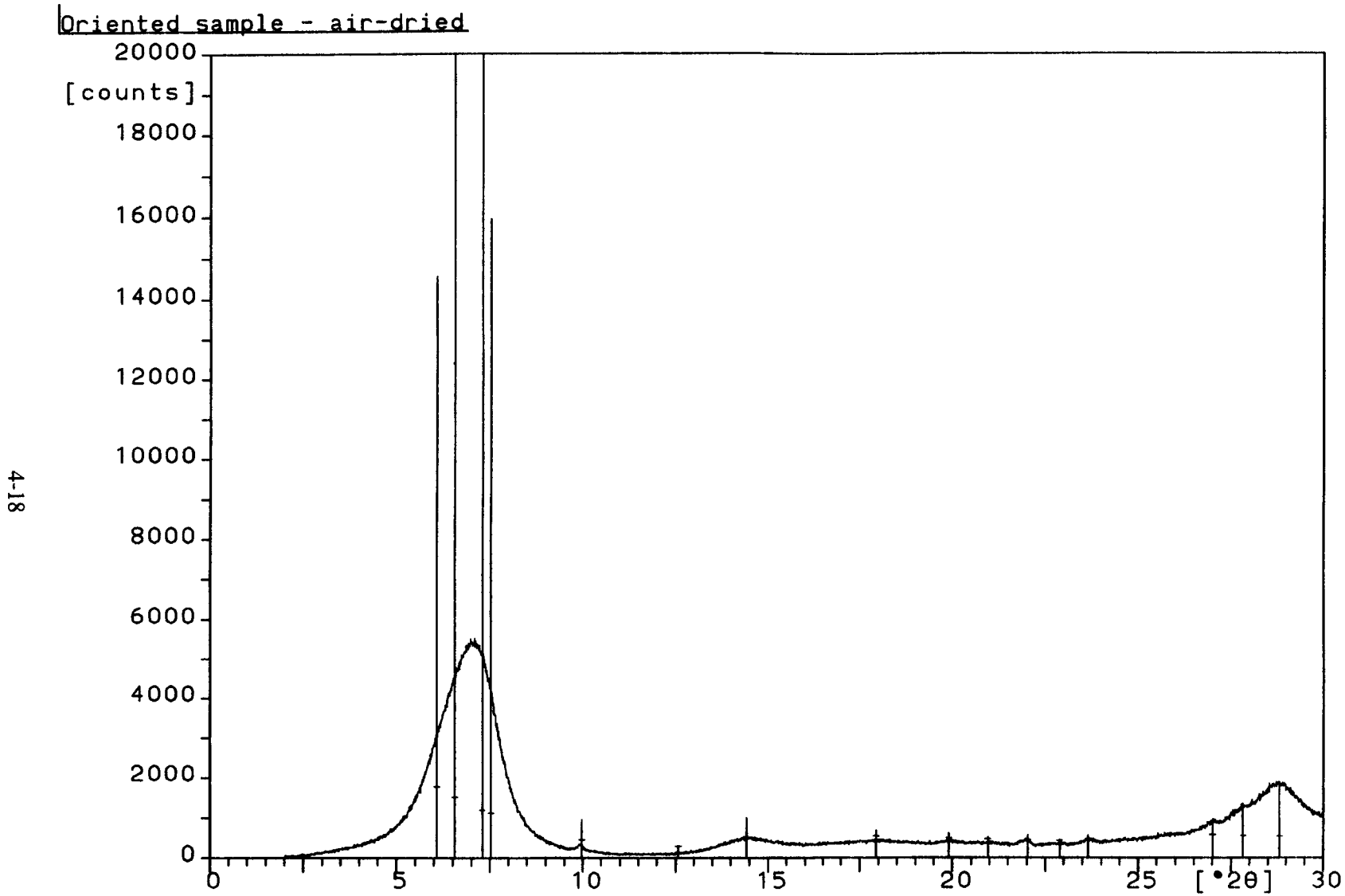


Figure 4-8b. X-ray results showing the clay mineralogy of the Solitario Canyon fault gouge (oriented sample: air-dried)

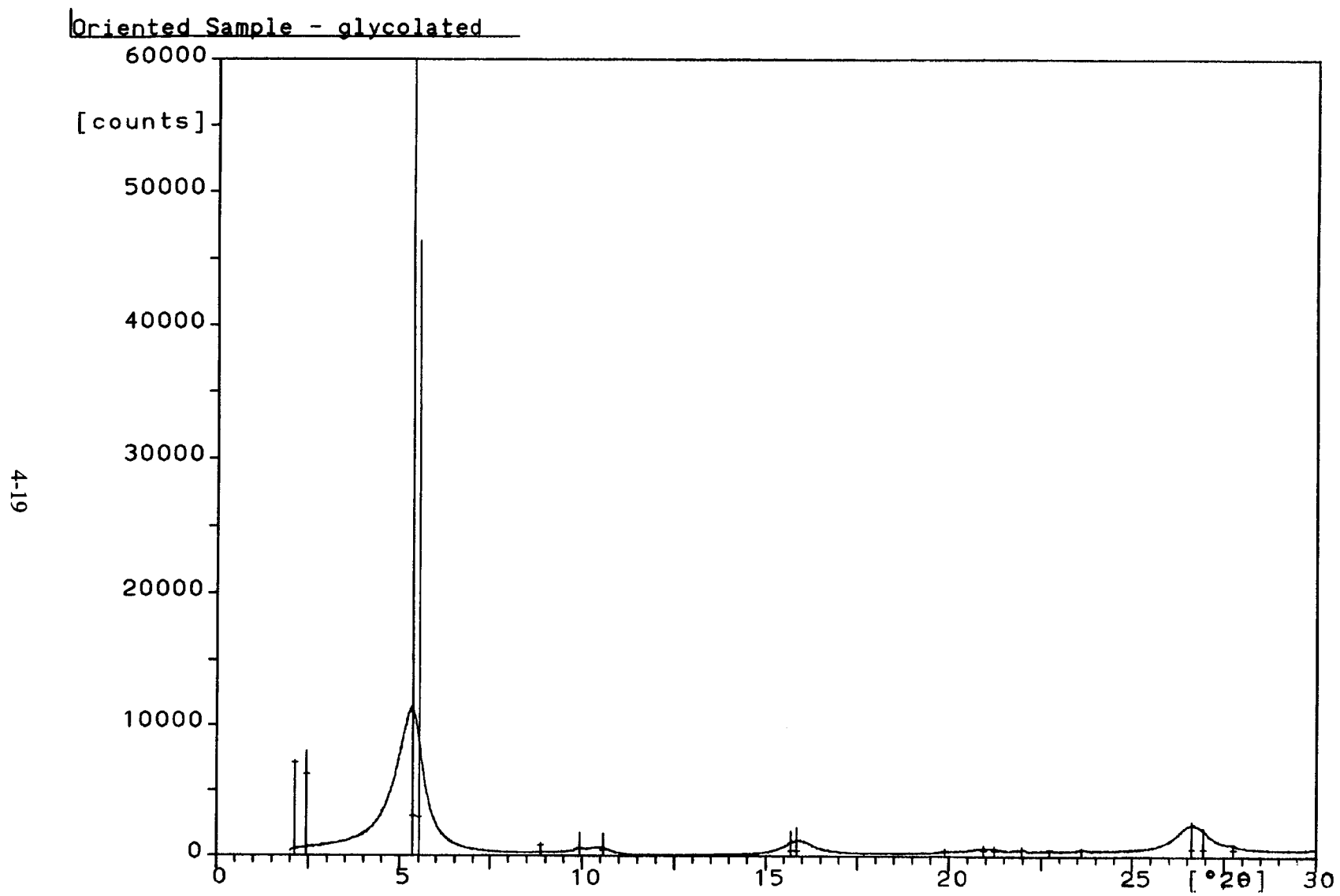


Figure 4-8c. X-ray results showing the clay mineralogy of the Solitario Canyon fault gouge (oriented sample: glycolated)

Comparison - Air-dried and glycolated samples

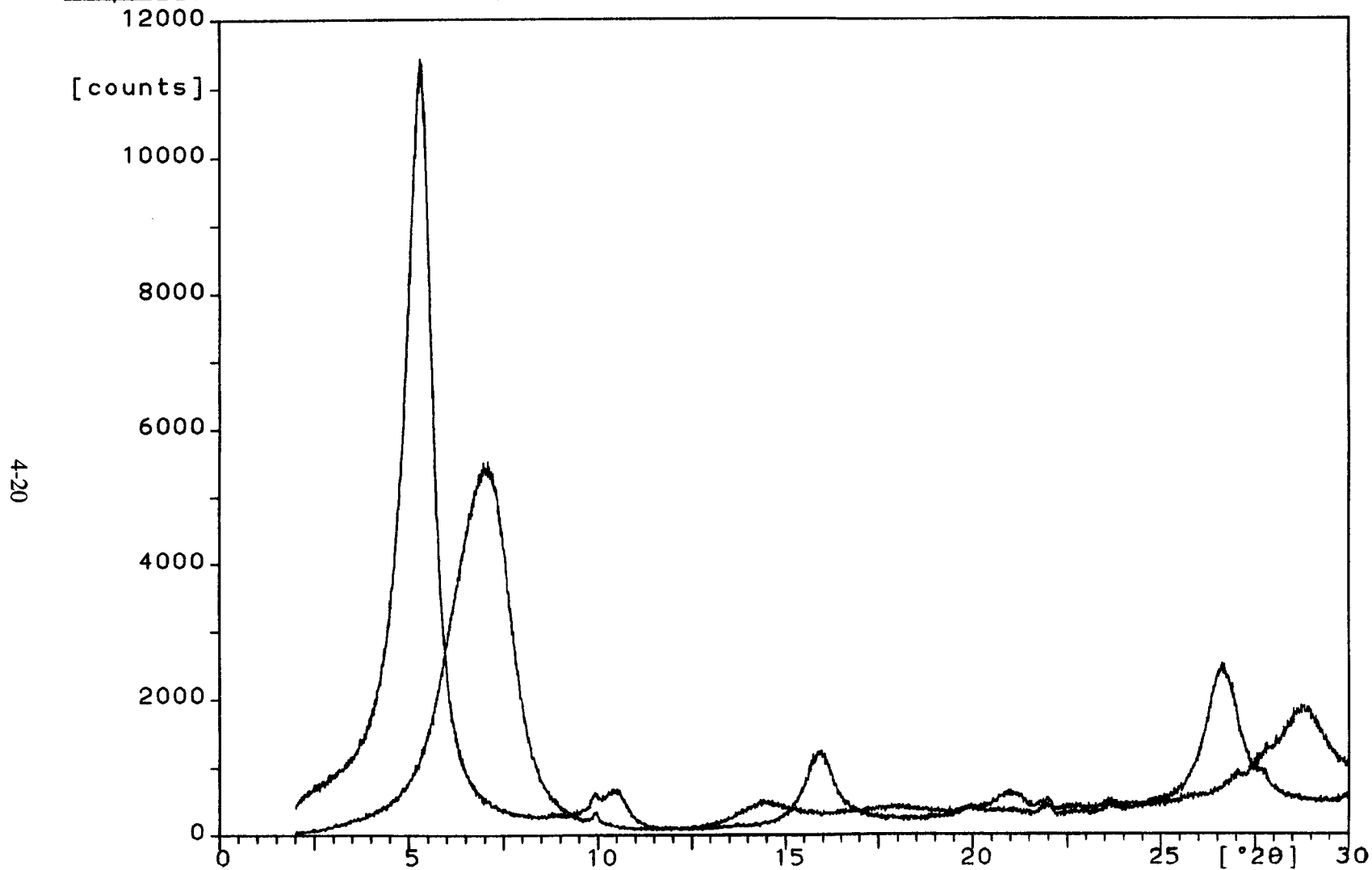


Figure 4-8d. X-ray results showing the clay mineralogy of the Solitario Canyon fault gouge (comparison: air-dried and glycolated samples)

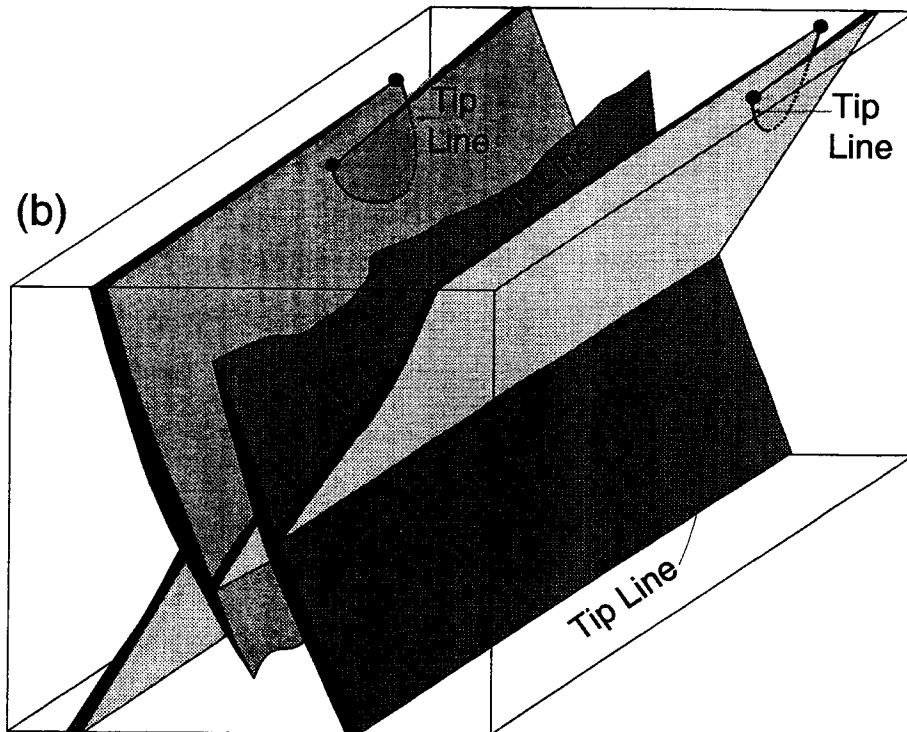
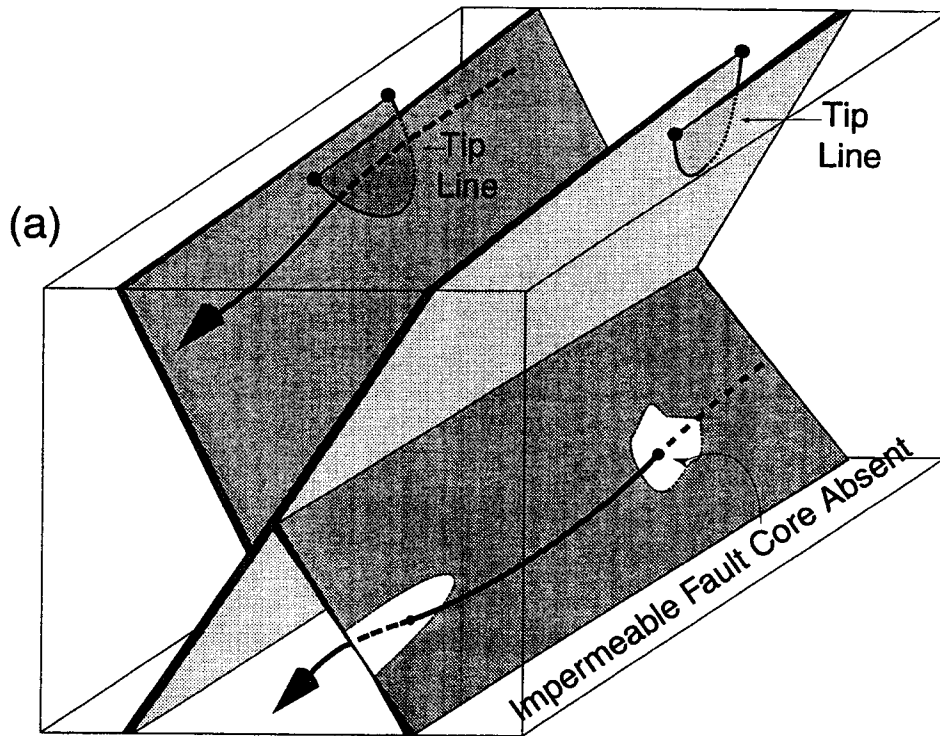


Figure 4-9. Schematic diagram illustrating effects of crossing conjugate normal faults on developing permeability anisotropy in rock where (a) fault zone deformation results in permeability decrease and (b) where fault zone deformation produces permeability increase

In nature, faults may contain all or only some of these deformation features. For example, in the ESF at YM, four fault types are identifiable based on these deformation characteristics. These four fault types match the generalized permeability fault types proposed by Caine et al. (1996). Of these, the SCF is most significant because it is one of the few faults to exhibit a well-developed fault gouge at its core surrounded by wide brecciated damage zones (13-m wide in the hanging wall and 3.5-m wide in the footwall), at least where it is exposed in the ECRB. X-ray analyses show that the fault gouge has been altered to a smectite clay, which would effectively clog the core and inhibit groundwater flow across the fault zone. In contrast, the large damage zones on either side of the SCF would possibly enhance groundwater flow parallel to the fault, with little cross-fault communication of fluids. If smectite is equally abundant in the fault zone within the SZ, this observation could explain the thermal anomalies at YM, where groundwater temperatures under the repository are significantly lower than those just west of the Solitario Canyon fault and in Crater Flat (Bredehoeft, 1997; Fridrich et al., 1994).

These effects of fault zones on groundwater flow are accentuated where faults form as conjugate pairs and intersect or cross each other (Ferrill et al., 1999c). Intersecting or crossing faults are common in extensional settings and tend to compartmentalize flow within the blocks bounded by the fault zones. This geometry establishes a permeability anisotropy, with maximum transmissivity parallel to fault intersections. At YM, the faults dip moderately to steeply and strike generally north-south. Thus, permeability is enhanced along the roughly north-south direction relative to all other directions. This trend is oblique to the northwest-southeast potentiometric gradient. Coupled with the effects of the regional stress field (Ferrill et al., 1999b), the permeability anisotropy would therefore deflect groundwater flow into a more north-south orientation than current flow models that are solely based on the potentiometric data alone and assumptions of isotropic and uniform permeability.

Because of the large uncertainties of the flow system in the SZ south of YM, incorporation and abstraction of these effects into YM, flow models are recommended. For example and as discussed in section 4.1, fault zone permeability depends in part on the stress field. Increasing confining pressures (depth) alone substantially alters fault rock permeability (Evans et al., 1997). To understand these effects, additional constraints on fault zone properties at YM or appropriate analogs are necessary. Possible approaches to assessing fault zone permeability at YM include

- Mini-permeameter testing of fault core, damage zone, and host rock
- Permeability plug testing of fault core, damage zone, and host rock under the different stress conditions indicative of the YMR following Evans et al. (1997)
- Fracman modeling of fault zone and numerical simulations of multidirectional fluid flow following Caine and Forster (1999)

The possibility that the SZ groundwater flow system is controlled to some degree by faults has important implications for YM repository performance. Groundwater flow enhanced along faults and restricted across faults could result in (i) faster travel times from YM to receptor locations, (ii) reduced dilution of waters contaminated with radionuclides from YM, and (iii) localized radionuclide migration pathways from YM to receptor locations.

4.4 HYDROCHEMISTRY OF GROUNDWATER IN THE YUCCA MOUNTAIN REGION

The chemical characteristics of groundwater in the vicinity of YM are functions of the recharge water chemistry and the rocks with which the groundwater interacts along the flow path (Luckey et al., 1996). This suggests that the hydrochemistry of groundwater within the YMR may be used to develop, evaluate, and constrain possible groundwater models. Luckey et al. (1996) indicated that some care is necessary when interpreting some of the hydrochemical data due to possible sample contamination. Further, Davisson et al. (1999) cautioned that, as flow systems become more complex or regional in extent, hydrochemical data may not provide single source and age determinations because of (i) an increase in the number of recharge mixing end-members contributing to groundwater flow, (ii) multiple water rock interactions working simultaneously or at different times within the flow history, and (iii) climate change and its effect on isotopic abundances.

4.4.1 Major Element Chemistry

4.4.1.1 Regional System

Winograd and Thordarson (1975) identified five distinct hydrochemical facies in the regional groundwater system:

1. The calcium magnesium bicarbonate facies typical of waters discharged from perched springs and regional springs in the carbonate units.
2. The sodium potassium bicarbonate facies typical of waters in the tuff aquifer.
3. The calcium magnesium sodium bicarbonate facies typical of waters found in the east-central Amargosa Desert and at Ash Meadows.
4. The sodium sulfate bicarbonate facies typical of waters discharged at Furnace Creek Wash and Nevares Springs in Death Valley.
5. A playa facies, high in total dissolved solids, typical of waters discharged by evapotranspiration at Franklin Lake Playa (Alkali Flat). Because waters sampled from the lower carbonate aquifer at the NTS are of the calcium magnesium sodium bicarbonate type, Winograd and Thordarson (1975) inferred downward flow from the tuffaceous units into the Paleozoic carbonate aquifer.

Waters discharging from the lower carbonate aquifer along the Ash Meadows spring line are also of the calcium magnesium sodium bicarbonate type. Waters in Pahrump Valley, which originate from recharge into carbonate rock that crops out in the Spring Mountains, are typical of the calcium magnesium bicarbonate facies. Because waters in Pahrump Valley contain much less sodium and sulphate than those discharged at Ash Meadows, Winograd and Thordarson (1975) believed that little, if any, water flows from Pahrump Valley to the Ash Meadows area.

Water from Indian Springs Valley, Three Lakes Valley, and northwest Las Vegas Valley has lower sodium, potassium, sulfate, and chloride concentrations than water from the NTS and Ash Meadows, suggesting that water does not flow eastward from the NTS (Winograd and Thordarson, 1975).

4.4.1.2 Yucca Mountain and Immediate Vicinity

The chemistry of water sampled from wells tapping the valley-fill aquifer in east-central Amargosa Desert is different from water sampled from other valley-fill aquifers in the NTS area. While these waters have a lower ionic strength, they belong to the same hydrochemical facies as water discharging at Ash Meadows. Winograd and Thordarson (1975) interpreted this difference as a mixing of recharging waters with up-flowing waters from the lower carbonate aquifer.

The chemical quality of water in the central Amargosa Desert varies spatially indicating the possibility of different sources. In this region, Winograd and Thordarson (1975) identified three possible categories of water: (i) water of the calcium magnesium sodium bicarbonate facies located in the southeast near the Ash Meadows spring line, (ii) water of the sodium potassium bicarbonate facies located southwest of Lathrop Wells, and (iii) water in the west-central and northwest portion of the Amargosa Desert. Category (i) water was interpreted as being derived from flow across the hydraulic barrier that causes the Ash Meadows spring line, category (ii) water was interpreted as originating from Jackass Flats, while category (iii) water was interpreted as originating from Oasis Valley.

Claassen (1985) contoured major element hydrochemistry data south of YM and identified a southeast trending trough of low concentrations centered beneath the main drainage emerging from Fortymile Canyon into the central Amargosa Desert (figure 4-10). Higher concentrations were found associated with readily dissolved playa deposits, whereas lower total dissolved solids (TDS) were found associated with coarser, more permeable deposits. Relative to the more dilute groundwater in the trough, higher ionic concentrations (e.g., Na^+ and Ca^{2+}) were measured for groundwater samples collected from the upstream reaches of the Amargosa River channel. Further downstream, below the confluence of the Fortymile Canyon and Amargosa River drainages, concentrations again decrease, suggesting a mixing of the two waters. The high Na^+ concentrations of Amargosa River groundwater samples from the upstream reaches suggest interaction with tuffaceous alluvium, whereas the elevated Ca^{2+} either may be due to mixing of alluvial waters with upwelling water from the underlying carbonate aquifers or to interaction with carbonate alluvium at the base of the Funeral Mountains.

Across the concentration gradient at the west side of the trough in west-central Amargosa Desert, Claassen (1985) noted east-west trends of decreasing Ca/Na in groundwaters from the tuffaceous alluvium. Because the potentiometric contours indicate a southerly flow, Claassen (1985) considered it unlikely that significant east-west mixing of fluids occurred; this is supported by the lack of significant changes in Cl^- concentration across the gradient. Groundwater diffusion with calcite precipitation to reduce Ca^{2+} was also considered inadequate by Claassen (1985) due to a lack of a corresponding decrease in calcite saturation. Claassen (1985) suggested that the observed trend was more likely due to continued evolution of the valley-fill water by interaction with tuffaceous alluvium and increased precipitation of clinoptilolite. No mineralogical evidence was presented to support this hypothesis.

Across the gradient on the east side of the trough, Schoff and Moore (1964) used increasing Ca/Na ratios in the east-central Amargosa Desert toward the Spring Mountains to indicate mixing between $\text{Na}^+ + \text{K}^+ + \text{HCO}_3^-$ tuffaceous waters from the north and $\text{Ca}^{2+} + \text{Mg}^{2+} + \text{HCO}_3^-$ groundwater recharged in the carbonates in the Spring Mountains. On the basis of the major ion hydrochemistry and a change in the potentiometric contours, Claassen (1985) proposed mixing across a region 5–10 km northeast of the Ash Meadows discharge zone. This region, west of Rock Valley Wash, occurs near the intersection of the Specter Range Thrust fault and Gravity fault and may represent a break in the hydrologic barrier separating the Ash Meadows spring line from the Amargosa Desert. Using major element chemistry and conservative ions such

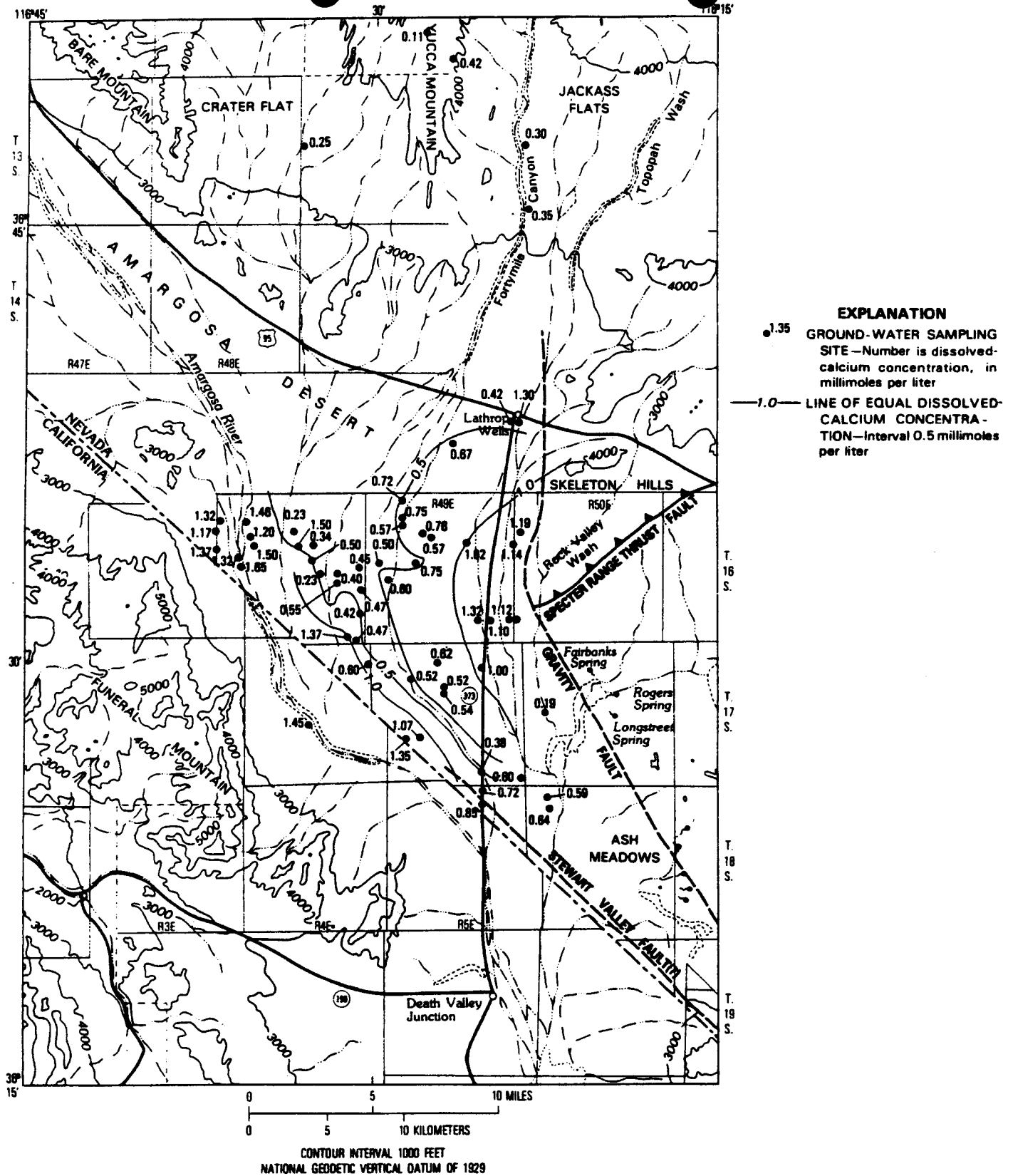


Figure 4-10a. Contour map of dissolved calcium in groundwater in the Yucca Mountain region (taken from Claassen, 1985)

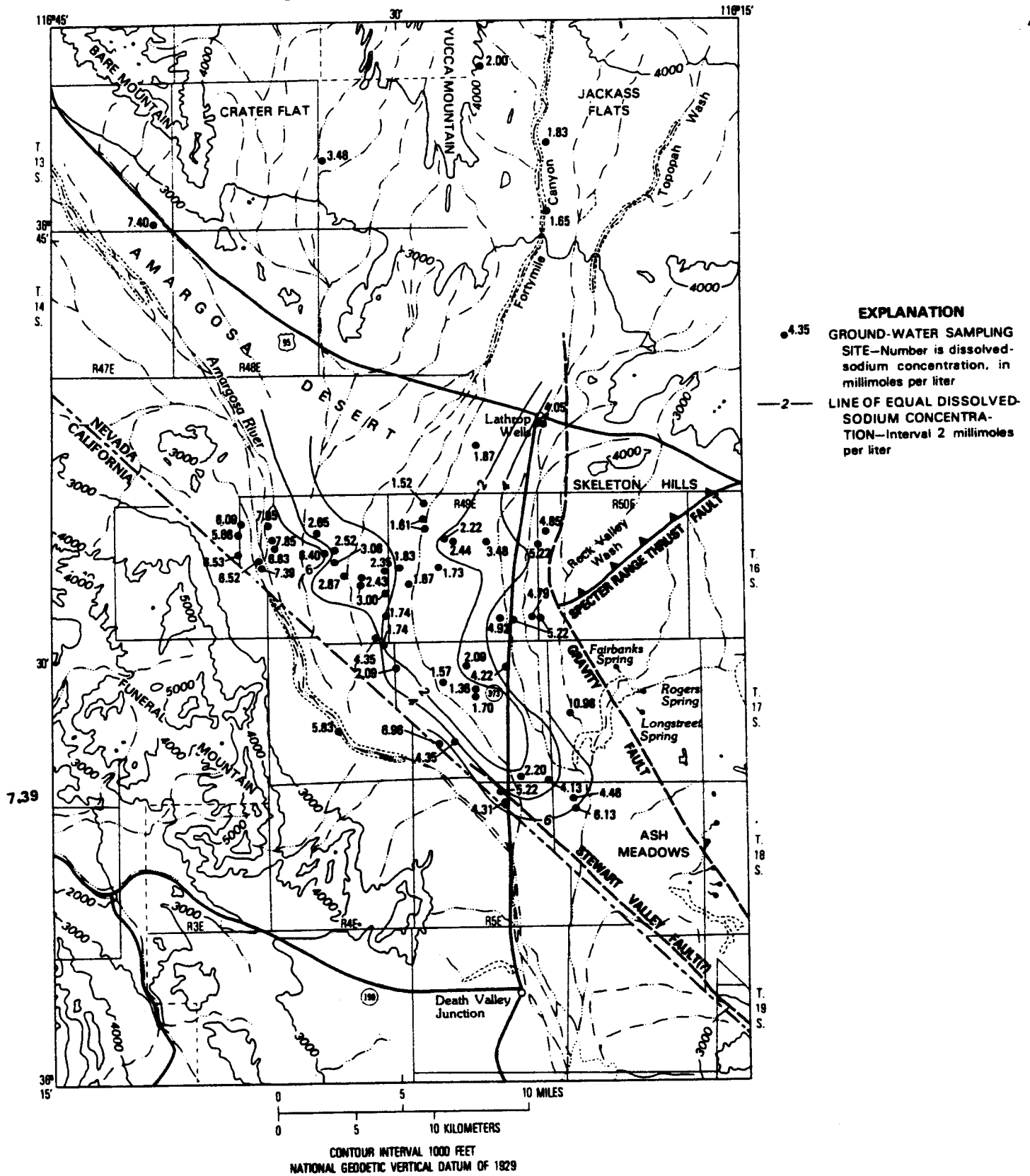


Figure 4-10b. Contour map of dissolved sodium in groundwater in the Yucca Mountain region (taken from Claassen, 1985)

as Cl^- , Claassen (1985) showed that progressive mixing of dilute waters from the center of the trough with mixed valley fill-carbonate waters leaking across the Gravity fault/Specter Thrust intersection could produce the observed hydrochemistry. Waters closer to the intersection were comprised of a larger component of carbonate water, while there is a rough increase in the tuff water component from north to south.

4.4.2 Stable Isotope Chemistry (δD , $\delta^{18}\text{O}$, and $\delta^{13}\text{C}$)

4.4.2.1 Regional System

Deuterium and ^{18}O values measured from waters collected from wells in tuffaceous aquifers in Pahute Mesa range between $\delta\text{D} = -109$ to -114 ‰ SMOW and $\delta^{18}\text{O} = -14.05$ to -14.75 ‰ SMOW (White and Chuma, 1987) and, as a result, are interpreted as being depleted. This observed depletion is assumed to be due in part to the elevation of Pahute Mesa. Similar deuterium and ^{18}O values were reported in springs and wells in the headwaters of Oasis Valley. White and Chuma (1987) attribute observed down-gradient enrichments in both deuterium and ^{18}O in the Oasis Valley basin to partial evaporation and progressive mixing between waters originating in Pahute Mesa and heavier waters recharging locally at lower elevations in Bullfrog Hills ($\delta\text{D} = -102$ and $\delta^{18}\text{O} = -13.3$ to -13.4 ‰ SMOW).

In general, the isotopic signatures overlap for waters from Tertiary volcanic and Quaternary alluvium aquifers within Pahute Mesa and Owens Valley. All the waters fall on a line that parallels the global meteoric water line (GMWL) of Craig (1961), but the line is shifted to slightly more depleted (~ 5 ‰) or deuterium values. This shift may be due to a cooler climate during the period of recharge (White and Chuma, 1987; Stuckless et al., 1991). Davisson et al. (1999) suggested the observed shifts from the global meteoric water line are due to evaporative processes that occur during precipitation and surface runoff. Evaporation may also occur from shallow groundwater systems.

Stable isotope signatures have been identified in the Ash Meadows discharge region. Winograd and Friedman (1972) suggested that the stable isotopic signatures in the Ash Meadows discharge area could result from mixing the groundwater from Pahrangat Valley with groundwater from the Spring Mountains. Davisson et al. (1999) suggested that such mixing is unlikely to occur because, based on ^{18}O contour maps for the region (figure 4-11; Davisson et al., 1999, figures 2 and 5), it is unlikely that groundwater can flow from Pahrangat Valley to the Ash Meadows region. Instead, Davisson et al. (1999) proposed two alternate models. One considers mixing Spring Mountains water with water migrating from Railroad Valley, while the second model considers mixing of Spring Mountains water with waters migrating south (beneath YM) from Pahute Mesa. The latter model is of interest because it supports the existence of groundwater flow paths from north of YM into the Amargosa Desert.

4.4.2.2 Yucca Mountain and Immediate Vicinity

Although waters collected from volcanic aquifers beneath YM are significantly heavier ($\delta\text{D} = -100$ to -108 ‰ and $\delta^{18}\text{O} = -13.4$ to -14.2 ‰ SMOW) than waters collected at Pahute Mesa, they are nevertheless still shifted to a line parallel to the GMWL. The observed shift however, is slightly less than that observed by White and Chuma (1987) for Pahute Mesa and Oasis Valley. Stuckless et al. (1991) argued that this indicates there is little communication between recharge at Pahute Mesa and the waters beneath YM.

Groundwater samples from Fortymile Canyon are enriched in both deuterium and ^{18}O relative to all other water samples from the YMR ($\delta\text{D} = -92.0$ to -97.5 ‰ and $\delta^{18}\text{O} = -12.4$ to -13.0 ‰ SMOW). White

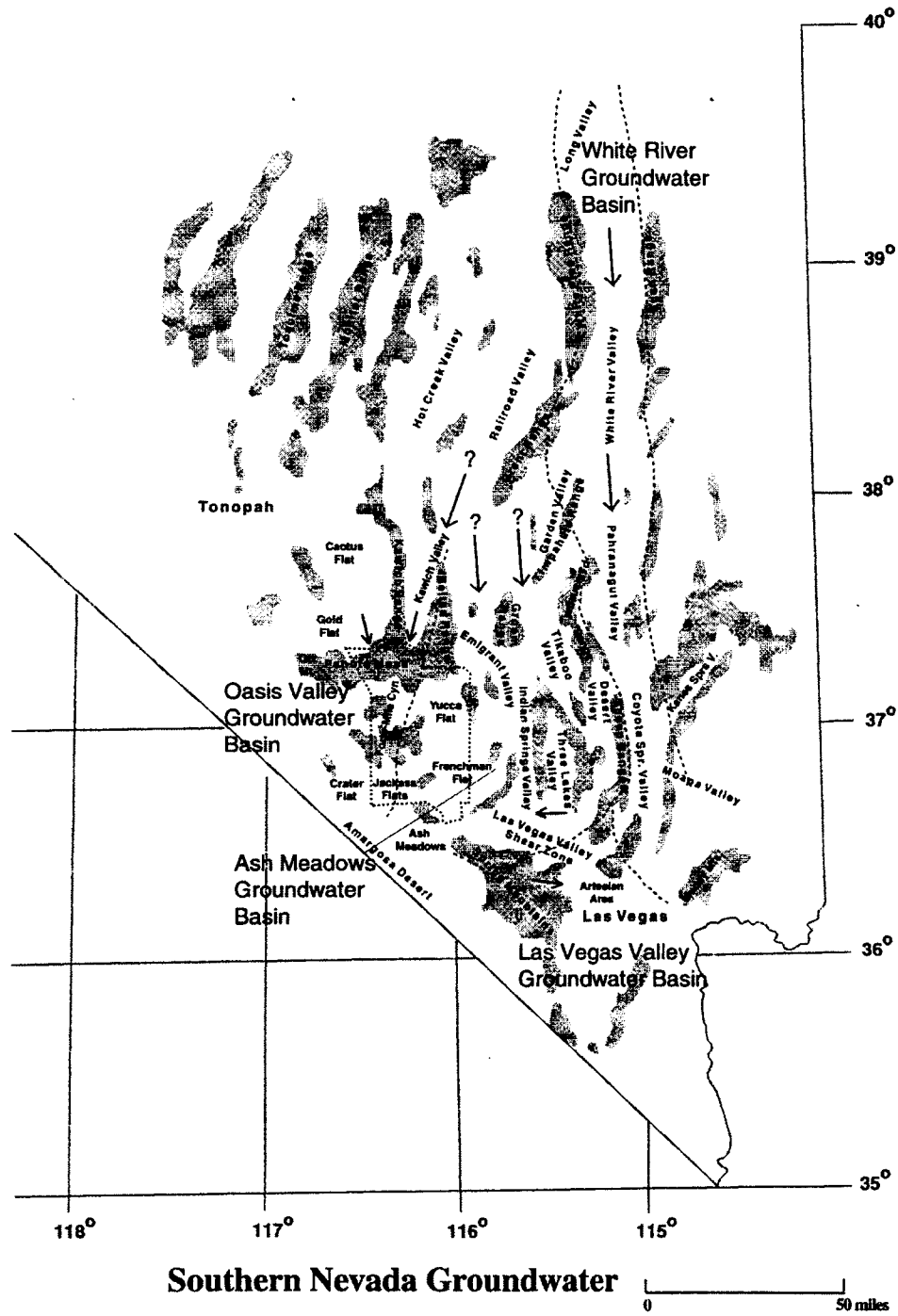


Figure 4-11a. Regional map for hydrochemical studies used by Davisson et al. (1999)

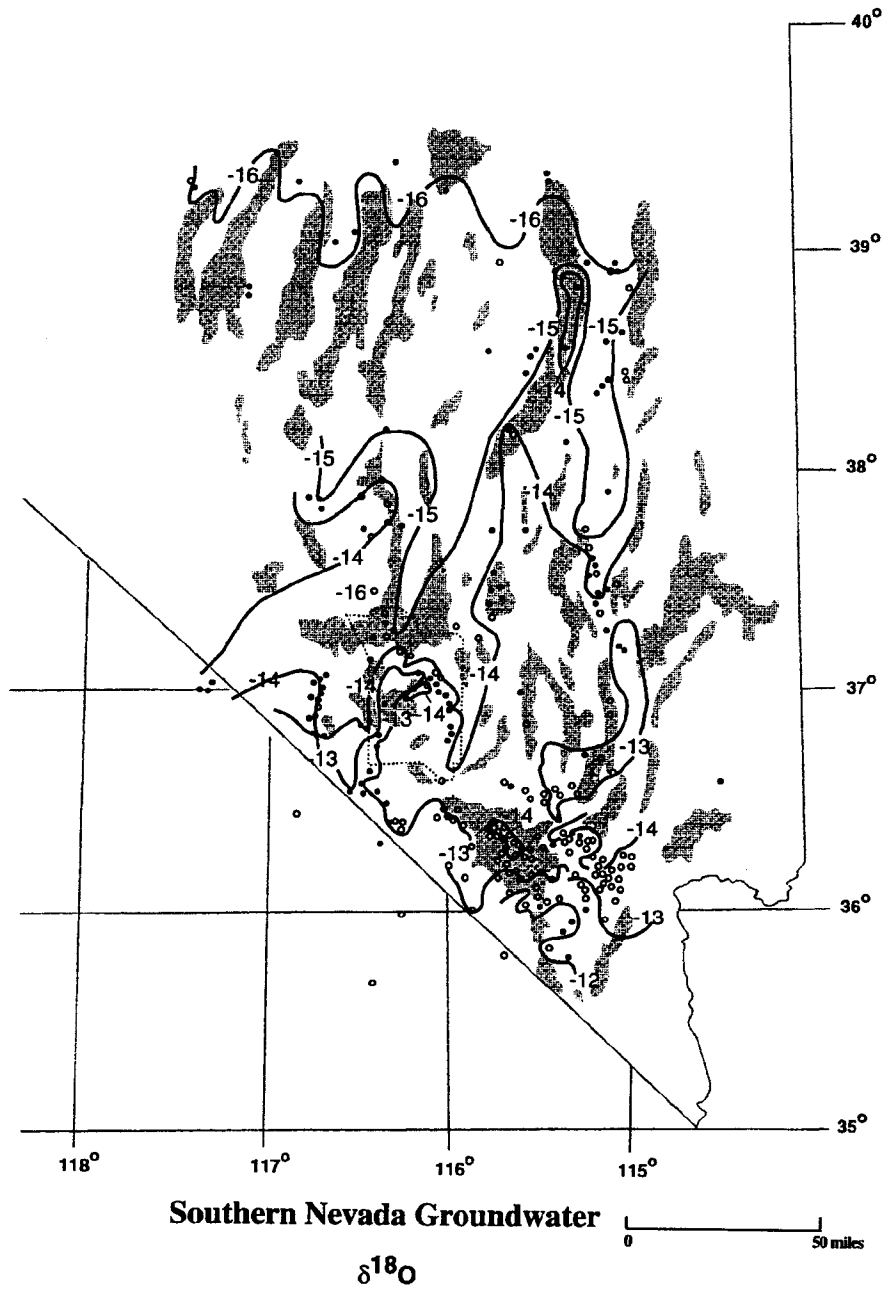


Figure 4-11b. Contour map of $\delta^{18}\text{O}$ in groundwater for the southern Nevada region [taken from Davisson et al. (1999)]

and Chuma (1987) and Stuckless et al. (1991) argued that this indicates there is little communication between the Tertiary aquifers beneath Fortymile Canyon and those under YM. Groundwater from the upper reaches of Fortymile Canyon is closer to the modern GMWL, suggesting local, relatively recent recharge, predominantly from summer precipitation at lower elevations. Claassen (1985) used this information to support inferred overland flow and recharge in Fortymile Canyon out into drainages in the Amargosa Desert. In this model, the chemical composition of the groundwater is principally determined by interaction with alluvial fill, with little input from upgradient tuff aquifers. This would tend to argue against significant mixing and dilution between tuff groundwaters beneath YM and those in the alluvial aquifers in Fortymile Canyon. An alternative proposal (White, 1981; White and Chuma, 1987) suggests that groundwater in the Amargosa Desert originated from tuffs in Fortymile Canyon with little interaction with alluvium. There is a gradual depletion in both deuterium and ^{18}O from wells UE-29a#1 and UE-29a#2 in the headwaters of Fortymile Canyon to wells J-12 and J-13, 15 km to the south. This trend is the opposite from the enrichment that one might expect because of progressive water-rock interaction or evaporation. Hence, the isotopic signatures of wells J-12 and J-13 instead might be due to mixing between waters flowing from beneath YM down-gradient to the southeast (Fridrich et al., 1994).

In Fortymile Canyon, measured groundwater $\delta^{13}\text{C}$ tends to increase from north ($\delta^{13}\text{C} = -13.1\text{‰ PDB}$ in UE-29 a#2) to values of about -7 to -8‰ PDB in the southern reaches of Fortymile Canyon and the northern Amargosa Desert (White and Chuma, 1987). Samples in the central Amargosa Desert, about 10–15 km south of the town of Amargosa Valley, are enriched still further (Claassen, 1985) to $\delta^{13}\text{C} = -3.4$ to -4.4‰ PDB . Heavier $\delta^{13}\text{C} = -5.7$ to -6.2‰ PDB are also reported (Claassen, 1985) in the south central Amargosa Desert near the Nevada-California state line at the base of the Funeral Mountains, just south of U.S. Highway 95 about 5 km south of Bare Mountain. Claassen (1985) used these carbon isotope results to support overland recharge through Fortymile Canyon into drainages in the northern and eastern Amargosa Desert. More negative values to the north are due to plant respiration ($\delta^{13}\text{C} \sim -24$ to 25‰) exerting a larger control on carbon isotope systematics at higher elevations and shallower depths to water in wells UE-29 a#1 and UE-29 a#2. With progressive flow to the south, $\delta^{13}\text{C}$ increases through increasing interaction with atmospheric CO_2 and fracture calcite. In the southern areas, the highest $\delta^{13}\text{C}$ values may be because of either progressive upward mixing with groundwaters from the carbonate aquifers (Claassen, 1985; Stuckless et al., 1991) or increased interaction with carbonate alluvium that originated in the Paleozoic carbonate uplands in the Spring, Funeral, and Bare Mountains (White and Chuma, 1987).

Fridrich et al. (1994) interpreted the $\delta^{13}\text{C}$ data as definitive evidence of the interaction between the carbonate and volcanic aquifers beneath YM. They interpreted the generally southward increase in $\delta^{13}\text{C}$ values as indicative of a southward increasing contribution of flow from the carbonate aquifer into the volcanic units. In addition, Fridrich et al. (1994) proposed that the pattern of $\delta^{13}\text{C}$ observed within the volcanic units results from the upwelling of groundwater along faults that intersect the underlying Paleozoic carbonate aquifer. Possible support for this model is seen in the thermal discussions in section 4.5.1.

4.4.3 Radiogenic Isotopes

4.4.3.1 Regional System

Peterman and Stuckless (1993) reported the results of Sr analyses for groundwaters in the vicinity of YM. In general, there is an increase in $\delta^{87}\text{Sr}$ from the Spring Mountains ($\delta^{87}\text{Sr} = -0.5\text{‰}$) toward the west and the springs at Ash Meadows ($\delta^{87}\text{Sr} = 6$ to 13.1‰) suggesting increased interaction with Cambrian and Precambrian clastics. There is also a general downgradient increase in $\delta^{87}\text{Sr}$ from Pahute Mesa to Franklin

Lake Playa. Peterman and Stuckless (1993) suggest this trend represents progressive water rock interaction within the volcanic units south to Amargosa Valley, where interaction with alluvial fill and increased mixing from groundwaters below the valley fill result in a general increase. The highest values to the south may be a result of upwelling or possible interaction with alluvial fill composed of Precambrian debris from the Funeral Mountains.

A large radiocarbon database exists for groundwaters in southern Nevada, however, the data are highly clustered in localized areas (figure 4-12a; Davisson et al., 1999). Further, little data exist where low ^{18}O recharge is inferred and most data are sampled from the Lower Carbonate Aquifer (Davisson et al., 1999). Within the Spring Mountains, ^{14}C values systematically increase with elevation, showing significant loading of modern recharge at high elevations. Increased ^{14}C values also are observed in the Fortymile Canyon region and are assumed to reflect modern recharge. Away from Fortymile Canyon and the Spring Mountains, most groundwater samples show considerably lower ^{14}C values (figure 4-12b).

4.4.3.2 Yucca Mountain and Immediate Vicinity

Peterman and Stuckless (1993) observed about 3-per-mil noise in the $\delta^{87}\text{Sr}$ data obtained from wells in volcanic tuffs north of the Amargosa Desert. This probably reflects the 10-per-mil range in $\delta^{87}\text{Sr}$ for the different volcanic units and the complex structure that results in different lithologic units at the water table and complex flow. The fact that these heterogeneities are to some extent preserved in the noise suggests that mixing of fluids may be limited beneath YM.

Age-dating using ^{14}C shows the youngest (uncorrected ^{14}C) measurements to be in UE-29 a#1 and UE-29 a#2 and increasing age to the south in wells J-12 and J-13. As is the case with deuterium and ^{18}O data, waters from Fortymile Canyon are distinctly younger (higher ^{14}C) than those in the tuff aquifers beneath YM. This appears to support the hypothesis of limited mixing between these two waters. Nevertheless, it is still possible that mixing between recharge waters in Fortymile Canyon with older groundwater from beneath YM produces the observed ages in wells J-12 and J-13, although the complexities of carbon systematics complicate the interpretation.

Carbon-14 data reported by Benson and McKinley (1985) show the oldest groundwater located beneath the crest of YM and the youngest water located further east beneath Fortymile Wash. Czarnecki et al. (1997) suggested these data, along with the west to east increase in the Ca/Na ratio reported by Claassen (1985), are consistent with (i) the SCF being a barrier to east-west groundwater flow, an observation consistent with the moderate hydraulic gradient found in this area (Ervin et al., 1994) and (ii) Fortymile Canyon being a recharge zone. However, hydrochemical data collected on either side of, and adjacent to, SCF appear similar and therefore do not support the former conclusion.

4.4.4 Summary of Implications of Hydrochemistry in Evaluating Structural Controls on Groundwater Flow in the Yucca Mountain Region

A significant amount of hydrochemical data has been collected in the YMR that can be used to evaluate the degree to which geologic structure influences groundwater flow. Major element chemistry can be used to define hydrochemical facies (Winograd and Thordarson, 1975) that can be related to both hydrostratigraphic units and structurally defined groundwater basins. Vertical mixing between aquifers and mixing across structural boundaries between basins potentially can be evaluated by considering conservative constituents such as chloride and sulfate. Other elements and ratios between major cations and anions can

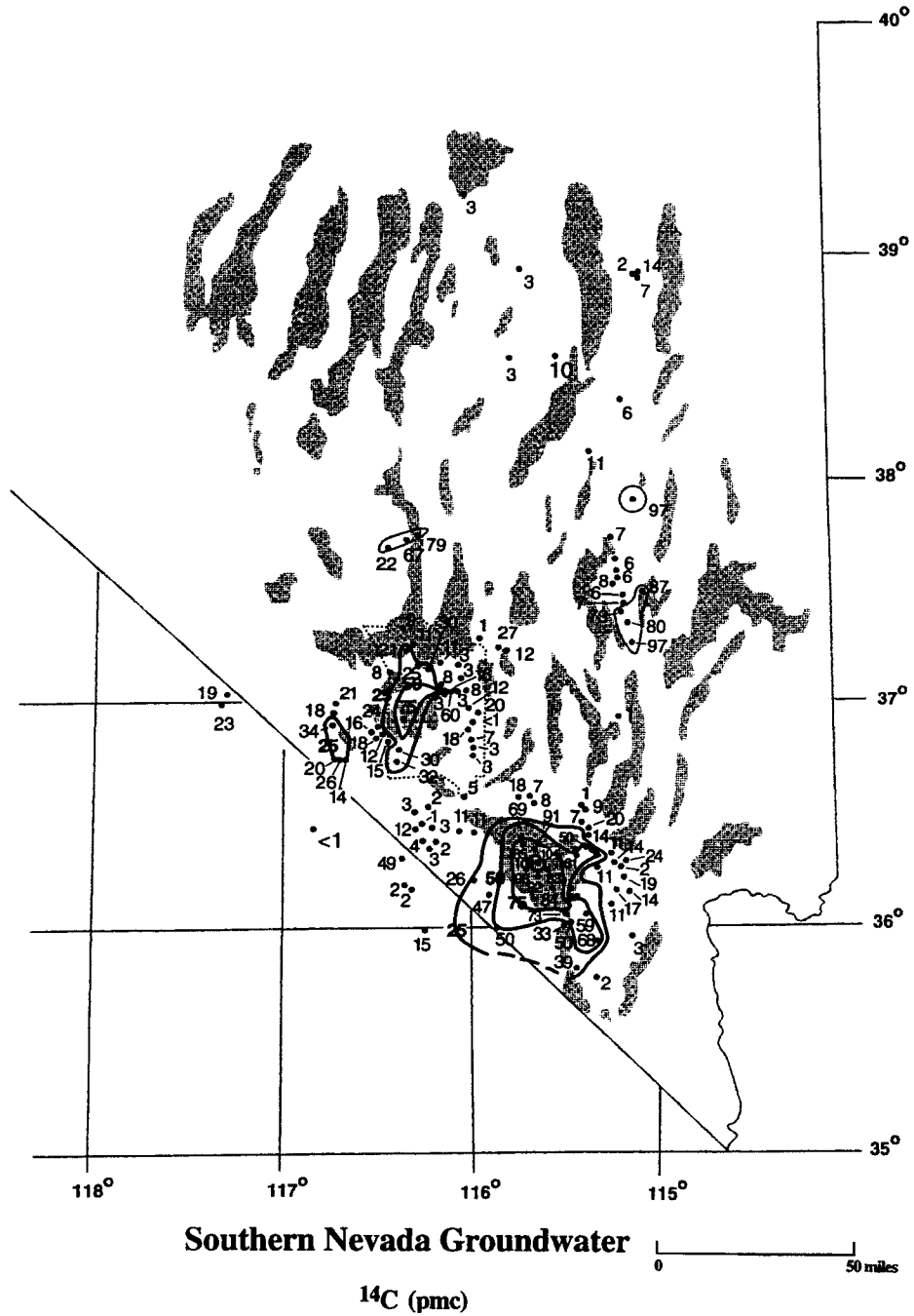


Figure 4-12a. Contour map of ^{14}C in groundwater for the southern Nevada region [taken from Davisson et al. (1999)]

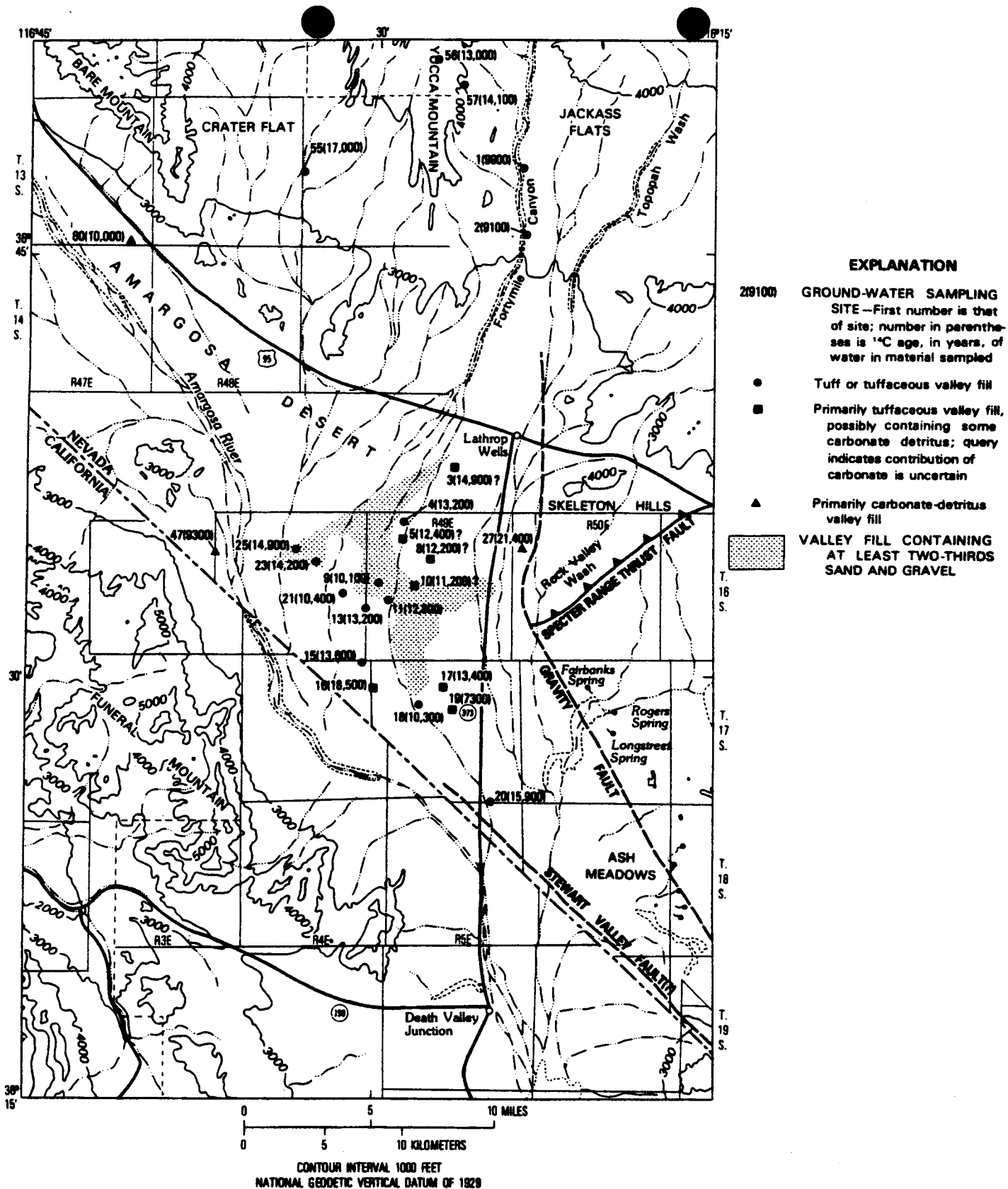


Figure 4-12b. Contour map of ¹⁴C in groundwater for the Yucca Mountain region [taken from Claassen (1985)]

be used as well, and careful consideration of potential water-rock interaction can be used to identify plausible flow paths that may be controlled by geologic structure. For example, geochemical modeling of aqueous speciation and mineral saturation can identify unique groundwaters and possible water-rock interaction along and across fault zones. As a complement to element chemistry data, light stable isotopes (^{18}O , ^2H , ^{13}C) can be used as tracers to identify recharge areas (Claassen, 1985; White and Chuma, 1987), potential flow paths, and estimate mixing (Winograd and Friedman, 1972) between different end-member waters. Deuterium and ^{18}O can also be used as a means of identifying evaporation (Davisson et al., 1999). Radiogenic isotopes such as ^{14}C can be used to estimate groundwater ages, bound flow rates, and constrain mixing estimates (Winograd and Pearson, 1976; Davisson et al., 1999).

SZ hydrochemistry is directly relevant to several of the Integrated Subissues identified in the Total System Performance Assessment Issue Resolution Status Report. As outlined previously, these data can be used to constrain flow rates in water production zones, retardation in water production zones and alluvium.

4.5 GEOPHYSICAL STUDIES IN THE YUCCA MOUNTAIN REGION

Geophysical methods provide a cost effective approach for mapping a variety of subsurface structures at varying scales, and are especially valuable where direct physical evidence such as borehole data are unavailable. Subsurface structures commonly mapped by geophysics include fault and fracture zones, as well as the spatial continuity and structural relationships between stratigraphic and hydrostratigraphic units. In addition to structural features, geophysical methods have been applied to hydrogeologic problems including water table and soil mapping, and contaminant delineation. This section presents a review of geophysical data considered relevant for evaluating structural controls on groundwater flow in the YMR at both local (tens to several hundreds of meters) and regional (several hundred meters to several kilometers) scales. The structures considered in this section include faults and fractures, the spatial continuity of hydrostratigraphic units, and the structural relationships between hydrostratigraphic units. The geophysical data reviewed were obtained from thermal, gravity, magnetic, electromagnetic and resistivity studies. It is important to recognize that the studies presented in this section represent only a small number of the total geophysical studies reported for the YMR.

4.5.1 The Heat Flow and Thermal Regime in the Yucca Mountain Region

YM is located near the southern boundary of the Eureka Low. Average heat flow within the Eureka Low is approximately half that seen in adjacent regions. Data collected during thermal studies in the YMR indicate that the thermal regime has been distorted by the effects of groundwater movement (Sass et al., 1980; Sass and Lachenbruch, 1982; Sass et al., 1995) and, as a result, may be used to complement hydrogeologic studies. The data also suggest that heat flow from below the water table is less than the regional average. Further, adjacent to YM, elevated heat flows and anomalously high water table temperatures are observed in Midway Valley and Solitario Canyon (figure 4-13).

4.5.1.1 Discussions of Heat Flow Data

Three models have been proposed to explain the observed heat flows in the YMR: (i) Lachenbruch and Sass (1977) showed that the observed thermal low can be produced by downward percolation, (ii) Sass and Lachenbruch (1982) proposed that the low heat flows recorded at YM were a southern extension of the Eureka Low, and (iii) Sass et al. (1988) proposed that the low heat flows at YM be considered part of an isolated thermal sink. For either interpretation, the tectonic implications of the heat flow data are largely

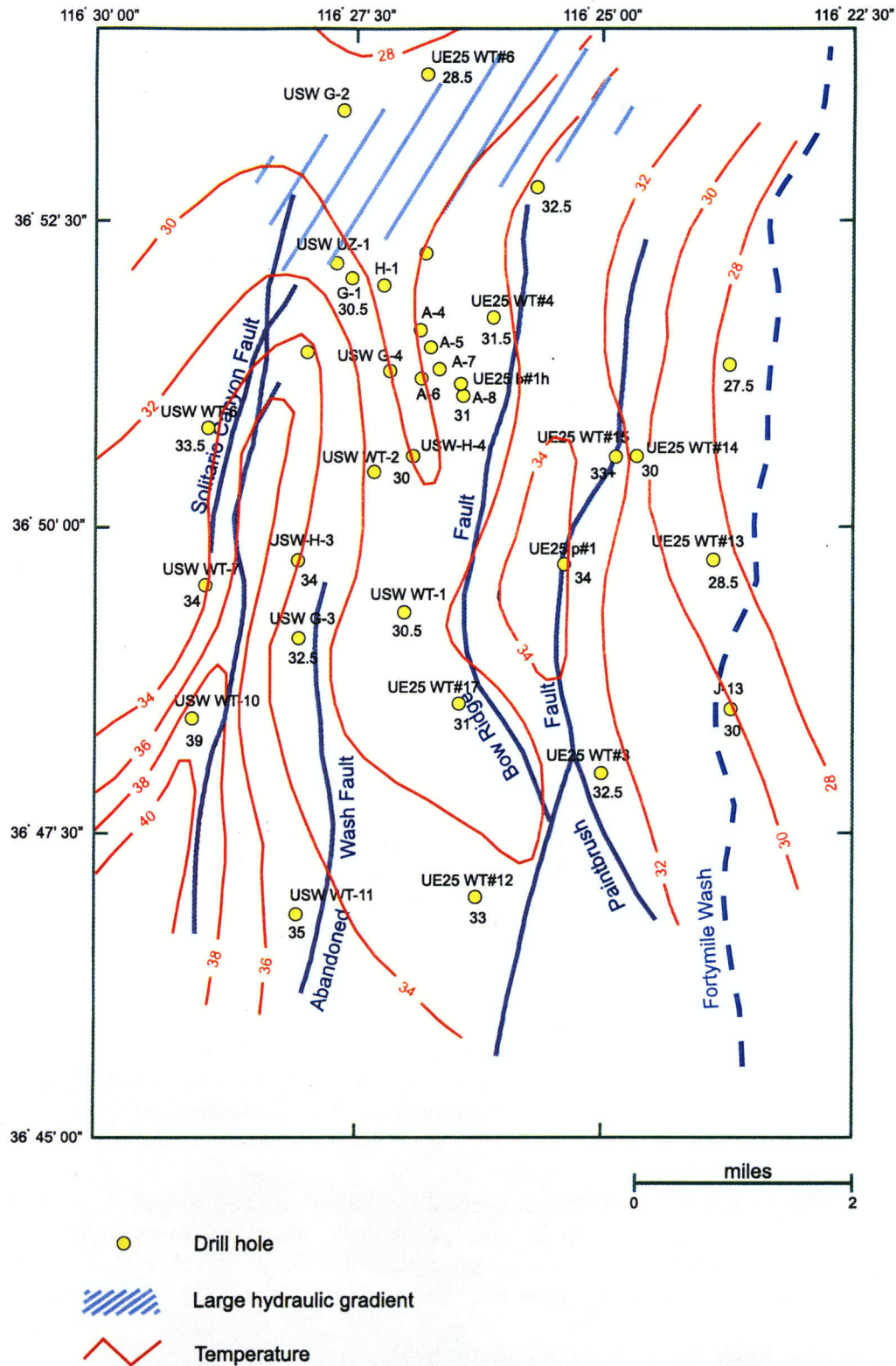


Figure 4-13. Map showing isotherms at the water table under Yucca Mountain, contoured with an interval of 2 °C [taken from Fridrich et al. (1994) and based on data from Sass et al. (1988)]

inconclusive, because the true regional heat flow is obscured by hydrologic processes (Sass et al., 1988). Nevertheless, the third model is the more widely accepted.

Based on their modeling efforts, Sass et al. (1988) concluded that at least 80 percent of the low-temperature anomaly observed beneath YM may be attributed to SZ processes, in particular, the flow of cool groundwaters within regional aquifer systems. Downward percolation of a few mm/year has also been proposed as a potential mechanism that may lead to the observed thermal low (Sass et al., 1988). However, for this mechanism to be plausible, downward components of groundwater flow must dominate upward components at the site-scale. Sass et al. (1988) point out that, while some segments of the YM SZ temperature profile indicate downward flow, upward flow is indicated by others. Hence, a pervasive downward flow model in the tuff aquifer in the vicinity of YM is not supported, especially considering the observed higher hydraulic heads in the underlying carbonate aquifer system.

Sass et al. (1988) suggest the large lateral variability of heat flow over distances of 1–2 km indicates a relatively shallow hydrologic source for the observed anomaly. This source may be primarily due to convection in the saturated tuffs and underlying carbonate aquifer (Sass et al., 1988). A numerical model demonstrating this behavior is presented in section 4.5.1.2.

Fridrich et al. (1994) extended the lateral flow model of Sass et al. (1988) by proposing the thermal anomaly beneath YM probably results from cool underflows in the deep carbonate aquifer. Support for this model was based on the anomalously low temperatures recorded in this aquifer. Fridrich et al. (1994) further postulated that the correspondence of the northern limit of the heat flow anomaly to the 300-m water table decline suggests that the effective northern limit of the deep carbonate aquifer and, by inference, the zone of downwelling into it, may coincide with the large hydraulic gradient under the northern part of YM. This proposed model of the northern limit of the carbonate unit appears consistent with structural interpretations based on the magnetic data (see section 4.5.3).

Hydraulically based arguments have been proposed to explain the linear zones of elevated temperature identified in the YMR. Szymanski (1989) suggested that, since these linear thermal highs correspond with the positions of major north-trending normal fault zones at the water table, they may represent upwelling along such structures. This upwelling appears consistent with the observations at UE25 p#1 that show higher hydraulic heads in the carbonate aquifer relative to the lower volcanic aquifer and provides a possible explanation for the smectites found within the fault gouge along the SCF (see section 4.3). Fridrich et al. (1994) provided support for this model by proposing that the maximum thermal difference (10 °C) observed at the site can only be accounted for by upward flow from the deep carbonate aquifer. The authors also pointed out that, if the linear thermal highs result primarily from upwelling from the deep carbonate aquifer, then the deep carbonate aquifer must extend beneath most of the YMR.

Finally, thermal logs in UE-25 p#1 located in Midway Valley appear qualitatively consistent with the interpretation of upward leakage of warm water along high-angle faults. Positive temperature anomalies within this borehole 100 m below the water table appear coincident with a permeable zone that corresponds approximately with the fault identified by Carr et al. (1986) and Sass et al. (1995).

4.5.1.2 Nonisothermal Modeling of Yucca Mountain Region

To determine whether the observed thermal anomalies could be produced by a nonstructurally controlled model, a nonisothermal modeling exercise was performed using the computer code METRA,

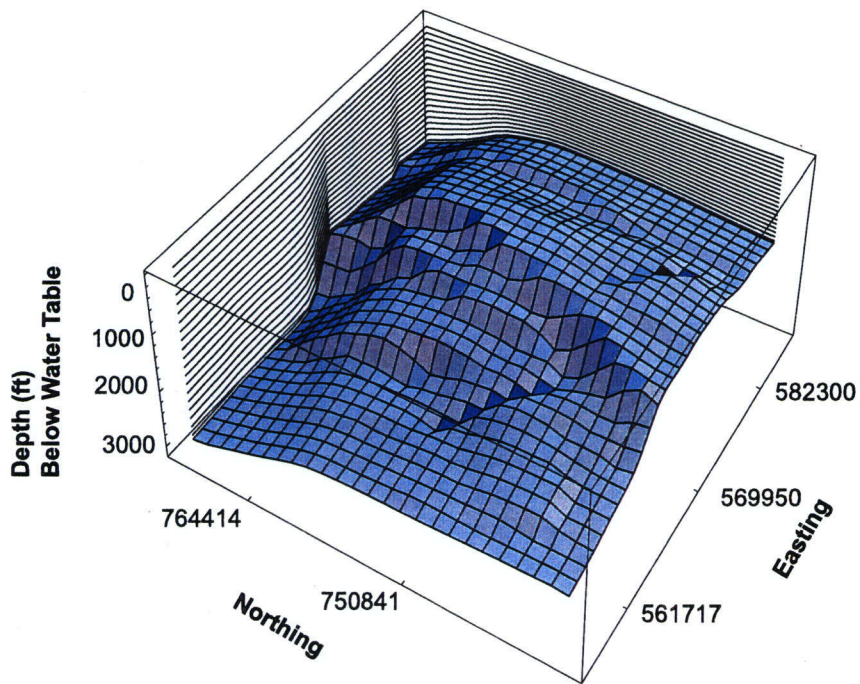
which is part of the MULTIFLO system of coupled flow and reactive transport models (Lichtner and Seth, 1998). The model domain covers an area of 8.5×10^8 ft². The domain includes the footprint of the proposed repository and the area immediately to the south and east. The west face is just to the east of the Solitario Canyon fault. The east face corresponds approximately to Fortymile Wash. This domain encloses structures within the Midway Valley system. The model grid used for this study is outlined in figure 4-14a. The nonuniform grid is logically rectangular with 20 layers and 30×25 cells in each layer. The base of the grid follows the top of the carbonate aquifer, and the top layer coincides with a potentiometric surface interpolated from hydraulic head measurements in the region. Nodes were assigned hydrologic properties according to a coarse representation of the hydrostratigraphy. The basecase permeability values for the four hydrostratigraphic units were obtained by calibration by Czarnecki et al. (1997) for their site-scale isothermal SZ model.

The boundary conditions for the model domain include (i) no flow from the underlying carbonates and a constant temperature of 55 °C was assigned to the base of the model; (ii) no fluid or heat flow from the east face corresponding to a presumed symmetry condition along Fortymile Wash; (iii) specified head and temperature along the remaining vertical faces and quasi-static conditions used to calculate vertical head distribution, and temperature were assumed to vary linearly with depth along each face; and (iv) no vertical flow at the top of the model, conductive heat flow from the water table to the land surface that was defined by a digital elevation map, and a constant temperature of 20 °C was specified at this surface.

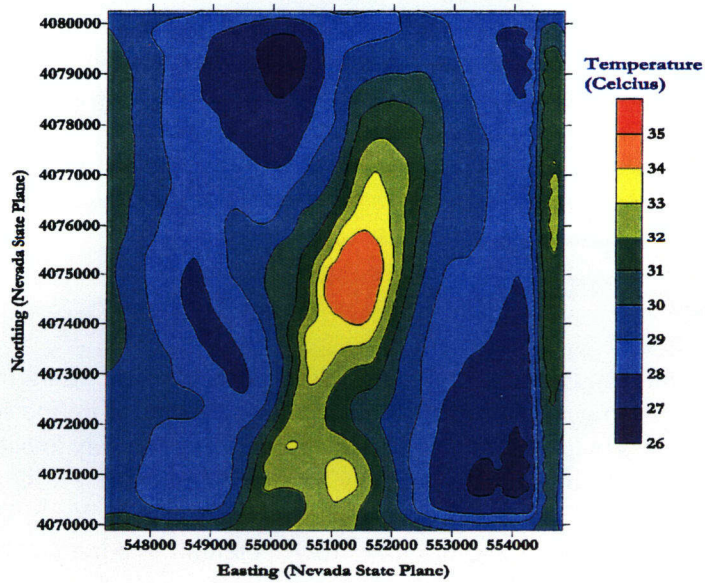
During the simulation, the zero pressure condition along the interpolated potentiometric surface was not imposed, but was monitored at several locations to check the calibration of the model. Using the permeability parameters obtained by Czarnecki et al. (1997) from their calibrated isothermal model, our model is also nearly calibrated when used in isothermal mode. However, the nonisothermal runs have a residual pressure head at the water table, indicating more calibration is needed. The magnitude of this residual pressure is a few meters when expressed in terms of equivalent head. This result suggests that permeability values obtained by calibration using isothermal models may contain significant errors in situations involving strong temperature variations. Model-simulated temperatures at the water surface are shown in figure 4-14b. The high-temperature anomaly near well UE-25 p#1 is reproduced accurately without any vertical upflow from the higher temperature carbonate unit. Similarly, the region of low temperature near the proposed repository is reproduced accurately without introducing any artificial downward flux. This modeling exercise also illustrates the importance of nonisothermal models for inverse modeling to attain better calibration.

4.5.2 Gravity Studies

Gravity methods essentially map density contrasts between adjacent stratigraphic units. From a hydrogeological perspective; the gravity data is important because it helps to define structural features at multiple scales and depths, such as fault and lithologic block geometries, that may impact groundwater flow and are essential in the development of groundwater flow models. Within the YMR, gravity studies have been performed on and around YM, in the Amargosa Desert, and in Fortymile Wash. This section provides a synthesis of the findings of these studies and discusses their potential importance regarding to possible structural controls on groundwater flow.



(a)



(b)

Figure 4-14. (a) Model grid for nonisothermal model domain showing the model grid on top of Paleozoic Carbonate; (b) Simulated temperatures at the water surface.

4.5.2.1 Discussions of Gravity Data

Yucca Mountain

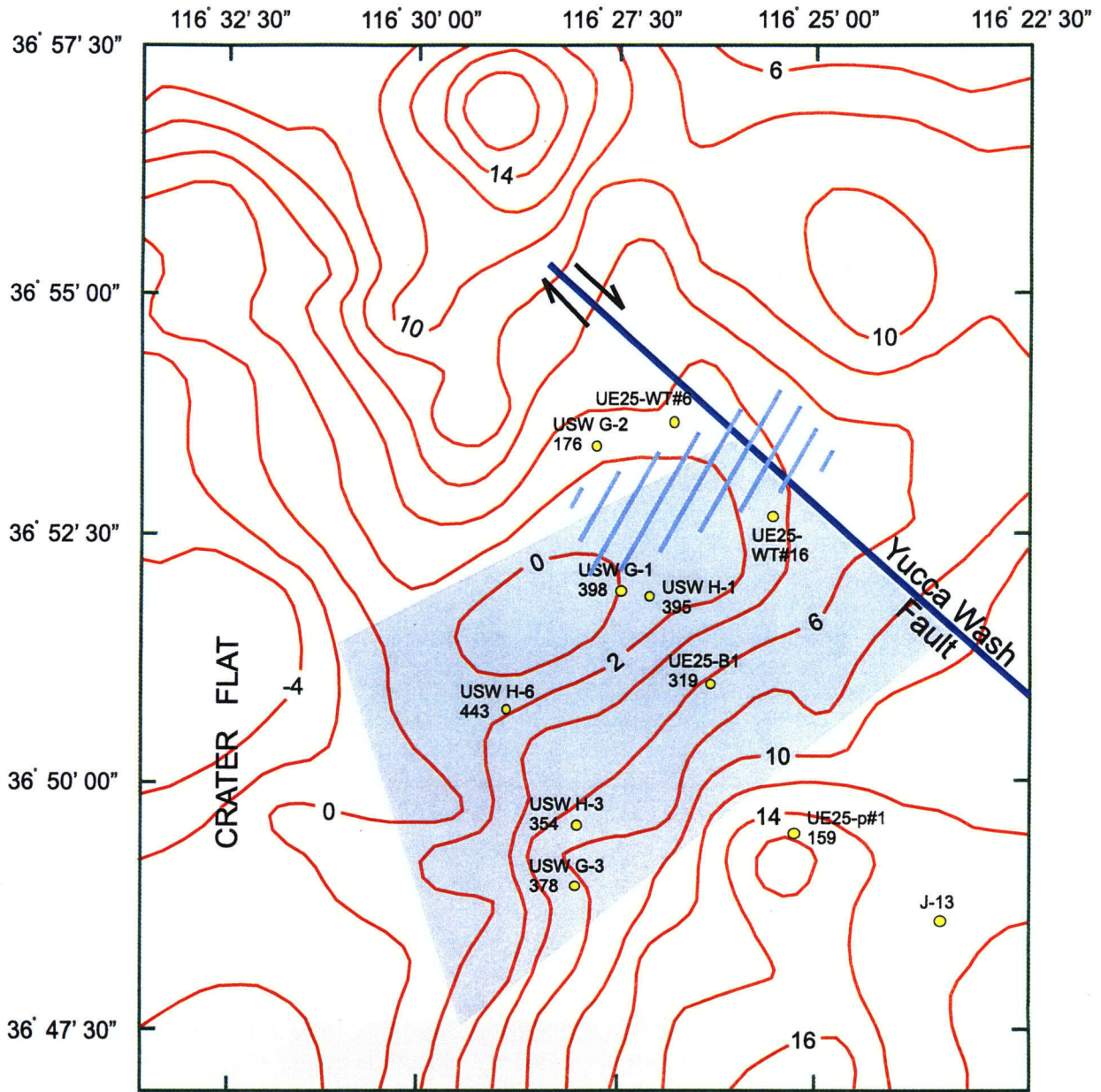
Gravity investigations in the YM and surrounding regions have been discussed in Healey and Miller (1971), Snyder and Carr (1984), Harris et al. (1986), Brocher et al. (1990, 1993), and Majer et al. (1996). Oliver et al. (1995) summarized some of the more salient aspects of these works.

According to Ponce and Oliver (1995), the three most significant gravity anomalies in the immediate vicinity of YM are (i) the northwestward decrease of approximately 20 mGal across YM, (ii) the sharp westward increase in gravity of about 30 mGal at the west side of Crater Flat, and (iii) the configuration and extent of the gravity low to the north of YM centered over the Silent Canyon caldera.

Several structural models were proposed to explain the gravity data in the immediate vicinity of YM. Snyder and Carr (1982, 1984) modeled the northwestward gravity decrease across YM as a 3–4-km-deep caldera extending from the repository area to Bare Mountain. Seismic studies by Hoffman and Mooney (1983) indicated a depth to basement of approximately 3.2 km, which appears to be in agreement with the depth reported by Snyder and Carr (1982, 1984). A tectonic model attributed to Fox by Ponce and Oliver (1995) also proposed to explain this observed decrease in gravity. The model assumes the existence of an east-dipping master detachment fault near the western edge of Bare Mountain, a listric normal fault forming the eastern face of Bare Mountain, and a west-dipping YM detachment terminating below Crater Flat. From a hydrogeologic perspective, the tectonic model is interesting because the faults provide possible pathways for the exchange of groundwater (and heat) between aquifer units as well as the establishment of hydrologic barriers caused by the juxtaposition of permeable and impermeable units, and impermeable fault gouge materials (see section 4.3).

As part of a hydrogeologic analysis, Fridrich et al. (1994) modeled the residual gravity field (see figure 4-15; Snyder and Carr, 1982) in the region of the northwest gravity decrease. Their model defined a graben in the dense Paleozoic rocks just south of the large hydraulic gradient zone that is filled with low-density Tertiary volcanic rocks. The throw of the trough was estimated to be approximately 0.5 km (Fridrich et al., 1994) (figure 4-16). Fridrich et al. (1994) conjectured that the proximity of this graben to the large hydraulic gradient appears to suggest the graben may be responsible, in part, for the observed gradient. Recent information collected at wells G-2 (see figure 4-16) and WT-24 (south of G-2) suggests possible perching of groundwater at various locations above the low-permeability Calico Hills formation, which occurs both within and north of this trough over the northern limits of the trough. Figure 4-16 indicates a significant hydraulic head drop within the Calico Hills formation. How these observations relate to the graben model is not well understood.

The gravity low under central YM has been interpreted by Spengler and Fox (1989) as an extensional axis covered by the older part of the volcanic section. Subsurface stratigraphic data collected at six bore holes drilled into the volcanic units in the area of the gravity low provide data that appear to support this interpretation. These drill holes identify volcanic sections approximately 50–100 percent thicker than those encountered in drill holes north and south of the gravity low. Moreover, the amount of stratigraphic thickening of the deep volcanic section into the area of the gravity low appears consistent with the 0.5 km estimate for the offset of the Paleozoic-Tertiary contact into the buried graben calculated from the gravity data.






-  Contour interval 2 mGals
-  Graben structure
-  Region of large hydraulic gradient

Figure 4-15. Map of the residual gravity field in the vicinity of Yucca Mountain; units in mGal. Data points represent thicknesses from the top of the Tram Member of the Crater Flat Tuff to the top of the Lithic Ridge Tuff, based on well data; units in meters. Note LHG represents Large Hydraulic Gradient [taken from Fridrich et al. (1994) and based on Snyder and Carr (1982)]

The results of a gravity survey, consisting of twelve lines, performed by Lawrence Berkeley National Laboratory along the eastern flanks of YM have been reported by Majer et al. (1996). In the survey, particular attention was given to areas where the gravity lines crossed mapped faults to determine whether the gravity anomalies can be used to place constraints on the location and amount of offset on the faults. In addition to indicating possible offsets across the GDF and Dune Wash faults, as well as other faults located near Boundary Ridge, the data showed a negative anomaly (maximum deviation equal to 1 mGal) extending over a distance of a few hundred meters from the BRF. Majer et al. (1996) conjectured that this is not the type of anomaly typical of a simple change in density across a fault, but is more suggestive of a zone of low density along the fault. The cause of this zone is currently unknown, but it may represent a damage zone around the fault with an enhanced secondary porosity or some other form of alteration. The former model is intriguing since it would provide potential fast pathways for groundwater flow. It is unclear whether this zone extends down into the SZ. The survey also located other anomalous structures that still have to be interpreted. Whether these features are of hydrological significance (i.e., whether they form significant barriers or conduits to groundwater flow) remains to be determined.

The north-south survey lines along the eastern flank of YM display residual gravity anomalies, characterized by an initial general negative trend in the anomaly toward the north followed by an interval of almost constant values (Majer et al., 1996). This negative trend appears consistent with the map of Snyder and Carr (1982) and discussions presented by Fridrich et al. (1994).

Fortymile Wash

Gravity measurements in Fortymile Wash have been discussed in Ponce et al. (1992) and Oliver et al. (1995). Fortymile Wash is associated with a gravity low that may be reflective of a deep basin filled with a significant thickness of alluvial material. Lipman and McKay (1965) suggested that Fortymile Wash is a fault-controlled structure. Since the Lipman and McKay assertions, several gravity surveys were conducted in the region to determine its structure. The largest gravity anomaly (approximately 2 mGal) identified in the vicinity of Fortymile Wash is the Paintbrush Canyon fault located on the west side of Fran Ridge. Models of the gravity data across this fault indicate an offset of approximately 180–240 m (Ponce and Oliver, 1995).

Gravity data collected within Fortymile Wash do not appear to support the presence of a major fault system beneath Fortymile Wash unless movement occurred between rocks of similar density (Ponce and Oliver, 1995). Several nearby faults have been mapped, however. In the vicinity of Fran Ridge, gravity and electrical studies identified several small displacement faults along the east side of the wash (Hoover et al., 1982; Ponce et al., 1992). Additional gravity anomalies were identified south of Busted Butte, near Fortymile Wash. It is of interest to note that one of the gravity lines of Ponce et al. (1992) that crossed Fortymile Wash immediately north of well J-12 (a zone of high transmissivity) did not detect any significant structural features. This suggests that the high-transmissivity zones identified at J-12 and J-13 are not caused by deformation associated with normal or reverse faulting. Whether the gravity anomalies identified south of Busted Butte represent faults or density changes within the alluvium requires further study.

North of Fran Ridge, gravity studies, supported by electromagnetic and seismic studies, in Fortymile Wash located a linear anomaly that appears continuous over approximately 2 km and correlates to the location of a fault mapped by Lipman and McKay (1965).

Amargosa Desert

Gravity investigations in the Amargosa Desert have been discussed in Healey and Miller (1971), Brocher et al. (1990), and Morin et al. (1998).

Healey and Miller (1971) developed three 2D cross sections based on coarse gravity data to infer the basement structure beneath the alluvial fill of the Amargosa Desert. Because of the coarseness of the data set only large-scale structures can be interpreted. Further, as pointed out by Oatfield and Czarnecki (1991), depth estimates presented in this model may be questionable because of the lack of reliable bulk density estimates for the alluvium in the Amargosa Desert. Nonetheless, the model proposed by Healey and Miller (1971) is of qualitative value. The cross-sections of Healey and Miller (1971) extended from (i) the Funeral Mountains to Striped Hills, (ii) the Funeral Mountains to Skeleton Hills, and (iii) the southern part of the Funeral Mountains to the northwest trending mountain belt southwest of Ash Meadows. The cross-sections showed the Amargosa Desert to be bounded on the east and west by high angle faults with displacements of several hundred meters. In addition to the basin bounding faults, a third fault was identified west of Ash Meadows. Whether this fault results in fluid exchanges between shallow and deep aquifers, thus influencing observed discharge processes and hydrochemistries in the Ash Meadows region (see section 4.4), requires further study. The cross-sections also demonstrate considerable variation in the depth to the pre-Cenozoic basement. The shallowest depth, of approximately a few hundred meters, occurs in the region of the Amargosa Desert gravity high, while depths of 1 km are observed in other locations. The spatial variation in the depth to the pre-Cenozoic basement reflects, in part, spatial variations in the thicknesses of post-Cenozoic units and may indicate varying thicknesses in aquifer and aquitard units that are important for groundwater flow modeling.

The results of a combined gravity and seismic survey (see also Young et al., 1992) performed south of the town of Amargosa Valley, between U.S. Route Nos. 373 and 160, and extending from the Amargosa Desert into Amargosa Flat have been discussed by Brocher et al. (1990, 1993). A model of the subsurface geology produced by a joint interpretation of the two data sets showed the topography of the basement fill-basement interface to be complex, with several basement highs identified (figure 4-17). A normal fault located along the western portion of the line appears to represent the eastern limit of the Amargosa Desert basin, whereas the eastern limit of the Amargosa Flat basin appears to coincide with a normal fault located along the eastern section of the line. In general, modeled Tertiary and post-Tertiary thicknesses along the line show considerable variability, with maximum thicknesses of about 1 km occurring along the western portion of the line. The model shows considerable thinning of some units within the pre-Tertiary basement. Whether thinning of these units promotes upward flow from the underlying aquifers into the overlying Tertiary and post-Tertiary units is not known. Gravity data have also been collected by CNWRA staff along a westward extension of this survey line, extending into the Amargosa Desert. Preliminary models of these gravity data indicate the presence of a fault-bounded basin beneath the central portion of the Amargosa Desert, the basement of which appears to be deformed by a number of extensional faults. The hydrogeologic significance of these faults, particularly those near the Ash Meadows discharge area, requires further study. Preliminary depth estimates along the eastern part of this line are consistent with those reported by Brocher et al. (1990, 1993), with shallowing of the basin occurring to the west.

A model of the Amargosa Desert based on a 3D inversion of gravity data has been developed by Morin et al. (1998). The model describes the Amargosa Desert as being underlain by a deep, steep-sided trough that varies in width from 15 to 20 km. The pre-Cenozoic basement of this trough, which is more than likely composed of carbonate rocks overlain by cessions of volcanic and sedimentary deposits, appears topographically complex. Because carbonate rocks are important aquifers in the region, the authors proposed

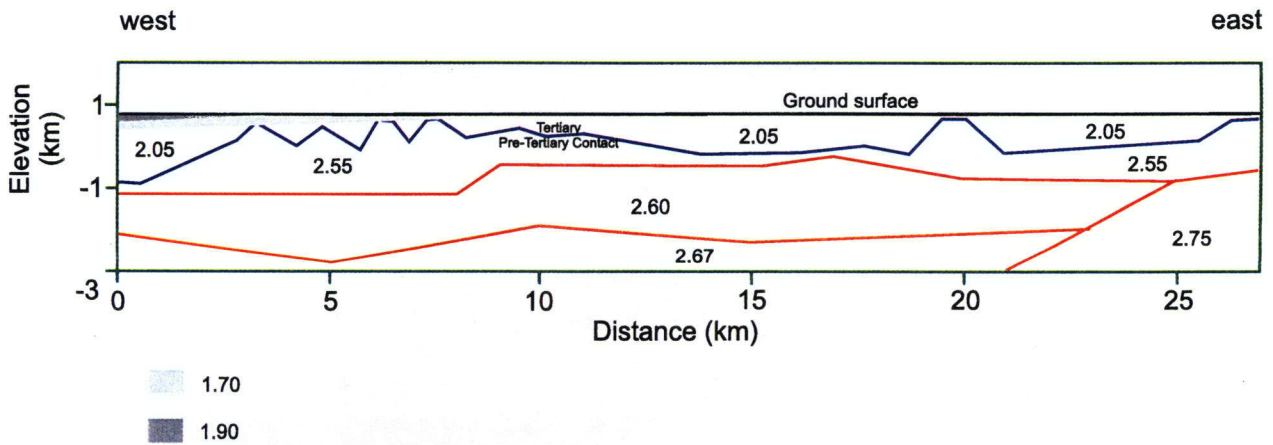
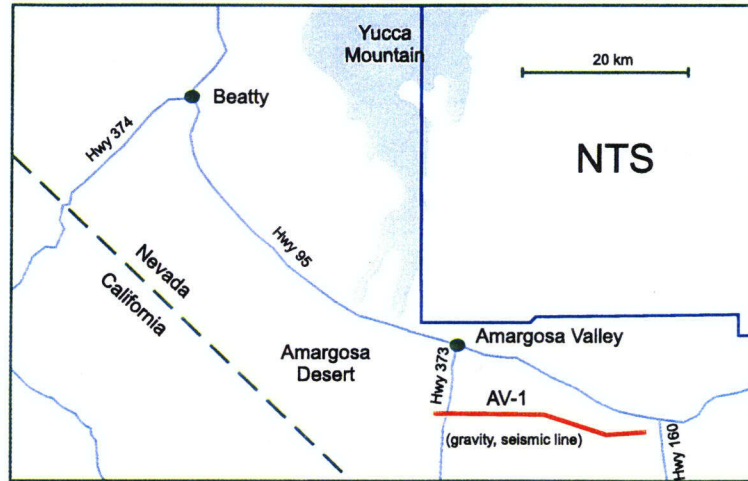


Figure 4-17. Subsurface model developed from gravity and seismic data collected along geophysical line AV-1 located south of the town of Amargosa Valley. Numbers on the figure represent densities; units in g/cm^3 [taken from Brocher et al. (1990)].

that the 3D aspects of the basement would strongly impact groundwater flow paths and transport rates. For example, they argue that the deeper parts of the Amargosa Desert trough, or faults that bound the western margin of the trough, interrupt the carbonate aquifer and thus may impede westward flow. If this is the case, they further argue that water discharging at Ash Meadows originates entirely from the carbonate flow system north and northeast of Ash Meadows, whereas water discharging at Furnace Creek originates from the volcanic flow path north and northwest of Furnace Creek.

4.5.3 Magnetic Studies

Magnetic methods essentially map variations in the magnetic intensities of stratigraphic units. From a hydrogeological perspective the magnetic data is important because it helps to define structural features at multiple scales, such as fault and lithologic block geometries, that may impact groundwater flow and are essential in the development of groundwater flow models. Within the YMR magnetic studies have been performed both on the local and regional scale. Regional scale studies traditionally have been performed using aeromagnetic surveys (Kane and Bracken, 1983; Kane et al., 1981; Langenheim et al., 1991), whereas local scale studies are commonly performed using ground-magnetic surveys (Ponce et al., 1992; Magsino et al., 1998). This section summarizes the findings of these studies and discusses their potential importance to structural controls on groundwater flow.

4.5.3.1 Discussions of Magnetic Data

Regional aeromagnetic maps for southern Nevada show a broad northwest trending magnetic high that traverses Wahmonie, the Calico Hills, the northern third of YM, and the Prospector Pass caldera. Across YM, the magnitude of this magnetic anomaly is approximately 100 to 250 nT. This anomaly is more than likely due to magnetite bearing units within the Eleana Formation being juxtaposed against carbonate units to the south. Analyses of the anomaly along the eastern edge of YM indicate the depth of contact between these units to be approximately 2.2 km (Oliver et al., 1995). Fridrich et al. (1994) compared existing aeromagnetic data to the water table data for YMR and demonstrated that the region of high hydraulic gradient, located between UE-25 wt#16 and UE-25 wt#6 north of YM, appeared to coincide with the location of the magnetic anomaly, thus indicating that the high-hydraulic gradient may be influenced by this contact.

Ground magnetic studies across the GDF identified a magnetic low centered approximately 15 m east of the fault, flanked by a distinctive high to the east (Oliver et al., 1994), that is indicative of possible down drop to the west. Models of these data indicated a possible tabular loss of magnetic remanence penetrating the normally polarized Topopah Spring Tuff. This may represent a zone of alteration or brecciation within the fault zone, or a shallow reversely polarized body within the fault plane such as a dike or mineralized zone with a greater reverse polarization than the Tiva Canyon Tuff (Oliver and Sikora, 1994). Because the anomaly along this fault has still to be determined, the hydrologic significance of this zone is not fully understood. The brecciation model, however, does appear consistent with the discussions presented in section 4-3.

CNWRA staff recently performed a number of north-south traverses along Fortymile Wash in an effort to map the tuff-alluvium interface along the wash. The survey lines were designed so lithologic data from wells J-13, J-12, JF-3, NC-EWDP-2D, NC-EWDP-Washburn-1X, and NC-EWDP-5S could be used to constrain modeling efforts. Preliminary models of this survey indicate a gradual pinch-out of the Tiva Canyon Tuff beneath the wash as well as a deepening of the alluvial deposits beyond well JF-3, which appears consistent with existing gravity data for the wash. The most obvious implication of this model is that

it provides a mechanism for estimating the location where the water table transitions from the tuff units into the alluvium, which is important for PA.

Magnetic data indicate the previously inferred position of the BRF may be incorrect (Oliver et al., 1995). In some locations, a 100-m displacement to the west may be required. Magnetic data further indicate the presence of a significant anomaly at shallow depth just north of UE-25 wt#6. The maximum depth to the top of this source has been estimated at 100 m (Oliver et al., 1995).

A number of magnetic anomalies have been identified within the Amargosa Desert (Langenheim et al., 1993; Magsino et al., 1998; Connor and Sanders, 1994). Several of these anomalies are shown in Connor and Sanders (1994, figure 7-4). These anomalies are recognized by their dipolar character, indicating they are the result of shallow, aurally restricted magnetized bodies. Currently, little information is available on the possible impacts these localized anomalies may have on the hydrogeology of the Amargosa Desert region.

4.5.4 Electrical Resistivity Studies

Electrical methods essentially map subsurface variation in electrical resistivity (or conductivity). Variations in subsurface electrical conductivity may result from changes in soil moisture content, changes in pore fluid chemistry, and changes in mineralogy. From a hydrogeological perspective the electrical data are important because they help define structural features at multiple scales, such as fault and lithologic block geometries, that may impact groundwater flow and are essential in the development of groundwater flow models. Within the YMR, electrical studies were performed both on the local and regional scale. Several have been used in the YMR to determine subsurface resistivities. These techniques include Schlumberger sounding and more sophisticated techniques, such as electromagnetic soundings, telluric soundings, and magnetotelluric soundings. This section summarizes the findings of these studies and discusses their potential importance to structural controls on groundwater flow.

4.5.4.1 Magnetotelluric Surveys

Magnetotelluric studies may be used to address the following issues related to structural controls on groundwater flow: (i) patterns of deep, conductive, hydrologic zones, as revealed by probable fault or fracture patterns of aquifers and aquitards; (ii) the extent and orientation of high-angle fault zones; and (iii) the extent of low-angle middle Tertiary extensional faults. Magnetotelluric surveys were conducted within the YMR during 1965–86. To date, little attention has been paid to the potential hydrological importance of the magnetotelluric data collected in the vicinity of YM. In this section, an attempt is made to infer the hydrological importance of this data set.

On the regional scale, the magnetotelluric data presented by Furgerson (1982) indicate a dominant west-northwest electrical strike that may be indicative of anisotropy in the electrical conductivity. This strike parallels the general trend of faults and fractures in the Walker Lane belt. The observed trend may be explained because it reflects considerable alteration of materials along and adjacent to regional faults. This alteration may result in an increased electrical conductivity of the altered materials. Another explanation discussed by Klein (1995) is that the observed electrical conductivity anisotropy may be caused by the presence of fluids with anomalously high TDS along the faults and fractures. Such zones may develop as a result of increased fracture porosity and fracturing along fault zones. Yet another explanation proposed by

Klein (1995) is that there may be one or two major discontinuities in resistivity within the region that (i) may parallel the primary axis of the conductivity anisotropy and (ii) may be fault controlled.

The Furgerson (1982) magnetotelluric data also indicate electrical conductivity zones that strike northeast. Klein (1995) suggests these anomalous strikes may reflect the superimposed influence of structures along the Walker Lane belt and structures that trend northeast across the Walker Lane belt such as north-northeast striking tectonic zones described by Carr (1984). Mechanisms similar to those described previously may be responsible for the enhanced electrical conductivity. Whether this information may be used to support anisotropy of material properties pertinent to groundwater flow in the YM area is not immediately clear and warrants further investigation. The orientation of the strike however, is consistent with fracture orientations reported for the YM site.

Magnetotelluric surveys have also been used to map lithologic units in the YMR (Klein, 1995). These studies identified several electrical resistivity layers which collectively extend to a depth of approximately 16 km. From a hydrological perspective, the most important of these layers are the low-resistivity (10 to 100 ohm-m) surficial layer that varies in depth 0.5–2.0 km, and an upper crustal zone of variable thickness and resistivity (50–500 ohm-m), which extends to a depth of between 4 km and 12 km (Klein, 1995). The low-resistivity surficial unit has been interpreted as a mixture of unconsolidated sedimentary units, volcanic rocks, and weathered zones in the Paleozoic bedrock of Bare Mountain, whereas the upper crustal zone has been interpreted as a combination of volcanic and Proterozoic and Paleozoic units (Klein, 1995). These definitions appear vague and may reflect some degree of subjectivity. Within the upper crustal zone, the lower resistivity units (50–150 ohm m) have been interpreted as volcanic rocks (Klein, 1995). The combined vertical depth of these zones may define the lower extent of the active regional flow system.

Preliminary work aimed at using magnetotelluric surveys to characterize hidden faults and geological heterogeneities at YM has been reported by Majer et al. (1996). The survey line used for this study extended in a northwest direction and crossed both the BRF and GDF as well as bore hole USW H-4. Since interpretation of this data appears preliminary, no discussion of these preliminary results is provided here.

4.5.4.2 Telluric Studies

Telluric studies conducted in the YMR consisted of two east-west telluric lines that extended from the YM area, across Fortymile Wash and into Jackass Flats, and two additional east-west lines located south of the town of Amargosa Valley. Line 1 of the survey was located approximately 0.6 km to the north of well J-13 and approximately 3 km south of line 2. Within Fortymile Wash, the surveys identified four north-south zones of low relative telluric voltages indicative of low earth resistivity, two on either side of the wash (figure 4-18a). These were interpreted as fault zones by Hoover et al. (1982), who hypothesized that the lower resistivity in these zones probably results from increased porosity due to fracturing along and adjacent to possible faults. If this hypothesis is indeed true, then this deformation may in part be responsible for the enhanced transmissivities observed within Fortymile Wash. The higher resistivity segments between the lows reflect more competent lower porosity rock (Hoover et al., 1982). If the assertions of Lipman and McKay (1965) are true (Fortymile Wash is fault controlled) and J-13 is assumed to lie within a graben, the two centered faults interpreted on the telluric profiles would define the Fortymile Wash graben (Hoover et al., 1982). Hoover et al. (1982) further asserted that based on the telluric data, sediment thickness within the graben should be rather thin. This assertion is supported by drill hole logs at J-13 (Hoover et al., 1982). The western most of these faults appears to coincide with the known location of Paintbrush Fault. Lines 1 and 2 also indicate a general decrease in telluric voltage to the west with significant steepening in some locations.

Hoover et al. (1982) correlated this steepening of the gradient to the steep gravity gradient across YM and indicated that the cause of this behavior may be due to thickening of the tuff units toward the west.

The telluric survey line immediately north of the town of Amargosa Valley (figure 4-18b) identified a number of contrasting telluric responses (Hoover et al., 1982). West of point 6E on line L-N, low telluric voltages are observed, whereas immediately east of this location higher responses occur. This response has been interpreted to represent carbonate rocks to the east juxtaposed with alluvium, and possible volcanics, to the west. This juxtaposition is coincident with the location of the Gravity fault. The declining trend further east is assumed to represent a thickening of the Tertiary volcanics toward the east. Possible faulting between points 1W and 3E along line L-N may also be inferred from the data, however, the presence of a fault in this location is not supported by other geophysical data in the region.

Telluric line L-S south of the town of Amargosa Valley (figure 4-18b) is virtually coincident with the AV-1 line used for gravity and seismic surveying in the region (see section 4.5.2.1). Along this line, the rapid change in resistivity observed near point 12 correlates to the location of the Gravity fault. The decline in resistivity toward the eastern end of this line correlates with a decline in Bouguer gravity along line AV-1 (see section 4.5.2.1) and is likely due to thickening of the saturated alluvium and Tertiary volcanic units in the Amargosa Flat basin.

4.5.4.3 Electromagnetic and Standard Resistivity Surveys

Flanigan (1981) described the application of the Slingram electromagnetic technique to investigate whether or not north-trending valleys in the YMR were fault controlled. The results of the surveys indicated that some of the northwest-trending valleys contained electromagnetic conductors that may be related to fracturing and faulting. Furthermore, the amplitude of the estimated conductivity values indicated a low electrical conductivity contrast between the fracture zones and the surrounding rocks, leading to the conclusion that the increase in porosity around faults may be small.

Time-domain electromagnetic (TDEM) surveys have been performed in the YMR² (figures 19a, b). One such survey designed to map water table topography and subsurface geology was performed along a line extending from Fortymile Wash to the Amargosa Farms region. The study indicated the presence of a conductive horizon at a depth that could be traced along the entire length of the survey line. Along the ends of the survey, the depth of the conductive structure showed good correlation to the measured depth of the water table in nearby wells. In general, the water table depths appeared much shallower beneath the Amargosa Desert than in Fortymile Wash; less than 60 m beneath the Amargosa Desert compared to greater than 150 m beneath Fortymile Wash. The results of the survey further indicated that the TDS of the groundwater system appeared to increase by a factor of 2 at the southern end of the survey line over that at the northern end. This supports the assumption of Fortymile Wash being a recharge zone. The increased TDS estimated at the southern end of the line reflects the interaction of the groundwater with the rock matrix along the flow path. The results of the survey also indicate two features of geological interest. This first is the apparent thickening of alluvial sediment along the northern sections of the survey line. This apparent thickening appears consistent with models of the Fortymile Wash which indicate thick sedimentary deposits in the southern section of the wash. The second feature of interest is represented by the apparent shallowing of the low electrical conductivity zone along the southern section of the line. This feature coincides with the local extension of the gravity high that extends toward the northeast across the northern section of the

²Center for Nuclear Waste Regulatory Analyses. 1998. unpublished data.

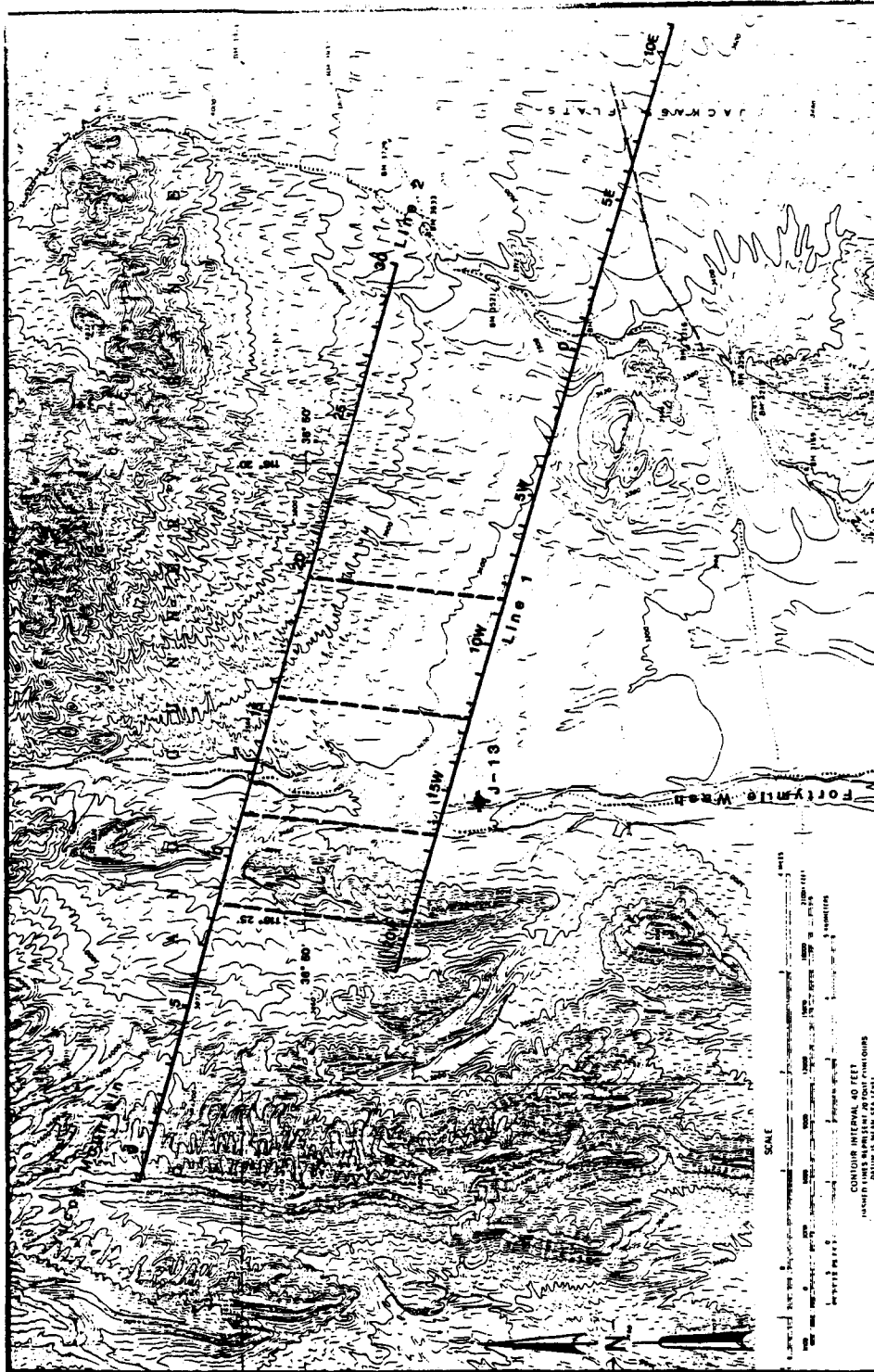


Figure 4-18a. Telluric lines 1 and 2 extending from Yucca Mountain across the northern portion of Fortymile Wash and into Jackass Flats [taken from Flanigan (1982)]

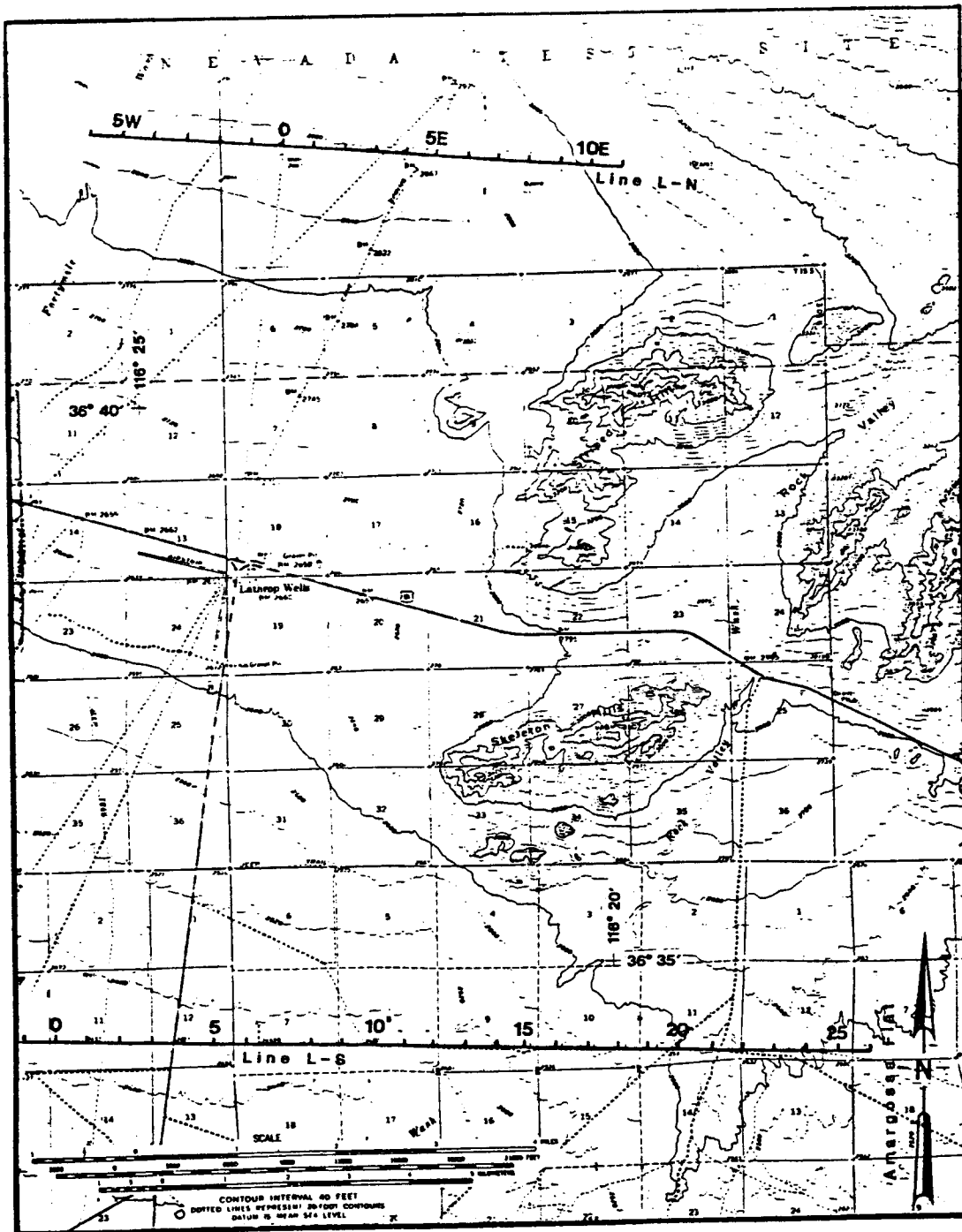
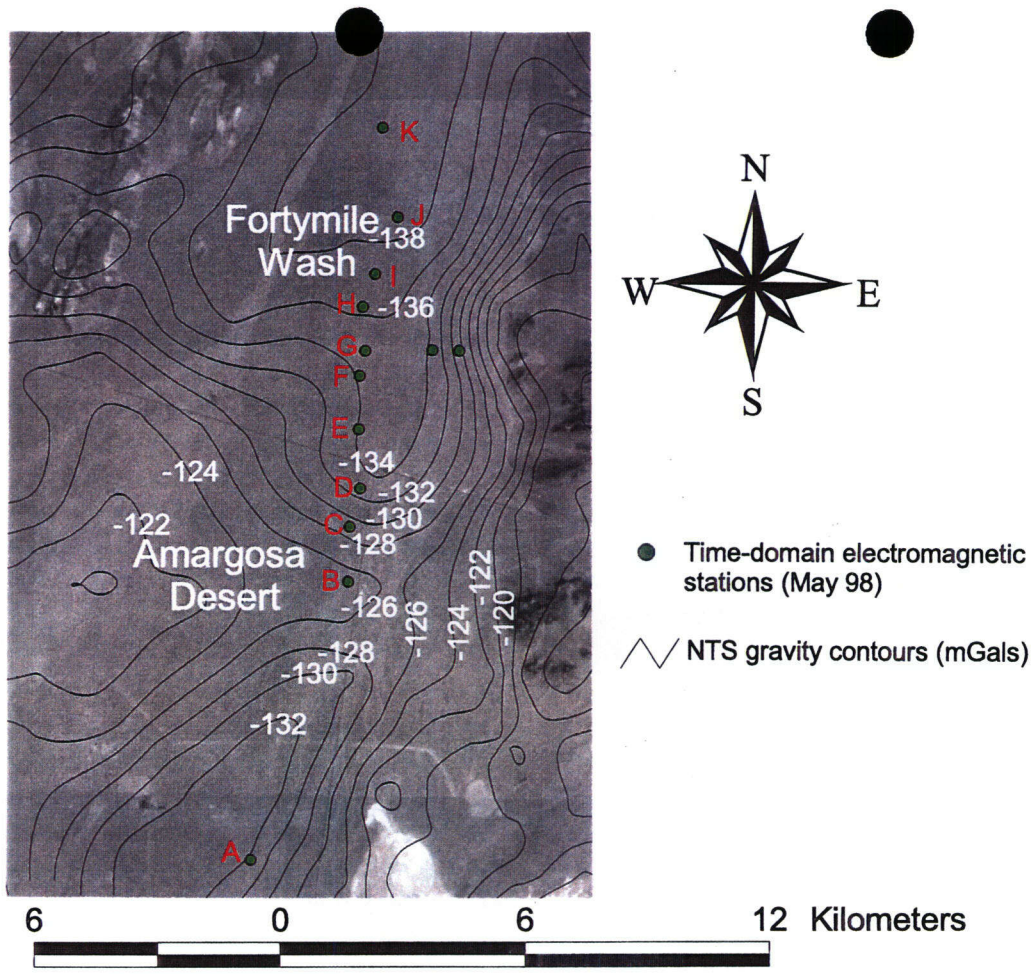
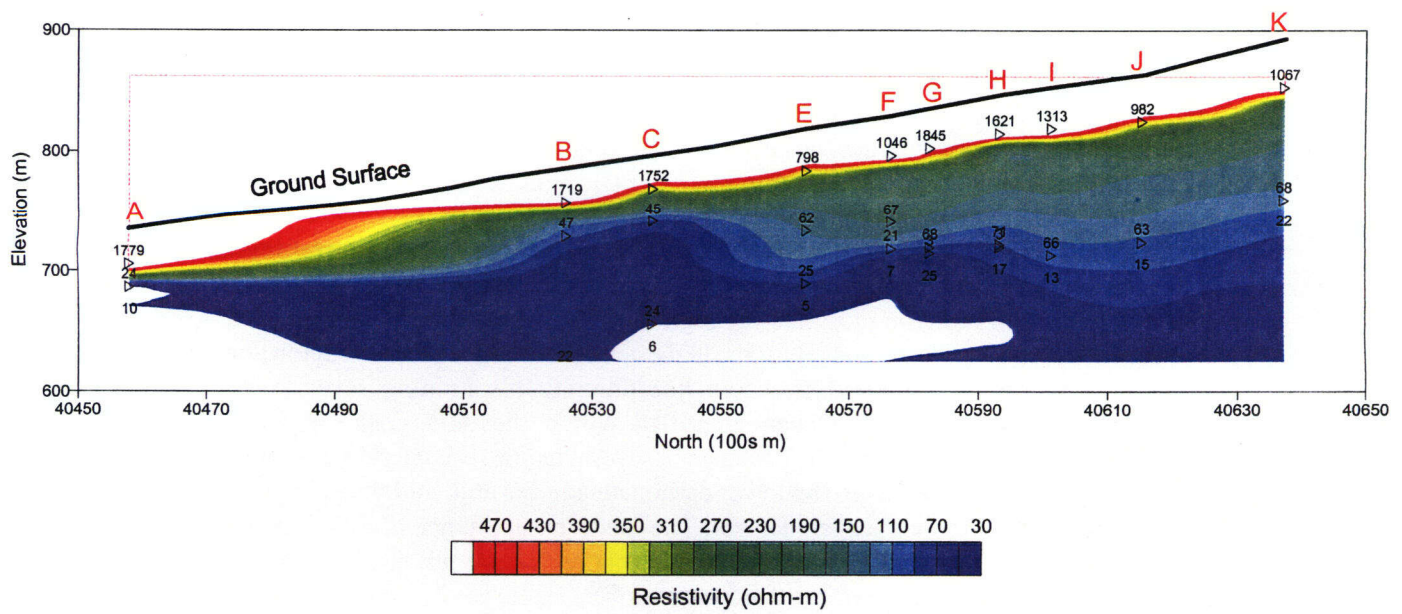


Figure 4-18b. Telluric lines 3 and 4 extending across the lower reaches of Fortymile Wash and the northern Amargosa Desert [taken from Flanigan (1982)]



(a)



(b)

Figure 4-19. (a) Electromagnetic sounding locations in Fortymile Wash and Amargosa Desert used by the Center for Nuclear Waste Regulatory Analyses (Bouguer gravity map superimposed); (b) Model based on electromagnetic data (triangles represent resistivity layer boundaries and numbers represent layer resistivities).

Amargosa Desert. Whether this feature reflects the impact of the basement high in the area on the water table is being investigated.

The shallowing trend observed in the electromagnetic data is also reflected in the Schlumberger resistivity data reported by Greenhaus and Zablocki (1982) [see also Oatfield and Czarnecki (1991)] as part of a study to define basement structure and basin-fill characteristics, which may or may not be influencing the hydrological systems of the region. Post-Paleozoic unit thicknesses in Fortymile Wash ranged between 800 and 1,200 m, while thicknesses of similar units south of the town of Amargosa Valley ranged between 200 and 800 m. Basin-fill characteristics examined in this study were found to be complex, with the fill being composed of spatially varying thicknesses (tens to hundreds of meters) of variably saturated sand, gravel, and clay units (Greenhaus and Zablocki, 1982, Appendix). This heterogeneity is also reflected in borehole data recently collected by Nye County and recent TDEM, IP and resistivity studies performed in Fortymile Wash and the Amargosa Desert.³ This heterogeneity can result in heterogeneous and bulk anisotropic flow and transport parameters within the basin fill deposits.

4.5.5 Summary of Implications of Geophysics Studies in Evaluating Structural Controls on Groundwater Flow in the Yucca Mountain Region

In the preceding, several geophysical studies for the YMR region were discussed. The geophysical studies allowed the identification of 3D structural relationships as well as 2D structural features. Thermal studies in the YMR assumed that the temperature data provided direct evidence that some block bounding faults, in particular the SCF and faults within Midway Valley, impacted groundwater flow. In fact, elevated water table temperatures in these regions attributed to warm upward flows along these faults from deeper aquifer units. Modeling studies presented in this report indicate that the observed temperature distribution may be caused by convection and conduction processes within the tuff aquifer. This contradicting result warrants a review of the existing thermal data and associated models. Gravity, magnetic, electrical, and electromagnetic studies were performed across faults within the YMR. In addition to providing estimates of possible fault displacements, some of these studies have indicated damaged or altered zones adjacent to faults that may result in modified porosities and permeabilities.

Geologic contacts pertinent to structural controls on groundwater flow have also been mapped using geophysical methods. For example, thermal, gravity, and magnetic studies have mapped structures north of the proposed repository location that appear conducive to the development of the large hydraulic gradient observed in this region. Integrated geophysical studies also were used to identify several linear features, interpreted to be possible faults, beneath Fortymile Wash that may be of significance to groundwater flow and recharge in this region. In the Amargosa Desert region, a limited number of integrated geophysical studies have been used to map large structural relations. In the central Amargosa Desert region, these surveys generally indicate that thinning of Tertiary units occurs. In addition to this thinning, several faults, some of which appear to be basin bounding, have been identified within the Amargosa Desert region. The combination of thinning of Tertiary units and the presence of several major faults within this region, provides a mechanism for possible upward flow from the lower carbonate aquifer unit, and thus provides a possible explanation for the observed hydrochemical signatures. The relative importance of these potential up-flow mechanisms and the general 3D structure of the geology in this region are not easily resolved due to the limited number of geophysical surveys performed in this region.

³Center for Nuclear Waste Regulatory Analyses. 1999. unpublished data.

Finally, due to the limited number of integrated geophysical surveys performed within the YMR, a comprehensive understanding of potential structural controls on groundwater flow is still lacking.

4.6 NUMERICAL STUDIES OF THE POTENTIAL IMPACTS OF AQUIFER ANISOTROPY AND HETEROGENEITY ON GROUNDWATER FLOW IN THE YUCCA MOUNTAIN REGION

An investigation of the potential impacts that aquifer anisotropy and large-scale heterogeneity could have on groundwater flow in the YMR has been conducted by staffs of the NRC and CNWRA. The approach used 2D numerical models designed to simulate groundwater flow in the region, considering varying degrees of anisotropy for the volcanic tuff aquifer system. It is important to note that the intent of the simulation exercise was not to develop a detailed, calibrated numerical model for the site but to demonstrate the potential impacts that issues raised in the conceptual model may have on groundwater flow and radionuclide transport at the site. Extensive new information for the saturated valley fill aquifer south of YM is being collected at this time by Nye County, Nevada. The nature of these new data, in the form of hydraulic heads and properties, stratigraphy, and water chemistry data, will probably lead to significant revisions of current flow models. The following discussion summarizes the models used in this study and the results.

The simulation domain encloses the YMR of the repository, Fortymile Wash and Jackass Flats, and the northern reaches of the Amargosa Desert north of U.S. Route 95. The periphery of the domain consists of line segments that connect wells where water surface elevations have been measured. Constant head boundary conditions were assumed for most of the exterior of the domain except along portions of the northern boundary where a specified flux was applied. The heads applied along the boundary were based on water surface elevations in peripheral wells. A linear variation in hydraulic head between wells was assumed. As is commonly the case for groundwater flow models of the YMR, steady-state conditions were assumed.

Material properties within the simulation domain were treated as spatially heterogeneous and isotropic with the exception of the tuff units, which were generally assumed anisotropic. For the tuffaceous units, the principal axis of anisotropy was assumed to vary between N0–30°E, with a value of N5°E most commonly used. This range in anisotropy is consistent with findings reported in section 4.2. Transmissivity (T) values used to represent the tuffaceous units were based on a long-term, 322-day aquifer test performed at the C-well complex by Geldon et al. (1997). Based on this test, an average T value of 1,300 m²/d was estimated. This value was used in the numerical model to represent T under isotropic conditions. For the anisotropic case, a value of 5,600 m²/d was used to represent T along the primary axis of the T ellipse. Along the minor axis, T was defined based on assumed ratios between the major and minor axes. Due to the lack of T data reported for the valley-fill aquifer south of YM, T values used in the modeling exercise varied 500 m²/d to 2,600 m²/d. The valley-fill aquifer was treated as being isotropic. Transmissivity values used to model the carbonate aquifer in the southeastern corner of the model were based on the broad range of hydraulic conductivities (5×10^{-4} to 225 m/d) provided by Czarnecki et al. (1997) and an estimated thickness of 500 m. In both the anisotropic and isotropic models, possible drain conditions in the highly permeable trough believed to exist beneath Fortymile Wash were simulated using zones of elevated T .

In the model, recharge to the SZ was assumed to occur along Fortymile Wash. Recharge estimates were based on the work of Savard (1998), who identified four recharge zones in the YM and Amargosa Desert regions: (i) Fortymile Canyon (74 m³/d), (ii) Upper Jackass Flats (3.0 m³/d), (iii) Lower Jackass Flats (45.0 m³/d), and (iv) Amargosa Desert (176 m³/d). Recharge within each zone was distributed between nodes falling within the zone. Note that recharge in the Upper Jackass Flats region was neglected in the model because it is small and unlikely to affect model results. Recharge within the Amargosa Desert

was not considered because it fell outside, or south, of the model domain. Positions of simulated equipotentials were influenced by the recharge along Fortymile Wash, although these effects were mostly eliminated in scenarios that placed a high- T drain along the wash. The potential impact on flow patterns of aerially distributed recharge from precipitation at YM also was considered in the model. For this case, a recharge rate of 10 mm/yr was used, consistent with current climatic conditions. Model results did not show major effects of this recharge from precipitation. Recharge, however, will be examined in greater detail when the models are updated with future Nye County data.

The impact of aquifer thickness on the groundwater flow system was also investigated. Recall that aquifer thickness is reflected in T estimates, where T is equivalent to hydraulic conductivity multiplied by the effective thickness of the aquifer. For this investigation, the thickness of the SZ aquifer was assumed to extend from the water table to approximately the lower half of the Tram Member of the Crater Flat Group. This is based on site data that include borehole flow surveys and analyses of rock cores that indicate below the Tram Tuff fractures are frequently filled with calcite mineralization. Also, wells USW H-1, USW H-3, and UE-25 p#1 demonstrate significant upward hydraulic gradients and the presence of an effective confining layer in the lower confining units. And finally, the C-Holes testing shows good vertical communication between the stratigraphic members of the Crater Flat Group, but the heads in the underlying Paleozoic aquifer do not appear affected by pumping in the Crater Flat Group.

The isotropic model with a drain was revised to incorporate scaled T values to represent varying aquifer thicknesses for the northwest corner of the model where thickness data were available. This model was run and the results compared to those obtained with a model that assumed constant thickness for the tuff aquifer. Only slight differences in equipotential lines were noted, showing that incorporating the detailed aquifer thickness data did not produce major changes in output.

Simulations were performed to evaluate the effects of varying degrees of anisotropy in the tuffs and varying T values in the valley-fill aquifer. Most of the anisotropic simulations assumed a principal axis of anisotropy to be oriented along N5°E. Simulations varied from isotropic conditions to varying degrees of anisotropy where T_{min}/T_{max} values of 50 percent, 20 percent, and 6 percent were used.

Preliminary conclusions based on the results of uncalibrated models are that anisotropy has the potential to alter groundwater flow paths to a more southerly direction, especially if greater degrees of anisotropy exist. It should be pointed out that the degree of anisotropy that may be present is poorly constrained. C-Holes analyses can support conditions that range from isotropic through a 6 percent value of T_{min}/T_{max} . Interestingly, the flow paths in both isotropic and anisotropic simulations appear to intersect at a distance of about 19 km from YM. The main difference is, compared to isotropic conditions, average flow paths in anisotropic simulations may be somewhat shorter and may include shorter flow paths in the saturated valley-fill aquifer. A continuum of average flow path can be envisioned based on varying degrees of anisotropy that converge on a common location south of YM. This approach should reasonably bound the set of average flow paths for consideration in PA.

Using a T_{min}/T_{max} ratio of 6 percent for the tuffs, of simulations were run using different values of T for the valley-fill aquifer. These values were 500; 1,000; 1,500; and 2,600 m²/d, with isotropic conditions assumed for the valley fill. It was found that a value of 1,000 m²/d without a central drain along Fortymile Wash produced quite low hydraulic gradients in the YM vicinity, similar to those seen in field observations. Although the model is not well calibrated, the results suggest that hydraulic properties of the valley-fill materials can have a substantial effect on water levels and gradients in the tuff aquifer system. These results

are also consistent with anecdotal reports from Nye County workers that wells along Fortymile Wash, including NC-EWDP-2D and Washburn 1-X, appear to have lower water-production potential than expected.

Based on drilling to date, the Nye County program reveals that a thick, saturated, valley-fill aquifer exists to the south of YM. The Paleozoic carbonate aquifer system has not been penetrated in any of the deep holes that have been drilled, but additional wells are planned for completion over the next 2 yr. The CNWRA staff await more detailed hydrologic information and documentation for the Nye County Wells to update the Micro-FEM models. At that time, an effort will be made to develop reasonably calibrated models to evaluate the effects of anisotropy in greater detail.

4.6.1 Summary of Implications of Numerical Studies in Evaluating Structural Controls on Groundwater Flow in the Yucca Mountain Region

In the preceding, a series of 2D numerical models was developed to examine the potential impacts of several structurally related phenomena on groundwater flow within the YMR. Since the goals of the study were to obtain a qualitative understanding of the impacts of these phenomena, rigorous calibration of the models to existing data was not performed. A primary finding of the study was that, for transmissivity anisotropies similar to those presented in section 4.2, groundwater flow directions were rotated in a more southerly direction compared to the isotropic case developed based on field observed data. Despite this rotation, flow paths computed under both assumptions eventually converged away from YM, with the anisotropic models producing the shortest flow paths to the point of convergence. This result is significant because it implies potentially shorter simulation times to receptor locations. This result suggests that an understanding of the anisotropic properties of the tuff aquifers is essential for accurate simulation of the hydraulic field in the YMR and, ultimately, to better estimate radionuclide doses to members of the critical group located at receptor locations. A second significant finding of the study was that model performance, in particular the hydraulic heads and gradients in the tuff aquifers, appeared sensitive to the hydraulic properties of the valley-fill aquifer. This sensitivity, which may result in model calibration difficulties, stresses the need for reliable hydraulic parameter estimates for the valley-fill sediments.

5 SUMMARY AND CONCLUSIONS

In an effort to evaluate possible structural controls on groundwater flow in the YMR, the CNWRA and the NRC assembled a multidisciplinary working group to review available hydrogeological, geophysical, hydrochemical, and structural geological data for the region. In addition to the review, the working group was encouraged to demonstrate, where possible, the potential impacts of their findings on groundwater flow in the region using simple flow models. In a future study, the impacts on the total system performance measure [i.e., annual total effective dose (TEDE) to an average member of the postulated critical group will also be evaluated]. This report summarizes the state of the information regarding structural control of groundwater flow.

The information included in this study indicate that groundwater flow within the YMR is impacted to varying degrees by existing structural features. Limited data for the region, however, do not allow for a comprehensive understanding of many of these impacts. Nonetheless, it is clear that in some localities, faults and fracture zones appear to provide pathways through which fluids may be exchanged between aquifer systems. Some of the regions where such exchanges occur appear to be delineated by thermal and hydrochemical data. Elevated temperatures at the water table have been interpreted as upwelling of warm waters along faults from deeper aquifer units. Although individual measurements represent local phenomena, collectively these data appear to indicate that, at the site-scale, some faults are capable of transmitting water along their entirety. Examples of such faults are the Solitario Canyon fault and faults within Midway Valley. Recent modeling exercises, however, indicate that this argument in support of upwelling may be questionable in light of the fact that similar temperature distributions at the water table may be produced by thermal convection and conduction. Flow along faults also has been proposed to explain the hydrochemistry of groundwater within the vicinity of YM. For example, Fridrich et al. (1994) proposed that the pattern of $\delta^{13}\text{C}$ observed within the volcanic units results from upwelling of groundwater along faults that intersect the Paleozoic aquifer.

Geophysical data collected along fault zones appear to indicate the existence of disturbed or altered zones adjacent to faults. In most cases, in-depth characterization of these zones has not been performed, and arguments related to their structure are, at best, speculative. Structural arguments for these zones range from brecciation to other forms of alteration. Brecciation models suggest the existence of zones of enhanced porosity, and perhaps permeability, adjacent to faults. Using such a model, it is possible for upwelling of fluids, recharge, and preferential lateral flow to occur. However, whether these near-surface observations extend to the depth of the SZ is not clear and requires further study.

Recent studies along the SCF found altered materials within the disturbed zone, which were identified as smectites. This result is significant because the low permeability of smectites can reduce the rate of groundwater flow across the fault. Further, because smectites may be formed by warm water contacting volcanic rocks, smectites along the SCF appear qualitatively consistent with upwelling of warm water from the underlying carbonate aquifer along the fault. It is of interest to note that the presence of saturated smectites within fault zones can also lead to enhanced electrical conductivities. Because the smectite observations are localized, it is difficult to generalize this conclusion to the entire length of the SCF. If smectites do occur along the entire length of the SCF then from a groundwater flow perspective, it is important to assess the thicknesses and spatial continuity of the smectite alteration zones. At this time, limited data precludes determining whether alteration products, such as smectites, occur along most faults in the region.

The information presented in this report show that, within the YMR, bulk transmissivities in the tuff units can be interpreted as anisotropic with the orientation of the primary axis being approximately N 33° E. This orientation appears to be consistent with fault and fracture orientations inferred from tuff units within this region and with predictions based on analyses of the regional stress field that indicate a strong likelihood for northeastwardly oriented fractures to be open and hydraulically transmissive. This suggests that existing fault and fracture orientations may exert strong influences on groundwater flow patterns within the tuff units. Although the transmissivity anisotropy ratio is poorly constrained, numerical studies demonstrate that it can result in a more southerly groundwater flow within the tuff units. This southerly flow may result in shorter travel distances through the alluvial deposits to receptor locations than currently envisioned. Such a scenario would reduce radionuclide transport times and diminish the overall effectiveness of the alluvial deposits as a natural attenuation mechanism. This emphasizes the need for accurate estimation of the transition zone between the tuff and alluvial units and in particular the zone where the water table transitions from the tuff units into the alluvium. In Fortymile Wash, this transition zone appears to be between Well JF-3 and the new Nye County well, Washburn IX. With the completion of Nye County Wells NC-EWDP-20D and NC-EWDP-10S on the NTS, and interpretation of magnetic and electromagnetic data collected in Fortymile Wash, the location of the transition zone will be constrained better. Little information currently exists with respect to the flow and transport properties of the alluvial materials. In the mathematical simulations reported in this report, crude, uniform estimates were used to represent the transmissivity of the alluvial unit. These simulations indicated that calibration of groundwater flow models for the YMR are sensitive to the hydraulic properties assigned to the alluvium. Recent drilling by Nye County and field studies by the CNWRA, however, have shown the alluvial deposits in the vicinity of YM to be heterogeneous. This heterogeneity may result in groundwater flow channeling that may impact estimates of radionuclide travel time to receptor locations.

Finally, although structural relationships have been used to gain a better understanding of some of the hydrogeological features observed at the site (e.g., the high hydraulic gradient region north of YM), structural data necessary for constructing 3D numerical models are limited for key areas along the flow path, such as Fortymile Wash and the Amargosa Desert region. For example, in Fortymile Wash, the existence of competing structural models based on geophysical and geological data precludes development of a single comprehensive conceptual model. It is clear, however, that structural features within this zone account for the observed high transmissivity and recharge. Interpretations of the limited geophysical data for the Amargosa Desert indicate a complex geology composed of variable unit thicknesses and potential faults. From the perspective of numerical modeling, an understanding of these layer thicknesses is a necessity. Within this region, extensive mixing of groundwater may be inferred based on hydrochemical data. Two causes of this mixing have been identified, one due to convergence of laterally flowing groundwater systems and the other due to upwelling waters from deeper aquifer units interacting with water present in the alluvial aquifer system. The upwelling observed may reflect either a thinning of units, faulting and fracturing, or other discontinuities.

Understanding of structural controls on groundwater flow can be enhanced by

- (i) Better definition the stratigraphy and hydrostratigraphy, as well as the hydraulic and transport properties of the alluvial units south of YM
- (ii) Establishing the hydraulic properties of the tuff aquifers using pump test and fracture data
- (iii) Evaluating the role of deformed zones around faults to determine under what conditions these zones may act as conduits or barriers to groundwater flow

- (iv) Correcting hydrochemical data to identify and constrain groundwater flow paths
- (v) Improved definition of large-scale structural relationship between hydrostratigraphic units in the vicinity of YM
- (vi) Evaluating appropriateness of the assumption of isothermal flow at YM

It should be noted that the primary regulatory reason for studying the effects of structural controls on groundwater flow at YM is to evaluate the eventual effect on potential annual dose to a receptor group located approximately 20 km from the proposed repository. Groundwater flow provides the primary pathway for transport of radionuclides from the engineered barriers of the repository to the receptor group. To delineate the relative importance of the various factors listed in the previous paragraph, a study to estimate the sensitivity of the total system performance to these factors needs to be undertaken. The current NRC/CNWRA sensitivity studies (Nuclear Regulatory Commission, 1999) indicate that the sorption processes in the alluvium part of flow path can play a significant role in moderating the estimated dose. Similar sensitivity studies, including the other factors such as hydraulic anisotropy, major faults, background thermal regime, and fracture distributions will be conducted in a future study.

6 REFERENCES

- Ahola, M.P., and B. Sagar. 1992. *Regional Groundwater Modeling of the Saturated Zone in the Vicinity of Yucca Mountain, Nevada—Iterative Performance Assessment, Phase 2*. NUREG/CR-5890. Washington, DC: Nuclear Regulatory Commission.
- Anderson, E.M. 1951. *The Dynamics of Faulting*. Edinburgh: Oliver & Boyd, Ltd.
- Barton, C.A., M.D. Zoback, and D. Moos. 1995. Fluid flow along potentially active faults in crystalline rock. *Geology* 23(8): 683–686.
- Bedinger, M.S., K.A. Sargent, and W.H. Langer. 1989. *Studies of Geology and Hydrology in the Basin and Range Province, Southwestern United States, for Isolation of High-level Radioactive Waste—Characterization of the Death Valley Region, Nevada and California*. USGS Professional Paper 1370–F. Denver, CO: U.S. Geological Survey.
- Benson, L.V., and P.W. McKinley. 1985. *Chemical Composition of Ground Water in the Yucca Mountain Area, Nevada, 1971–84*. USGS Open-File Report 85–484. Denver, CO: U.S. Geological Survey.
- Bredehoeft, J.D. 1997. Fault permeability near Yucca Mountain. *Water Resources Research* 33: 2,459–2,463.
- Brocher, T.M., M.D. Carr, K.F. Fox, Jr., and P.E. Hart. 1993. Seismic reflection profiling across Tertiary extension structures in the eastern Amargosa Desert, southern Nevada Basin and Range province. *GSA Bulletin* 105: 30–46.
- Brocher, T.M., P.E. Hart, and S.F. Carle. 1990. *Feasibility Study of the Seismic Reflection Method in Amargosa Desert, Nye County, Nevada*. USGS Open-File Report 89-133. Menlo Park, CA: U.S. Geological Survey.
- Byerlee, J.D. 1978. Friction of rocks. *Pure and Applied Geophysics* 116: 615–626.
- Caine, J.S., and C.B. Forster. 1999. Fault zone architecture and fluid flow. *Insights from field data and numerical modeling. Faults and Subsurface Fluid Flow*. Handberg et al., eds. Washington, DC: American Geophysical Union.
- Caine, J.S., J.P. Evans, and C.B. Forster. 1996. Fault zone architecture and permeability structure. *Geology* 24: 1,025–1,028.
- Carlsson, A., and T. Olsson. 1979. Hydraulic conductivity and its stress dependence. *Proceedings of the 1979 Workshop Low-Flow, Low-Permeability Measurements in Largely Impermeable Rocks*. Paris, France: 249–259.
- Carr, W.J. 1984. *Regional Structural Setting of Yucca Mountain, Southwestern Nevada, and Late Cenozoic Rates of Tectonic Activity in Part of the Southwestern Great Basin, Nevada and California*. USGS Open-File Report 88–854. Denver, CO: U.S. Geological Survey.

- Carr, M.D. 1990. Styles of extension in the Nevada Test Site region, southern Walker Lane Belt—An integration of volcano-tectonic and detachment fault models. Basin and Range Extensional Tectonics near the Latitude of Las Vegas, Nevada. B.P. Wernicke, ed. *Geological Society of America Memoir* 176: 283–303.
- Carr, M.D., S.J. Waddell, G.S. Vick, J.M. Stock, S.A. Monsen, A.G. Harris, B.S. Cork, and F.M. Byers, Jr. 1986. *Geology of Drill Hole UE-25 p#1: A Test Hole to Pre-Tertiary Rocks near Yucca Mountain, Southern Nevada*. USGS Open-File Report 86–175. Denver, CO: U.S. Geological Survey.
- Castagna, J. 1996. Exploration questions: the sequel. *The Leading Edge*: January.
- Chester, F.M., and J.M. Logan. 1986. Composite planar fabric of gouge from the Punchbowl fault, California. *Journal of Structural Geology* 9: 621–634.
- Claassen, H.C. 1985. *Sources and Mechanisms of Recharge for Ground Water in the West-Central Amargosa Desert, Nevada—A Geochemical Interpretation*. USGS Professional Paper 712–F. Washington, DC: U.S. Geological Survey.
- Clayton, R.W., W.P. Zelinski, and C.A. Rautman. 1997. *ISM2.0: A 3-D geologic framework and integrated site model of Yucca Mountain, Rev 00*. Las Vegas Nevada: Civilian Radioactive Waste Management System Management and Operating Contractor.
- Cohen, A.J.B., C.M. Oldenburg, A.M. Simmons, A.K. Mishra, and J. Hinds. 1997. *S⁴Z: Sub-site Scale Saturated Zone Model for Yucca Mountain*. Ernest Orlando, Level 4 Milestone SP25UM4. Berkeley, CA: Lawrence Berkeley National Laboratory.
- Connor, C.B., and C.O. Sanders. 1994. *Geophysics review topical report: Applications of seismic tomographic and magnetic methods to issues of basaltic volcanism*. CNWRA94-013. San Antonio, TX: Center for Nuclear Waste Regulatory Analyses.
- Cowen, D.S., and R.L. Bruhn. 1992. Late Jurassic to early Cretaceous geology of the U.S. Cordillera. *The Cordilleran Orogen: Conterminous U.S., The Geology of North America Volume G-3*. B.C. Burchfiel, P.W. Lipman, and M.L. Zoback, eds. Boulder, CO: Geological Society of America, Inc. 205–260.
- Craig, H. 1961. Isotopic variations in meteoric waters. *Science* 133: 1,702–1,703.
- Crider, J.G., and D.D. Pollard. 1998. Fault linkage: Three-dimensional mechanical interaction between echelon normal faults. *Journal of Geophysical Research* 103: 24,373–24,391.
- Czarnecki, J.B. 1985. *Simulated Effects of Increased Recharge on the Ground-water Flow System of Yucca Mountain and Vicinity, Nevada-California*. USGS Water-Resources Investigations Report 84–4344. Denver, CO: U.S. Geological Survey.
- Czarnecki, J.B. 1989. Characterization of the subregional ground-water flow system at Yucca Mountain and vicinity, Nevada-California. *Radioactive Waste Management and the Nuclear Fuel Cycle* 13: 51–61.

- Czarnecki, J.B., and R.K. Waddell. 1984. *Finite-element Simulations of Groundwater Flow in the Vicinity of Yucca Mountain, Nevada-California*. USGS Water-Resources Investigations Report 84-4349. Denver, CO: U.S. Geological Survey.
- Czarnecki, J.B., C.C. Faunt, C.W. Gable, and G.A. Zyvoloski. 1997. *Hydrogeology and Preliminary Three-Dimensional Finite-Element Ground-Water Flow Model of the Site-Saturated Zone, Yucca Mountain, Nevada*. SP23NM3. Denver, CO: U.S. Geological Survey.
- D'Agnese, F.A., C.C. Faunt, A.K. Turner, and M.C. Hill. 1997. *Hydrogeological Evaluation and Numerical Simulation of the Death Valley Regional Groundwater Flow System, Nevada and California, Using Geoscientific Information Systems*. USGS Water-Resources Investigations Report 96-4300. Denver, CO: U.S. Geological Survey.
- Dalziel, I.W.D. 1996. Neoproterozoic-Paleozoic geography and tectonics: Reviews, hypothesis, environmental speculation. *Geological Society of America Bulletin* 109: 16-42.
- Davison, M.L., D.K. Smith, J. Kenneally, and T.P. Rose. 1999. Isotope hydrology of southern Nevada groundwater: Stable isotopes and radiocarbon. *Water Resources Research* 35: 1,279-1,294.
- Day, W.C., C.J. Potter, D. Sweetkind, R.P. Dickerson, and C.A. San Juan. 1998a. *Bedrock Geologic Map of the Central Block Area, Yucca Mountain, Nye County, Nevada: Scale 1:6000*. U.S. Geological Survey Miscellaneous Investigations Series Map I-2601. Reston, VA: U.S. Geological Survey.
- Day, W.C., R.P. Dickerson, C.J. Potter, D.S. Sweetkind, C.A. San Juan, R.M. Drake, II, and C.J. Fridrich. 1998b. *Geologic map of the Yucca Mountain Area, Nye County, Nevada, Scale 1:24,000*. Geological Investigations Series I-2627. Reston, VA: U.S. Geological Survey.
- Dudley, W.W., and J.D. Larson. 1976. *Effect of Irrigation Pumping on the Desert Pupfish Habitat in Ash Meadows, Nye County, Nevada*. Reston, VA: Geological Survey Professional Paper 927.
- Ervin, E.M., R.R. Luckey, and D.J. Burkhardt. 1993. Summary of revised potentiometric-surface map for Yucca Mountain and vicinity, Nevada. *Proceedings of the Fourth Annual International Conference on High-Level Radioactive Waste Management, Las Vegas, Nevada, April 26-30, 1993*. La Grange Park, IL: American Nuclear Society: 1,554-1,558.
- Ervin, E.M., R.R. Luckey, and D.J. Burkhardt. 1994. *Revised Potentiometric-Surface Map, Yucca Mountain and Vicinity, Nevada*. USGS Water-Resources Investigations Report 93-4,000. Denver, CO: U.S. Geological Survey.
- Evans, J.P., C.B. Forster, and J.V. Goddard. 1997. Permeability of fault-related rocks, and implications for hydraulic structure of fault zones. *Journal of Structural Geology* 19: 1,393-1,404.
- Fabryka-Martin, J.T., A.V. Wolfsberg, S.S. Levy, K. Campbell, P. Tseng, J.L. Roach, and L. Wolfsberg. 1998. *Evaluation of Flow and Transport Models of Yucca Mountain, Based on Chlorine-36 Studies for FY98*. Yucca Mountain Project Milestone Report SP33DDM4. Los Alamos, NM: Los Alamos National Laboratory.

- Faulds, J.E., J.W. Bell, D.L. Feuerbach, and A.R. Ramelli. 1994. *Geologic map of the Crater Flat Area, Nevada*. Nevada Bureau of Mines and Geology Map, Scale 1:24,000.
- Feeney, T.A., M.E. Campana, and R.L. Jacobson. 1987. *A Deuterium-Calibrated Groundwater Flow Model of the Western Nevada Test Site and Vicinity*. Water Resources Publication 45057/DOE/NV/10384-16. Reno, NV: Desert Research Institute.
- Ferrill, D.A., G.L. Stirewalt, D.B. Henderson, J.A. Stamatakos, K.H. Spivey, and B.P. Wernicke. 1996a. *Faulting in the Yucca Mountain Region, Critical Review and Analyses of Tectonic Data from the Central Basin and Range*. NUREG/CR-6401. Washington, DC: Nuclear Regulatory Commission.
- Ferrill, D.A., J.A. Stamatakos, S.M. Jones, B. Rahe, H.L. McKague, R.H. Martin, and A.P. Morris. 1996b. Quaternary slip history of the Bare Mountain Fault (Nevada) from the morphology and distribution of alluvial fan deposits. *Geology* 24: 559-562.
- Ferrill, D. A., A. P. Morris, S. M. Jones, and J. A. Stamatakos. 1998. Extensional layer-parallel shear and normal faulting. *Journal of Structural Geology* 20: 355-362.
- Ferrill, D. A., J.A. Stamatakos, and D. Sims. 1999a. Normal fault corrugation: Implications for growth and seismicity of active normal faults. *Journal of Structural Geology*. In press.
- Ferrill, D.A., J.R. Winterle, G. Wittmeyer, D. Sims, S. Colton, and A. Armstrong. 1999b. Stressed rock strains groundwater at Yucca Mountain, Nevada. *GSA Today* 9 (5): 2-8.
- Ferrill, D.A., A.P. Morris, J.A. Stamatakos, and D.A. Sims. 1999c. Crossing conjugate normal faults. *American Association of Petroleum Geologist*.
- Caine, J.S., and C.B. Forster. 1999. Fault zone architecture and fluid flow. *Insights from field data and numerical modeling. Faults and Subsurface Fluid Flow*. Handberg et al., eds. Washington, DC: American Geophysical Union.
- Finkbeiner, T., C.A. Barton, and M.D. Zoback. 1997. Relationships among *in-situ* stress, fractures and faults, and fluid flow: Monterey formation, Santa Maria Basin, California. *American Association of Petroleum Geologist Bulletin* 81(12): 1,975-1,999.
- Flanigan, V.J. 1981. *A Slingram Survey at Yucca Mountain on the Nevada Test Site*. USGS Open-File Report 81-980 Denver, CO: U.S. Geological Survey.
- Fleck, R.J., B.D. Turrin, D.A. Sawyer, R.G. Warren, D.E. Champion, M.R. Hudson, and S.A. Minor. 1996. Age and character of basaltic rocks of the Yucca Mountain region, southern Nevada. *Journal Geophysical Research* 101: 8,205-8,227.
- Fridrich, C.J. 1998. *Tectonic Evolution of the Crater Flat Basin, Yucca Mountain Region, Nevada, Cenozoic Basins of the Death Valley Region*. USGS Open-File Report 98-33. Denver, CO: U.S. Geological Survey: 43.
- Fridrich, C.J., W.W. Dudley, Jr., and J.S. Stuckless. 1994. Hydrogeologic analysis of the saturated-zone ground-water system, under Yucca Mountain, Nevada. *Journal of Hydrology* 154:133-168.

- Frizzel, V.A., and J. Shulters. 1990. *Geologic Map of the Nevada Test Site, southern Nevada. Scale 1:100,000*. U.S. Geological Survey Miscellaneous Investigations Series Map I-2046.
- Furgerson, R.B. 1982. *Remote-reference magnetelluric survey, Nevada Test Site and vicinity, Nevada and California*. With an introduction by D.B. Hoover. USGS Open-File Report 82-465. Denver, CO: U.S. Geological Survey.
- Geldon, A.L. 1993. *Preliminary Hydrologic Assessment of Boreholes UE-25C #1, UE-25C #2. Yucca Mountain, Nye County, Nevada*: U.S. Geological Survey Water-Resources Investigations Report 92-4016. Las Vegas, NV. U.S. Geological Survey.
- Geldon, A.L., A.M.A. Umari, M.F. Fahy, J.D. Earle, J.M. Gemmel, and J. Darnell. 1997. *Results of Hydraulic and Conservative Tracer Tests in Miocene Tuffaceous Rocks at the C-Hole Complex, 1995 to 1997, Yucca Mountain, Nevada*. Milestone Report SP23PM3. Las Vegas, NV: U.S. Geological Survey.
- Geldon, A.L., A.M.A. Umari, J.D. Earle, M.F. Fahy, J.M. Gemmel, and J. Darnell. 1998. *Analysis of a Multiple-Well Interference Test in Miocene Tuffaceous Rocks at the C-Hole Complex, May-June, 1995, Yucca Mountain, Nye County, Nevada*. Water Resources Investigations Report 94-4166. Denver, CO: U.S. Geological Survey.
- Geomatrix Consultants, Inc., and TRW Environmental Safety, Inc. 1998. *Saturated Zone Flow and Transport Expert Elicitation Project*. WBW 1.2.5.7. San Francisco, CA: U.S. Department of Energy.
- Goddard, J.V., and J.P. Evans. 1995. Chemical changes and fluid-rock interactions in faults of crystalline thrust sheets, northwestern Wyoming, U.S.A. *Journal of Structural Geology* 17: 533-547.
- Gray, M.B., J.A. Stamatakos, and D.A. Ferrill. 1998. Microstructural and microtextural analyses of faulting at Yucca Mountain, Nevada. *EOS, Transactions of the American Geophysical Union* 79 (45): F823.
- Greenhaus, M.R., and C.J. Zablocki. 1982. *A Schlumberger Resistivity Survey in the Amargosa Desert, Southern Nevada*. USGS Open-File Report 82-897. Denver, CO: U.S. Geological Survey.
- Harmsen, S. C. 1994. The Little Skull Mountain earthquake of 29 June 1992: Aftershock focal mechanisms and tectonic stress field implications. *Bulletin of the Seismological Society of America* 84: 1,484-1,505.
- Harrill, J.R., J.S. Gates, and J.M. Thomas. 1988. *Major Ground-Water Flow Systems in the Great Basin Region of Nevada, Utah, and Adjacent States*. USGS Hydrologic Investigations Atlas HA-694-C. Denver, CO: U.S. Geological Survey.
- Harris, R.N., H.W. Oliver, and D.L. Healey. 1986. Structural implications of an isostatic residual gravity map of the Nevada Test Site, Nevada: *EOS, Transactions of the American Geophysical Union* 67(44): 262.
- Healey, D.L., and C.H. Miller. 1971. *Gravity Survey of the Amargosa Desert Area of Nevada and California*. USGS Open-File Report 474-136. Denver, CO: U.S. Geological Survey.

- Heizler, M.T., T.I. Wilch, and J. Stroud. 1997. $^{40}\text{Ar}/^{39}\text{Ar}$ dating of basalts younger than 100 ka. *EOS, Transactions of the American Geophysical Union* 78(46): F771.
- Hoffman, L.R., and W.D. Mooney. 1983. *A Seismic Study of Yucca Mountain and Vicinity, Southern Nevada; Data Report and Preliminary Results*. USGS Open-File Report 83-588. Denver, CO: U.S. Geological Survey.
- Hoover, D.B., M.P. Chornack, and M.M. Broker. 1982. *E-Field Ratio Telluric traverses near Fortymile Wash, Nevada Test Site, Nevada*. USGS Open-File Report 82-1042. Denver, CO: U.S. Geological Survey.
- Horsfield, W.T. 1980. Contemporaneous movement along crossing conjugate normal faults. *Journal of Structural Geology* 2: 305-310.
- Hudson, M.R., D.A. Sawyer, and R.G. Warren. 1994. Paleomagnetism and rotation constraints for the Miocene southwestern Nevada volcanic field. *Tectonics* 13: 258-277.
- Jaeger, J. C., and N. G. W. Cook. 1979. *Fundamentals of Rock Mechanics* (3rd Edition). London, United Kingdom: Chapman and Hall.
- Kane, M.F., and R.E. Bracken. 1983. *Aeromagnetic Map of Yucca Mountain and Surrounding Regions, Southwest Nevada*. USGS Open-File Report 83-616. Reston, VA: U.S. Geological Survey.
- Kane, M.F., M.W. Webring, and B.K. Bhattacharyya. 1981. *A preliminary analysis of gravity and aeromagnetic surveys of the Timber Mountain area, southern Nevada*. USGS Open-File Report 81-189. Reston, VA: U.S. Geological Survey.
- Klein, D.P. 1995. Regional magnetotelluric investigations in H.W. Oliver, D.A. Ponce, and W.C. Hunter, eds., *Major Results of Geophysical Investigations at Yucca Mountain and Vicinity, Southern Nevada*. USGS Open File Report 95-74. Reston, VA: U.S. Geological Survey.
- Krantz, R.W. 1988. Multiple fault sets and three-dimensional strain: theory and application. *Journal of Structural Geology* 10: 225-237.
- Lachenbruch, A.H., and J.H. Sass. 1977. Heat flow in the United States and the thermal regime of the crust. The Earth's Crust. J.G. Heacock, ed. *Geophysical Monograph* 20: 626-675. Washington, DC: American Geophysical Union.
- Langenheim, V.E., S.F. Carle, D.A. Ponce, and J.D. Phillips. 1991. *Revision of an Aeromagnetic Survey in the Lathrop Wells Area, Nevada*. USGS Open-File Report 91-46. Reston, VA: U.S. Geological Survey.
- Langenheim, V.E., K.S. Kirchoff-Stein, and H.W. Oliver. 1993. Geophysical investigations of buried volcanic centers near Yucca Mountain, southwest Nevada. *Proceedings of the Fourth Annual International Conference on High Level Radioactive Waste Management 2*: La Grange, IL: American Nuclear Society. 1,840-1,846.

- Lehman, L.L., and T.P. Brown. 1995. An alternative conceptual model for the saturated zone at Yucca Mountain, Nevada. *Proceedings of Waste Management '95*. Tucson, AZ.
- Lehman, L.L., and T.P. Brown. 1996. *Summary of State of Nevada—Funded Studies of the Saturated Zone at Yucca Mountain, Nevada*. Las Vegas, NV: L. Lehman & Associates, Inc.
- Levy, S. S., D.S. Sweetkind, J.T. Fabryka-Martin, P.R. Dixon, J.L. Roach, L.E. Wolfsberg, D. Elmore, and P. Sharma. 1997. *Investigations of Structural Controls and Mineralogic Associations of Chlorine-36 Fast Pathways in the ESF*: Los Alamos Milestone SP2301M4. Los Alamos, NM: Los Alamos National Laboratory.
- Lichtner, P.C., and M.S. Seth. 1998. Two-phase nonisothermal coupled thermal-hydrologic-chemical flow simulator. *MULTIFLO User's Manual. MULTIFLO Version 1.2β*. San Antonio, TX: Center for Nuclear Waste Regulatory Analyses.
- Lipman, P.W., and E.J. McKay. 1965. *Geological Map of the Topopah Spring SW Quadrangle, Nye County, Nevada*. U.S. Geological Survey Geologic Quadrangle Map GQ-439, Scale 1:24,000.
- Luckey, R.R., P. Tucci, C.C. Faunt, E.M. Ervin, W.C. Steinkampf, F.A. D'Agnesse, and G.L. Patterson. 1996. *Status of Understanding of the Saturated-Zone Ground-Water Flow System at Yucca Mountain, Nevada, as of 1995*. USGS Open-File Report 96-4077. Denver, CO: U.S. Geological Survey.
- Lundstrom, S.C., J.B. Paces, and S.A. Mahan. 1998. Late Quaternary history of Fortymile Wash in the area near the H-road crossing. *Quaternary Geology of the Yucca Mountain Area, Southern Nevada*. E.M. Taylor, editor. Friends of the Pleistocene: Pacific Cell. 64-66.
- Magsino, S.L., C.B. Connor, B.E. Hill, J.A. Stamatakos, P.C. La Femina, D.A. Sims, and R.A. Martin. 1998. *CNWRA ground magnetic surveys in the Yucca Mountain region, Nevada (1996-1997)*. CNWRA 98-001. San Antonio, TX: Center for Nuclear Waste Regulatory Analyses.
- Majer, E.L., L. Johnson, K. Lee, T. Daley, E. Karageorgi, P. Parker, T. Smith, K. Williams, A. Romero, and T. McEvelly. 1996. *Milestone OBB02: Results of Geophysical Surveys along the North-South and South ESF Alignment; Milestone OBB03: Summary Report: Interpretation of Multiple Geophysical Surveys*. Berkeley, CA: Orlando Lawrence Berkeley National Laboratory.
- McKague, H.L., J.A. Stamatakos, and D.A. Ferrill. 1996. *Type I faults in the Yucca Mountain region*. CNWRA 96-007. San Antonio, TX: Center for Nuclear Waste Regulatory Analyses.
- Minor, S.A., M.R. Hudson, and C.J. Fridrich. 1997. *Fault-Slip Data, Paleomagnetic Data, and Paleostress Analyses Bearing on the Neogene tectonic Evolution of Northern Crater Flat Basin, Nevada*. USGS Open-File Report 97-285. Denver, CO: U.S. Geological Survey: 41p.
- Moore, D.M., and R.C. Reynolds. 1989. *X-ray Diffraction and the Identification and Analysis of Clay Minerals*. Oxford, England: Oxford University Press.
- Morin, R.L., R.J. Blakey, E.H. McKee, K.M. Schmidt, V.E. Langenheim, and G.L. Dixon. 1998. Three-dimensional model of pre-Cenozoic basement beneath Amargosa Desert and Pahrump Valley,

California and Nevada: Implications for tectonic evolution and water resources. *EOS, Transactions of the American Geophysical Union*: Supplement 79(45).

Morris, A.P., D.A. Ferrill, and D.B. Henderson. 1996. Slip tendency analysis and fault reactivation. *Geology* 24: 275–278.

National Research Council. 1996. *Rock Fractures and Fluid Flow*. Washington, DC: National Academy Press.

Nicol, A., J.J. Walsh, J. Watterson, and P.G. Bretan. 1995. Three-dimensional geometry and growth of conjugate normal faults. *Journal of Structural Geology* 17: 847–862.

Nuclear Regulatory Commission. 1999. *NRC Sensitivity and Uncertainty Analyses for a Proposed HLW Repository at Yucca Mountain, Nevada, Using TPA 3.1*. NUREG-1668, Volume 2. Washington, DC: U.S. Nuclear Regulatory Commission.

Oatfield, W.J., and J.B. Czarnecki. 1991. Hydrogeologic inferences from driller's logs and from gravity and resistivity surveys in the Amargosa Desert, southern Nevada. *Journal of Hydrology* 24: 131–158.

Oliver, H.W., and R.F. Sikora. 1994. *Gravity and Magnetic Data Across the Ghost Dance Fault in WT-2 Wash, Yucca Mountain, Nevada*. USGS Open-File Report 94–413–A. Denver, CO: U.S. Geological Survey.

Oliver, H.W., E.L. Majer, and R.W. Spengler. 1994. Geophysical Investigations of the Ghost Dance Fault, Yucca Mountain, Nevada [abs]. *Geological Society of America, Cordilleran Section Meetings, Abstracts with Programs* 26(2): 78.

Oliver, H.W., D.A. Ponce, and H.R. Blank. 1995. Magnetic investigations. *Major Results of Geophysical Investigations at Yucca Mountain and Vicinity, Southern Nevada*. H.W. Oliver, D.A. Ponce, and W.C. Hunter, eds. USGS Open File Report 95–74, Reston, VA: U.S. Geological Survey.

Papadopoulos, I.S. 1965. Nonsteady flow to a well in an infinite anisotropic aquifer. International Symposium of Scientific Hydrology. *Proceedings, Dubrovnik Symposium on the Hydrology of Fractured Rocks*. 21–31.

Peacock, D.C.P., and D.J. Sanderson. 1994. Geometry and development of relay ramps in normal fault systems. *American Association of Petroleum Geologists Bulletin* 78: 147–165.

Peterman, Z.E., and J.S. Stuckless. 1993. Isotopic evidence of complex ground-water flow at Yucca Mountain, Nevada, USA. *Proceedings of the Fourth Annual International Conference on High-Level Radioactive Waste Management*. La Grange Park, IL: American Nuclear Society: 1,559–1,566.

Plume, R.W. 1996. *Hydrogeologic Framework of the Great Basin region of Nevada, Utah, and Adjacent States*. U.S. Geological Survey Professional Paper 1409–B. Washington, DC: U.S. Geological Survey.

- Ponce, D.A., and H.W. Oliver. 1995. Gravity investigations. *Major Results of Geophysical Investigations at Yucca Mountain and Vicinity, Southern Nevada*. H.W. Oliver, D.A. Ponce, and W.C. Hunter, eds. USGS Open File Report 95-74. Reston, VA: U.S. Geological Survey.
- Ponce, D.A., S.B. Kohn, and S. Waddell. 1992. *Gravity and Magnetic Data of Fortymile Wash, Nevada Test Site, Nevada*. USGS Open-File Report 93-343. Denver, CO: U.S. Geological Survey.
- Prave, A.R. 1999. Two diamictites, two caps carbonates, two $\delta^{13}\text{C}$ excursions, two rifts: The Neoproterozoic Kingston Peak Formation, Death Valley, California. *Geology* 27: 339-342.
- Rice, W.A. 1984. *Preliminary Two-Dimensional Regional Hydrologic Model of the Nevada Test Site and Vicinity*. SAND83-7466. Albuquerque, NM: Sandia National Laboratories.
- Robison, J.H. 1984. *Structure of pre-Cenozoic Rocks in the Vicinity of Yucca Mountain, Nye County, Nevada—A Potential Nuclear-Waste Disposal Site: U.S. Geological Survey Bulletin 1647*. Las Vegas, NV: U.S. Geological Survey.
- Rush, F.E. 1970. *Regional Ground-Water Systems in the Nevada Test Site Area, Nye, Lincoln, and Clark Counties, Nevada*. Water Resources Reconnaissance Series Report 54. Las Vegas, NV: Nevada Department of Conservation and Natural Resources.
- Sadler, W.R., M.E. Campana, R.L. Jacobson, and N.L. Ingraham. 1992. *A Deuterium-Calibrated, Discrete-State Compartment Model of Regional Groundwater Flow, Nevada Test Site and Vicinity*. Water Resources Publication 45088/DOE/NV/10845-09. Reno, NV: Desert Research Institute.
- Sass, J.H., and A.H. Lachenbruch. 1982. *Preliminary Interpretation of Thermal Data from the Nevada Test Site*. USGS Open-File Report 82-973. Reston, VA: U.S. Geological Survey.
- Sass, J.H., A.H. Lachenbruch, and C.W. Maze. 1980. *Analysis of Thermal Data from Drill Holes UE25a-3 and UE25a-1, Calico Hills and Yucca Mountain, Nevada Test Site*. USGS Open-File Report 80-826. Reston, VA: U.S. Geological Survey.
- Sass, J.H., A.H. Lachenbruch, W.W. Dudley, Jr., S.S. Priest, and R.J. Munroe. 1988. *Temperature, Thermal Conductivity, and Heat Flow near Yucca Mountain, Nevada: Some Tectonic and Hydrologic Implications*. USGS Open-File Report 87-649. Denver, CO: U.S. Geological Survey.
- Sass, J.H., W.W. Dudley, Jr., and A.H. Lachenbruch. 1995. Regional thermal setting. *Major Results of Geophysical Investigations at Yucca Mountain and Vicinity, Southern Nevada*. H.W. Oliver, D.A. Ponce, and W.C. Hunter, eds. USGS Open File Report 95-74. Reston, VA: U.S. Geological Survey.
- Savard, C.S. 1994. Ground-water recharge in Fortymile Wash near Yucca Mountain, Nevada. *Proceedings High Level Radioactive Waste Management of the Fifth Annual International Conference*. Las Vegas, NV: American Nuclear Society. 1,805-1,813.
- Savard, C.S. 1998. *Estimating Ground-Water Recharge from Streamflow in Fortymile Wash near Yucca Mountain, Nevada*. USGS Water-Resources Investigations Report 97-4273. Denver, CO: U.S. Geological Survey: p. 30.

- Sawyer, D.R., R.J. Fleck, M.A. Lanphere, R.G. Warren, D.E. Broxton, and M.R. Hudson. 1994. Episodic caldera volcanism in the Miocene southwestern Nevada volcanic field: Revised stratigraphic framework, $^{40}\text{Ar}/^{39}\text{Ar}$ geochronology, and implications for magmatism and extension. *Geological Society of America Bulletin* 106: 1,304–1,318.
- Schoff, S.L., and J.A. Moore. 1964. *Chemistry and Movement of Ground Water, Nevada Test Site*. USGS Open-File Report TEI-838. Washington, DC: U.S. Geological Survey.
- Schweickert, R.A., and M.M. Lahren. 1997. Strike-slip fault system in Amargosa Valley and Yucca Mountain, Nevada. *Tectonophysics* 272: 25–41.
- Scott, R.B. 1990. *Tectonic Setting of the Yucca Mountain Region, Southwest Nevada*. Geological Society of America Memoir 176. Boulder, CO: Geological Society of America: 251–282.
- Scott, R.B., and J. Bonk. 1984. *Preliminary Geologic Map of Yucca Mountain, Nye County, Nevada with Geologic Sections*. Scale 1:12000. USGS Open-File Report 84-494. Denver, CO: U.S. Geological Survey:
- Seront, B., W. Fong, J.S. Caine, C.B. Forster, and R.L. Bruhn. 1998. Laboratory characterization of hydrodynamical properties of a seismogenic normal fault system. *Journal of Structural Geology* 20: 86–881.
- Sibson, R.H. 1977. Fault rocks and fault mechanisms. *Geological Society of London Journal* 133: 191–231.
- Simonds, W. F., J.W. Whitney, K. Fox, A. Ramelli, J.C. Yount, M.D. Carr, C.D. Menges, R. Dickerson, and R.B. Scott. 1995. *Map of Fault Activity of the Yucca Mountain Area, Nye County, Nevada*. USGS Miscellaneous Investigations Series Map, I-2,520. Reston, VA: U.S. Geological Survey: 1–2,520.
- Snow, J.K. 1992. Large-magnitude Permian shortening and continental-margin tectonics in the southern Cordillera. *Geological Society of America Bulletin* 104: 80–105.
- Snyder, D.B., and W.J. Carr. 1982. *Preliminary Results of Gravity Investigations at Yucca Mountain and Vicinity, Southern Nye County, Nevada*. USGS Open-File Report 82-701. Denver, CO: U.S. Geological Survey.
- Snyder, D.B., and W.J. Carr. 1984. Interpretation of gravity data in a complex volcano-tectonic setting, southwestern Nevada. *Journal of Geophysical Research* 89: 10,193–10,206.
- Sonnenthal, E.L., C. Ahlers, and G. Bodvarsson. 1997. Fracture and fault properties for the UZ site-scale flow model. *The Site-Scale Unsaturated Zone Model of Yucca Mountain, Nevada, for the Viability Assessment*. G. Bodvarsson, T. Bandurraga, and Y. Wu, eds. LBNL-40376. Berkeley, CA: Lawrence Berkeley National Laboratory.
- Spengler, R.W., and K.F. Fox, Jr. 1989. Stratigraphy and structural framework of Yucca Mountain, Nevada. A.M. Platt, D.R. Anderson, and F. Girardi, eds. *Radioactive Waste Management and the Nuclear Fuel Cycle. Special Issue* 13: 21–36.

- Spengler, R.W., M.P. Chornack, D.C. Muller, and J.E. Kibler. 1984. Stratigraphic and Structural Characterization of Volcanic Rocks in Borehole USNG-4. Yucca Mountain, Nye County Nevada. U.S. Geological Survey Open-File Report 84-789. U.S. Geological Survey.
- Stamatakos, J.A., C. B. Connor, and R.H. Martin. 1997. Quaternary basin evolution and basaltic magmatism of Crater Flat, Nevada from detailed ground magnetic surveys of the Little Cones. *Journal of Geology* 105: 319–330.
- Stamatakos, J.A., and D.A. Ferrill. 1998. Strike-slip fault system in Amargosa Valley and Yucca Mountain, Nevada—comment. *Tectonophysics* 294: 151-160.
- Starkey, H.C., P.D. Blackmon, and P.L. Hauff. 1984. *The Routine Mineralogical Analysis of Clay-Bearing Samples*. USGS Bulletin B 1563. Reston, VA: U.S. Geological Survey.
- Stock, J. M., J.H. Healy, S.H. Hickman, and M.D. Zoback. 1985. Hydraulic fracturing stress measurements at Yucca Mountain, Nevada, and relationship to regional stress field. *Journal of Geophysical Research* 90: 8,691–8,706.
- Stuckless, J.S., J.F. Whelan, and W.C. Steinkampf. 1991. Isotopic discontinuities in ground water beneath Yucca Mountain, Nevada. *Proceedings of the Second Annual International Conference on High-Level Radioactive Waste Management*. La Grange Park, IL: American Nuclear Society: 1,410–1,415.
- Swadely, W.C., and L.D. Parrish. 1988. *Surficial Geologic Map of the Bare Mountain Quadrangle, Nevada, Scale 1:34,000*. USGS Miscellaneous Investigations Series Map I-1826. Reston, VA: U.S. Geological Survey.
- Sweetkind, D. S., and S.C. Williams-Stroud. 1996. *Characteristics of fractures at Yucca Mountain, Nevada: Synthesis Report*. Administrative Report. Denver, CO: U.S. Geological Survey.
- Szymanski, J.S. 1989. *Conceptual Considerations of the Yucca Mountain Groundwater System with Special Emphasis on the Adequacy of this System to Accommodate a High-Level Nuclear Waste Repository*. Unpublished report available from the Department of Energy, Yucca Mountain Project Office, 5 Volumes. Las Vegas, NV.
- Throckmorton, C.K., and E.R. Verbeek. 1995. *Joint networks in the TIVA Canyon and Topopah Spring Tuffs of the Paintbrush Group, Southwestern Nevada*. USGS Open-File Report 95-2. Denver, CO: U.S. Geological Survey.
- Trexler, J.H., Jr., J.C. Cole, and P.H. Cashman. 1996. Middle Devonian-Mississippian stratigraphy on and near the Nevada Test Site: Implications for hydrocarbon potential. *American Association of Petroleum Geologists Bulletin* 80: 1,736–1,762.
- Trudgill, B., and J. Cartwright. 1994. Relay-ramp forms and normal-fault linkages, Canyonlands National Park, Utah. *Geological Society of America Bulletin* 106: 1,143–1,157.
- Turrin, D.B., D. Champion, and R.J. Fleck. 1991. $^{40}\text{Ar}/^{39}\text{Ar}$ age of the Lathrop Wells Volcanic Center, Yucca Mountain, Nevada. *Science* 253: 253–257.

- U.S. Department of Energy. 1998. *Viability Assessment of a Repository at Yucca Mountain: Total System Performance Assessment, December 1998*. Volume 1. DOE/RW-0508. Las Vegas NV. U.S. Department of Energy. Office of the Civilian Radioactive Waste Management.
- Waddell, R.K. 1982. *Two-Dimensional, Steady-State Model of Ground-Water Flow, Nevada Test Site and Vicinity, Nevada-California*. USGS Water-Resources Investigations Report 82-4085: Denver, CO: U.S. Geological Survey.
- Waddell, R.K., J.H. Robinson, and R.K. Blankenagel. 1984. *Hydrology of Yucca Mountain and Vicinity, Nevada-California, Investigative Results through Mid-1983*. USGS Water Resources Investigations Report 84-4267. Denver, CO: U.S. Geological Survey.
- Watterson, J., A. Nicol, J.J. Walsh, and D. Meier. 1998. Strains at the intersections of synchronous conjugate normal faults. *Journal of Structural Geology* 20: 363-370.
- Wernicke, B.P. 1992. Cenozoic extensional tectonics of the western Cordiller. *The Cordilleran Orogen: Conterminous U.S., The Geology of North America Volume G-3*. B.C Burchfiel, P.W. Lipman, and M.L. Zoback, eds. Boulder, CO: Geological Society of America, Inc.: 553-581.
- White, A.F. 1981. Controls on isotopic compositions of groundwater in southern Nevada. *EOS, Transactions of the American Geophysical Union* 62: 286.
- White, A.F., and N.J. Chuma. 1987. Carbon and isotopic mass balance models of Oasis Valley-Fortymile Canyon Groundwater basin, southern Nevada. *Water Resources Research* 23: 571-582.
- Winograd, I.J., and I.J. Friedman. 1972. Deuterium as a tracer of regional ground-water flow, southern Great Basin, Nevada and California. *Geological Society of America Bulletin* 83: 3,691-3,708.
- Winograd, I. J., and W. Thordarson. 1975. Hydrogeologic and hydrochemical framework. South-Central Great Basin, Nevada-California, with Special Reference to the Nevada Test Site: *Geological Survey Professional Paper 712-C*.
- Winograd, I.J., and F.J. Pearson, Jr. 1976. Major carbon 14 anomaly in a regional carbonate aquifer: Possible evidence for a megascale channeling, south central Great Basin. *Water Resources Research* 12: 1,125-1,143.
- Wittmeyer, G.W., and D.R. Turner. 1995. *Conceptual and Mathematical Models of the Death Valley Regional Groundwater Flow System*. CNWRA95-019. San Antonio, TX: Center for Nuclear Waste Regulatory Analyses.
- Woods, E.P. 1988. Extensional structures of the Jabiru Terrace, Vulcan subbasin in the North Shelf, Australia. *Proceedings of Petroleum Exploration Society, Australia Symposium*.
- Woods, E.P. 1992. Vulcan subbasin fault styles-implications for hydrocarbon migration and entrapment: *The Australian Petroleum Production and Exploration Association Journal* 32: 138-158.
- Young, S.R., A.P. Morris, G.L. Stirewalt. 1992. Preliminary Structural Interpretation of Reflection Seismic Line AV-1. CNWRA 92-024. San Antonio, Texas: Center for Nuclear Waste Regulatory Analyses.

- Zoback, M. L., R.E. Anderson, and G.A.Thompson. 1981. Cenozoic evolution of the state of stress and style of tectonism of the Basin and Range Province of the western United States. *Philosophical Transactions of the Royal Society of London* 300: 407-434.
- Zoback, M.L. 1992. First- and second-order patterns of stress in the lithosphere: The World Stress Map Project. *Journal of Geophysical Research* 97(B8): 11,703-11,728.
- Zyvoloski, G.A., B.A. Robinson, K.H. Birdsell, C.W. Gable, J. Czarnecki, K.M. Bower, and C. Faunt. 1997. *Saturated Zone Radionuclide Transport Model*. Civilian Radioactive Waste Management System Management and Operating Contractor. Milestone Report SP25CCM3A. Los Alamos, NM. Los Alamos National Laboratory.